November 2017

Resolving chronological and temperature constraints on Antarctic deglacial evolution through improved dating methodology

Cristina Subt
University of South Florida, csubt@mail.usf.edu

RESOLVING CHRONOLOGICAL AND TEMPERATURE CONSTRAINTS ON ANTARCTIC DEGLACIAL EVOLUTION THROUGH IMPROVED DATING METHODOLOGY

by

Cristina Subt

A dissertation submitted in partial fulfillment
of the requirements for the degree of
Doctor of Philosophy in Marine Science
with a concentration in Geological Oceanography
College of Marine Science
University of South Florida

Major Professor: Brad E. Rosenheim, Ph.D.
Amelia E. Shevenell, Ph.D.
Tim M. Conway, Ph.D.
John M. Jaeger, Ph.D.
Christina R. Riesselman, Ph.D.

Date of Approval:
October 25, 2017

Keywords: Last Glacial Maximum, radiocarbon, TEX_{86}, Ramped PyrOx

ACKNOWLEDGMENTS

First and foremost, I would like to thank my advisor, Brad Rosenheim, and to the members of my committee, whose help and guidance have made me a better scientist. He continually challenged me to take initiative, strive to do better, and learn from all my mistakes. Thank you to all the members of the Paleolab: their dedication inspired me, their support fueled me, and their discussions guided me. Thank you to my committee for always providing exciting challenges and insights that allowed me to discover new ways of thinking about science.

I would also like to acknowledge the scientists at the Korea Polar Research Institute for offering so many opportunities to collaborate with them, and learn from them. Thank you also to the scientists, crew and support staff aboard the Research Vessels Lawrence M. Gould and Araon. Their assistance in the field and in the laboratory was invaluable to my success.

I would like to express my gratitude to the College of Marine Science at the University of South Florida, the Florida-Georgia Louis Stokes Alliance for Minority Participation Bridge to the Doctorate Program at the University of South Florida (NSF Award # 1400837), and to the Alfred P. Sloan Foundation's Minority Ph.D. Program for providing the funding support necessary to allow me to complete this dissertation.

TABLE OF CONTENTS

LIST OF TABLES

LIST OF FIGURES

ABSTRACT

In order to determine the timing of Antarctic ice sheet retreat and advance during the Late Quaternary, various tools are used to measure the age of marginal marine sediments. Carbonate ^{14}C dating is a well-established approach, but requires foraminiferal microfossils, shells or other carbonate materials that are rare in most Antarctic regions, and may also suffer from vital effects, which can result in variability of up to 500 years in living organisms. Bulk acid insoluble organic (AIO) ^{14}C dates are frequently as an alternative, but this approach works best where high productivity and sedimentation rates reign, and not too well in condensed sequences where high proportions of detritus are present. Compound specific dating methods have also been employed, but these may still yield an average age from a mixture of components and require very large sample sizes. Alternate methods of applying a chronology have also been used, such as magnetic intensity dating, or regional correlation with well-dated cores, but these may not always provide accurate and precise dates. Here I present work, some published with co-authors, of progressive improvements of Ramped PyrOx ^{14}C dating, which utilizes the thermochemical degradation of components within a bulk AIO sediment sample. This dissertation focuses on the study, improvement and application of advanced Ramped PyrOx techniques. These improvements include novel techniques, such as compositing and isotope dilution that I use to date sediments where the proportion of contemporaneously deposited carbon is very small relative to other detrital components, and maximize the accuracy of resulting dates while minimizing costs in precision from utilizing ultra-small fractions of the bulk sample. Ramped PyrOx ^{14}C dating techniques allows us to generate chronologies for cores

that would otherwise go undated. Furthermore, these techniques can be used to push the limits of radiocarbon dating not only to regions where accurate core chronologies have been difficult to come by, but also further back in time, into marine sediment horizons deposited at or before the last glacial maximum (LGM), where highly detrital material has precluded radiocarbon dating in the past. Wider use of these techniques can enable more coordinated *a priori* coring efforts to constrain regional glacial responses to rapid warming.

CHAPTER 1:
INTRODUCTION

1.1 Sea Level Forcing Mechanisms

The effects of ocean warming on ice sheet disintegration at high latitudes, such as the breakup of the Larsen ice shelf observed through satellite imagery since 1989, have spurred the advancement of research concerning Antarctic glacial advance and retreat in recent years. Polar ice sheets comprise a crucial component of global sea level change during glacial cycles. Antarctic ice volume is equivalent to ~61 m of sea level, most of which is locked up in the Weddell and Ross ice shelves (Huybrechts, 2002). The Antarctic Ice Sheet is divided into 2 parts: the East Antarctic Ice Sheet (EAIS), which rests on a major land mass and is generally considered to be more stable (e.g. Sugden et al., 1993; Hughes, 1973), and the West Antarctic Ice Sheet (WAIS), which is classified as a marine-based ice sheet (it is grounded below sea level) (e.g. Bindschadler et al., 2003; Bougamont et al., 2003; Joughin and Alley, 2011; Joughin et al., 2005; Joughin and Tulaczyk, 2002; Livingstone et al., 2012; MacAyeal, 1992; Mercer, 1978; Oppenheimer, 1998). More recent research has also challenged the belief that the EAIS was relatively stable (e.g. Bart and Anderson, 2000; Mackintosh et al., 2014). The bases of ice sheets are generally warmer than the surface due to geothermal heat, and in places where basal melting occurs, the meltwater acts as a lubricant, creating corridors of fast-flowing ice known as ice streams (e.g. Livingstone, 2012). Where the ice sheets meet the coastline, thick ice shelves often form and can extend far beyond the grounding line. Recognizing features left

behind by ice streams is a crucial step in determining the geometry of grounded ice, as well as the direction and thickness of ice flow.

At the Last Glacial Maximum (LGM; ~23 to 19 ka), the total eustatic sea level depression was between 125 and 135 m (Fairbanks, 1989; Yokoyama et al., 2000). Constraining the timing and contribution of Antarctic glacial ice to Late Pleistocene – Holocene sea-level changes and the major forcing mechanisms controlling these changes can therefore be used to make inferences and models to predict future melting and associated sea level rise (e.g. DeConto and Pollard, 2016; Overpeck et al., 2006). However, this is complicated by the complex ice sheet dynamics in Antarctica (e.g. Clark and Mix, 2002; Overpeck et al., 2006; Rignot et al., 2011a), and the out-of-phase glacial cycles not only between hemispheres (Blunier et al., 1998), but also between the East and West Antarctic Ice Sheets (EAIS and WAIS, respectively). A change in ice sheet dynamics could have profound effects for sea level and global ocean circulation. WAIS, being a marine-based ice sheet, poses the most immediate threat for sea-level rise due to its potential instability (e.g. Oppenheimer, 1998; Overpeck et al., 2006; Schoof, 2007; Schoof, 2012) Ice sheets are also a central component of the climate system due to their effects on heat transport, and carbon cycling, but are a major source of uncertainty for rates of sea level change (e.g. DeConto and Pollard, 2016; Golledge et al., 2015; Rignot et al., 2011b).

The utility of any paleoclimate record hinges on the accuracy of its chronology. Much has been learned about post-LGM deglaciation in the past few decades of research. For example, it is now known that the Antarctic Ice Sheet contributed ~10-18 m to eustatic sea level rise (significantly less than the total 61 m sea-level equivalent stored in Antarctic ice volume), mostly from the Ross and Weddell Sea regions (Denton and Hughes, 2002; Golledge et al., 2014; Pollard and DeConto, 2009). However, constraining the timing of these contributions has encountered many difficulties that have limited the advancement of our

understanding of these systems (Andrews et al., 1999; Rosenheim et al., 2008; Rosenheim et al., 2013b; Subt et al., 2016). This dissertation seeks to improve novel radiocarbon (^{14}C) dating techniques to expand the horizons for constraining accurate chronologies, both spatially (by targeting regions where accurate core chronologies have been limited) and chronologically (by dating marine sediment horizons deposited at or before the LGM, where highly detrital material has precluded ^{14}C dating in the past). Wider application of improved techniques could enable more coordinated a priori coring efforts to constrain regional glacial responses to rapid warming.

1.2 Late Quaternary Antarctic Deglacial Reconstructions

Reconstructions of past ice sheet/ice shelf response to large climate perturbations provide a context to place recent observations of ice shelf collapse and accelerated flow from outlet glaciers (e.g. Ó Cofaigh et al., 2014; Vaughan and Doake, 1996). As the current climate continues to warm, reconstructing past shifts from glacial to interglacial conditions can lend a deeper understanding of the cryosphere's responses to climatic changes. Studies of post-LGM deglaciation offer the densest and most complete record of a deglacial transition and are therefore the best source for understanding present and future climate and sea level changes through models and reconstructions (Bentley, 2010; Bentley et al., 2014; DeConto and Pollard, 2016; Overpeck et al., 2006). Thus, it is important to study the mechanisms by which Antarctic deglaciation has occurred in the past if we are to understand future changes. Many discoveries have been made on the mode of retreat of Antarctic ice sheets, but constraints on the timing of those changes have been difficult to attain due to problems found within the sediments (e.g. Andrews et al., 1999; Berger and Johnson, 1978; Cearreta and Murray, 2000; Domack et al., 2001).

Previous attempts at reconstructing post-LGM ice sheet extent in Antarctica have been limited by more than the reliability of available chronologies. The volume of ice and timing of release of the Antarctic contribution of melting ice sheets to sea level at the LGM have been difficult to quantify due to a mismatch between previously constrained ice extent and ice mass volume (Bentley, 1999). The lack of a clear understanding of how ice sheets can impact and are impacted by climate have caused difficulties for modelers seeking to develop accurate reconstructions (e.g. Clark and Mix, 2002; Denton and Hughes, 2002). However, techniques used to acquire and analyze data for developing records of ice-sheet thickness and extent have been refined or developed in recent years. These improvements have led to great improvements in existing reconstructions and a better understanding of these processes (Anderson and Andrews, 1999; Anderson et al., 2002; Bentley, 1999; Denton and Hughes, 2002; Livingstone et al., 2012; Wright et al., 2008).

Outlet glaciers drain the interior of Antarctic ice sheets to the coast along continental margins and can be used to track the direction of ice flows, which can be helpful for interpreting patterns of past deglaciations. Geophysical observations of the seafloor with multibeam swath bathymetry allow for the identification of mega-scale glacial lineations (MSGLs), which indicate ice streams that mark zones of fast-flowing ice where outlet glaciers are preferentially drained (Livingstone et al., 2012; Ottesen et al., 2005). Geophysical observations also record the past extent of formerly grounded ice in marine settings, appearing in the form of mega-scale glacial lineations (MSGL), grounding-zone wedges (GZW), transverse ridges and channels. . Although the availability of seafloor bathymetry data is limited around Antarctic margins due to ice extent and extreme seasonality, today there is more Antarctic seafloor data than ever before, thus providing us with more understanding of paleo-ice flow locations and dynamics. By synthesizing knowledge of key characteristics in paleo-ice streams,

including bathymetry, geology and geomorphology, we can investigate relationships between dated and inferred modes of retreat and the factors that control them (Livingstone et al., 2012). Thus, it is imperative to constrain the timing of the events that form these features, despite the many difficulties doing so may present.

1.3 The Difficulties of ^{14}C Dating Antarctic Sediments

Our ability to apply a chronology to any marine sediment-based ice sheet reconstruction is key to being able to understand the rates and timing of important ice sheet retreat events. However, many regions of the Antarctic margins pose difficulties for dating. Carbonate ^{14}C dating of Antarctic marginal marine sediments is a relatively simple and well-established method of constraining the timing of events within cores, that produces minimal uncertainty in most cases. However, carbonate microfossils in these regions are often rare due to low abundances in the water column and the dissolution effects of carbonates caused by cold temperatures and deep continental shelves in Antarctica (Licht et al., 1998; Mackintosh et al., 2014). Thus, alternate methods of attaining chronologies are often employed, such as ^{14}C dating the acid insoluble organic (AIO) fraction of the sediment (e.g. Andrews et al., 1999; Cunningham et al., 1999; DeMaster et al., 1996; Domack et al., 2001; Licht et al., 1998; Licht et al., 1996), diatom-bound compound-specific (CS) ^{14}C dating (Yokoyama et al., 2016) or by geomagnetic field paleo-intensity tuning with an independently dated reference curve (Brachfeld et al., 2003; Stoner et al., 1994; Van Geel and Mook, 1989; Wigley et al., 1990; Xiao et al., 2016), each with its own set of difficulties. Moreover, ^{14}C dating from carbonate microfossils carry their own share of problems that need to be accounted for, such as reworking through sediment transport, bioturbation, sediment gravity flows and winnowing, and may be representative of a

range of ages at the time of deposition due to geological uncertainty (Rosenheim et al., 2008; Rosenheim et al., 2013b; Subt et al., 2016).

Bulk AIO ^{14}C dating is the most typical approach for 'absolute' dating of Antarctic late Quaternary sediments where carbonate material is unavailable, but often yields ages much older than the age of contemporaneous carbon deposition. These older ages are mostly the result of the admixing of old organic carbon from regional erosion and re-sedimentation, which can change the relative proportions of detrital material in the sediments (Andrews et al., 1999; Domack et al., 1999a; Domack et al., 2001; Yamane et al., 2014). This also accounts for the large spatial variability in core-top ages found within the Antarctic margins (Andrews et al., 1999). Core-top ages in marginal Antarctic sediments are often older than the designated reservoir correction (usually between 1200 and 1300 ^{14}C years) determined from marine carbonates in the region (Berkman and Forman, 1996; Domack et al., 1989; Gordon and Harkness, 1992); this suggests secondary processes are also taking place which affect the ^{14}C activity measured in sediments (Andrews et al., 1999). Other processes that can impact the anomalously old ages in Antarctic marginal sediments include geochemical processes such as vital effects (Gordon and Harkness, 1992), biological effects associated with sea ice limitation on CO_2 exchange, and bioturbation (Andrews et al., 1999). For these reasons, the AIOM age of the core-top sediments is typically subtracted from all subsequent ages down-core, known as the constant offset approach; however, this may result in inaccurate dating. The constant offset assumes constant relative proportions of old organic carbon from terrigenous sources, comparable to modern ratios, have been advected into the system through time, but this is not necessarily accurate in all regions (Andrews et al., 1999; Hall and Henderson, 2001; Michalchuk et al., 2009; Pudsey et al., 1994; Rosenheim et al., 2013b). Although AIO ^{14}C dating has been historically problematic, it is still a relatively easy approach that can provide a good first-order

estimation of ages in sediments where the relict detrital component is not large (e.g. Cunningham et al., 1999; Domack et al., 2001; McKay et al., 2008; Smith et al., 2014).

One of the most common difficulties that arise from ^{14}C dating Antarctic marginal sediments is the effects of the very old carbon reservoir (e.g. Andrews et al., 1999; Berkman and Forman, 1996; Gordon and Harkness, 1992; Hall and Henderson, 2001; Stuiver et al., 1986b). That is, the water in which productivity occurs and, where possible, carbonate precipitates, may have an initial age that is up to thousands of years old. It is the result of the inherited age (the age derived from the input of old carbon such as glacial meltwater) and the residence age (the natural age of water masses sealed from the atmosphere) (Hall and Henderson, 2001; Hendy and Hall, 2006). The ocean has a long residence time of ^{14}C relative to atmosphere, and water mass circulation varies greatly geographically, resulting in the oldest surface waters residing in the Southern Ocean (Broecker, 1963; Berkman and Forman, 1996). The unique water mass circulation patterns around Antarctica thus result in a large spatial variability in reservoir age, which generates further complications, precluding standardization of a regional reservoir correction (e.g. Conway et al., 1999; Gordon and Harkness, 1992; Hall and Henderson, 2001; Hendy and Hall, 2006). Reservoir corrections in Antarctic sediments can range from 1200 to 3000 years (Andrews et al., 1999; Berkman and Forman, 1996; Domack et al., 1989; Gordon and Harkness, 1992). There is also great uncertainty in the changes in reservoir age that can take place over time as a result of changes in circulation regimes (Burke and Robinson, 2012; Carré et al., 2016; Hall and Henderson, 2001; Sarnthein et al., 2007).

1.4 Recent Developments of Methods for Dating Antarctic Sediments

Improvements in separating pools of organic carbon within the sediment have been made by employing compound specific (CS) ^{14}C dating (Eglinton et al., 1996; Eglinton et al.,

1997; Ingalls et al., 2004; Ohkouchi and Eglinton, 2006; Ohkouchi and Eglinton, 2008; Ohkouchi et al., 2003; Pearson et al., 1998) and Ramped PyrOx (RP) ^{14}C dating (Rosenheim et al., 2008; Rosenheim et al., 2013b). The compound-specific technique involves the chemical extraction of specific compounds (biomarkers) associated with organism-specific processes. Targeted compounds for this approach may include fatty acids, sterols and hydrocarbons (e.g. Eglinton et al., 1996). Early work utilizing this technique had difficulties with the large amounts of material required for ^{14}C analysis (Ingalls and Pearson, 2005). Although CS ^{14}C dating has since been developed more recently for sediments, which contain greater quantities of the necessary pools of carbon, recent work targeting CS ^{14}C ages in Antarctic regions in the Ross Sea and the Wilkes Land Coast illustrates large uncertainties that result from applying compound-specific ^{14}C dating to hemipelagic sediments (Ohkouchi et al., 2003; Ohkouchi and Eglinton, 2006, 2008; Yamane et al., 2014; Yokoyama et al., 2016). The high degradation rate of specific compounds for ^{14}C dating can lead to low abundances in relict organic material. Moreover, this approach requires large amounts of sediment for extraction to produce an accurate chronology.

Alternatively, Ramped PyrOx ^{14}C dating has also offered recent advances in the separation of pools of organic carbon through thermochemical degradation (Rosenheim et al., 2008; Rosenheim et al., 2013b). The partitioning of samples into several components produces a spectrum of ^{14}C ages, ranging from youngest to oldest with increasing pyrolysis temperature. Both compound specific and Ramped PyrOx dating may still yield an average age from a mixture of components. In Ramped PyrOx, the least diagenetically stable (lowest temperature) component of the sediment is generally the least thermochemically stable and is thus the first aliquot of CO_2 to be collected, but this can vary due to the physical and chemical properties of these components. Early work shows that aliquots collected at high-resolution low-temperature

intervals approached foraminiferal ages, but lower resolution intervals did not (Rosenheim et al., 2008). Additionally, contributions from different pools changed downcore and constant age offsets were found to be potentially erroneous (Rosenheim et al., 2013b). Further advancements have been made by using smaller aliquots, collected at lower temperatures of the reaction to reduce the amount of older CO_2 incorporated into the aliquot (Fernandez et al., 2014). Although carbonate ^{14}C dating is not without its own problems, the match in ages between two mutually exclusive components of the sediment lends support to the applicability of Ramped PyrOx for sediments with mixed components of ^{14}C.

This research focuses on the development of Ramped PyrOx for dating purposes in Antarctic sediments. However, it should be noted that Ramped PyrOx, previously termed Ramped Pyrolysis, provides a thermogravimetric analysis of organic samples that can be applied to any organic material, and be useful for a wide variety of reasons. For example, Distributed Activation Energy Models (DAEM) for pyrolysis of organic materials can be a valuable resource for determining energy potentials of specific biomass constituents that can be used as fuel (e.g. de Jong et al., 2003; Kirtania and Bhattacharya, 2012), or simply analyzing reaction kinetics of the bulk material (e.g. Hemingway, in prep; Issler and Snowdon, 1990; Please et al., 2003). Polycyclic aromatic carbon (PAH) pollution and composition from the *Deepwater Horizon* oil spill in the Gulf of Mexico sediments has been determined through diagnostic Ramped PyrOx analyses (e.g. Adhikari et al., 2016; Pendergraft and Rosenheim, 2014). Pyrolysis experiments have also been conducted on tobacco to determine relationships between tobacco components and smoke products (Baker and Bishop, 2004). Ramped PyrOx is also a powerful tool when coupled with isotopic analysis or as a diagnostic tool to analyze constituents within a sample. However, little research has been done to analyze Antarctic sediments in this way (Rosenheim

et al., 2008; Rosenheim et al., 2013b). For this reason, this research includes sections that evaluate the thermochemical decomposition of the organic material analyzed.

The relatively recent developments and improvements in dating Antarctic sediments and the availability of increasingly complex and detailed datasets have allowed for investigating the post-LGM Antarctic deglaciation with increasing detail. Continuing this trend can expand the limits of Antarctic research not only for the improvement of accuracy of deglacial chronologies across the continent, but also to broaden exploration through regions where typical dating methods have been impractical or ineffectual. In essence, we can take one step closer to surpassing the limitations of dating sediments where it is possible, and instead date where it is preferable. Improvements in dating also provide the opportunity to make use of existing cores where the chronology has been problematic, and to extend the dating further downcore to develop a better understanding of glaciation processes (Andrews et al., 1999; Ohkouchi et al., 2003; Rosenheim et al., 2008; Rosenheim et al., 2013). However, despite the many incremental advances that have been made to improve the accuracy and precision of dates from marine deposits around Antarctica, problematic chronologies persist. For example, ^{14}C dates remain ambiguous in regions with high reworking of older sediment, low accumulation rates and corrosive waters where $CaCO_3$ microfossils are not preserved. Moreover, maximum age constraints determined through Ramped PyrOx ^{14}C dating require further analysis to improve the approach by extending its applicability to increasingly detrital samples. Much of the research conducted in Antarctic marine sediments is still highly dependent on the ability to retrieve high resolution sediment cores with sufficient carbonate material for dating, or other indicators that carbonate or AIO ^{14}C dating is likely to be fruitful. Removing such limitations through improved AIO ^{14}C dating may allow sediments under ice shelves, glacial tills or siliceous muds and oozes (SMOs) buried prior to the LGM to be dated. Sub-ice shelf sediments, for example, could serve

as a modern analog for Cryogenian research (e.g. Vincent et al., 2000). It would also allow researchers to study ice sheet behavior not only during the deglacial period but into the glacial period as well.

1.5 Research Objectives

The research presented in this dissertation is designed to test the overarching hypothesis that alternative dating techniques improve ^{14}C dates of organic material in Antarctic sediments through more effective separation of pre-aged C from contemporaneously-deposited organic material. Three distinct study sites (Lapeyrère Bay, Larsen C ice shelf, and Drygalski Trough) are analyzed with a variety of methods to determine the effectiveness of the Ramped PyrOx ^{14}C dating approach.

The first main objective of this dissertation is to apply the Ramped PyrOx ^{14}C dating approach to develop chronologies for a wider range of Antarctic marginal marine sediments than has previously been possible. The applicability of Ramped PyrOx has only begun to break ground in Antarctic research, but shows great potential for improving the accuracy of ^{14}C dates required for most Quaternary research. Thus, it is important to show it can be used for diverse settings under different conditions. We targeted three locations for our analyses: Chapter 2 presents data from a sediment core from Lapeyrère Bay, located off Anvers Island in the western Antarctic Peninsula, which contains sediment from a relatively productive region where organic carbon as well as carbonate sediments are found in sufficient quantities for ^{14}C dating throughout most of the core. Chapter 3 focuses on sub-ice shelf sediments adjacent to the Larsen C Ice Shelf, on the eastern Antarctic Peninsula, where extremely high proportions of detrital material overwhelm the typical AIO ^{14}C measurement. Finally, Chapter 4 focuses on

sediments near the Drygalski Ice Tongue in the Ross Sea, which can provide clues into a multiple-recession scenario for the Ross Ice Shelf through the LGM deglaciation.

Typical ^{14}C dating techniques used in these regions are often limited by the types of sediments that can be used. Therefore, the second objective of this research is to demonstrate the improvement in accuracy of the Ramped PyrOx ^{14}C dating approach and to expand its applicability to a wide range of sediment types along the Antarctic margins where other approaches are limited. In Chapter 2, I show that Ramped PyrOx ^{14}C dating can produce a chronology of equivalent, if not higher, accuracy than carbonate ^{14}C, which is commonly perceived as the "gold standard" for ^{14}C dates. In Chapter 3, I improve upon this approach by applying a number of techniques that modify Ramped PyrOx ^{14}C dating to illustrate its advantages while also demonstrating the limitations of each new technique.

The third and final objective is to explore patterns of ice sheet retreat and advance in regions where ^{14}C dating has proven difficult in the past. A good chronology should lead to straightforward interpretations of proxies, thus Chapter 4 utilizes TEX_{86} as a temperature proxy to test the timing of open ocean events in the Ross Sea since the LGM. This study also applies the improved techniques developed in Chapters 2 and 3 to sediments from the western Ross Sea. The TEX_{86} paleothermometry applied in this study is used to examine the effect that water mass temperature may have had on ice shelf disintegration.

CHAPTER 2:

SEDIMENT CHRONOLOGY IN ANTARCTIC DEGLACIAL SEDIMENTS: RECONCILING ORGANIC CARBON ^{14}C AGES TO CARBONATE ^{14}C AGES USING RAMPED PYROX

2.1 Note to Reader

This chapter includes materials previously published in *The Holocene; Volume:* 26; Issue:2; Pages: 265-273; doi: 10.1177/0959683615608688;

Authors: Cristina Subt[1], Kimberly A. Fangman[2], Julia S. Wellner[2], Brad E. Rosenheim[1]

[1]College of Marine Science, University of South Florida, USA

[2]Department of Earth and Atmospheric Sciences, University of Houston, USA

C. Subt (first author) analyzed data and prepared the manuscript. K. Fangman originally analyzed sediments, re-analyzed by Matthew Pendergraft. Useful input, discussions and editing were provided by co-authors J. Wellner and B. Rosenheim.

Sections 2.2 through 2.7 incorporate all materials included in the publication listed above with only minor changes to the text. Sections 2.8 and 2.9 contain additional information and analysis pertinent to this chapter that is unpublished.

2.2 Abstract

We present the first study which directly compares carbonate radiocarbon (^{14}C) dates with the Ramped PyrOx (RP) radiocarbon dating technique within a single sediment core, and we confirm the utility for the latter constructing chronologies of high latitude, Holocene marine margin sediment successions. Historically, the heavily detrital nature of Antarctic margin sedimentary organic material and lack of carbonate preservation have made these sediments difficult to date accurately. Here, we use archived cores with existing foraminiferal ages to compare with RP dates at equal or similar depth intervals. The lowest temperature RP splits were integrated over narrower intervals than in previous studies to reduce the amount of mixing with older, more thermochemically stable end-members during pyrolytic decomposition. Ages of the low-temperature RP splits coincide with their corresponding carbonate counterparts, suggesting that the RP ^{14}C dating method is a reliable alternative to carbonate dates in sediments where carbonates are absent or not sufficiently preserved for ^{14}C dating. The rarity of calcareous material in most Antarctic sediments often obligates the use of the bulk acid insoluble organic (AIO) fraction of the sediment, which can be problematic because of contamination by older carbon. The bulk AIO ^{14}C ages, which are calculated using the weighted arithmetic mean of all RP splits of individual samples, show that age reversals and biases can occur using bulk AIO dates for age models because of variable proportions of pre-aged organic matter down-core. The application of the RP dating method can reduce these effects to produce a more reliable chronology that is statistically identical to the foraminiferal dating chronology.

2.3 Introduction

Interpreting past changes in climate and the forces controlling them can provide context for current climate shifts. Many studies have focused heavily on the last ice age, as it has the

most significant relatively well-preserved record of climate change in the geologic record, and may be able to provide a long-term baseline with which to detect anthropogenic effects on climate (Mix et al., 2001). The high latitudes are some of the most sensitive regions to climate change, and the melting of polar ice can have extensive effects on climate, ocean circulation, and sea level (Cook et al., 2005; Stammerjohn et al., 2008). Understanding ice shelf response to past warming periods recorded in the geologic record can lead to more reasonable expectations of changes in ice volume that may occur under current warming (Bentley et al., 2014). Maximum global ice volume during the Last Glacial Maximum (LGM) is estimated by both global and local Antarctic sea level records and occurred between 26.5 and 19 ka, ending with the onset of sea level rise ~20 to 19 ka (Carlson and Clark, 2012; Clark et al., 2009; Mix et al., 2001). However, not enough is known about the style of deglaciation and source of water that contributed to sea level rise (Carlson and Clark, 2012; Deschamps et al., 2012; Mackintosh et al., 2011).

The Antarctic Peninsula (AP) Ice Sheet was drained by paleo-ice streams, regions of accelerated ice flow sourced by deep continental ice in the

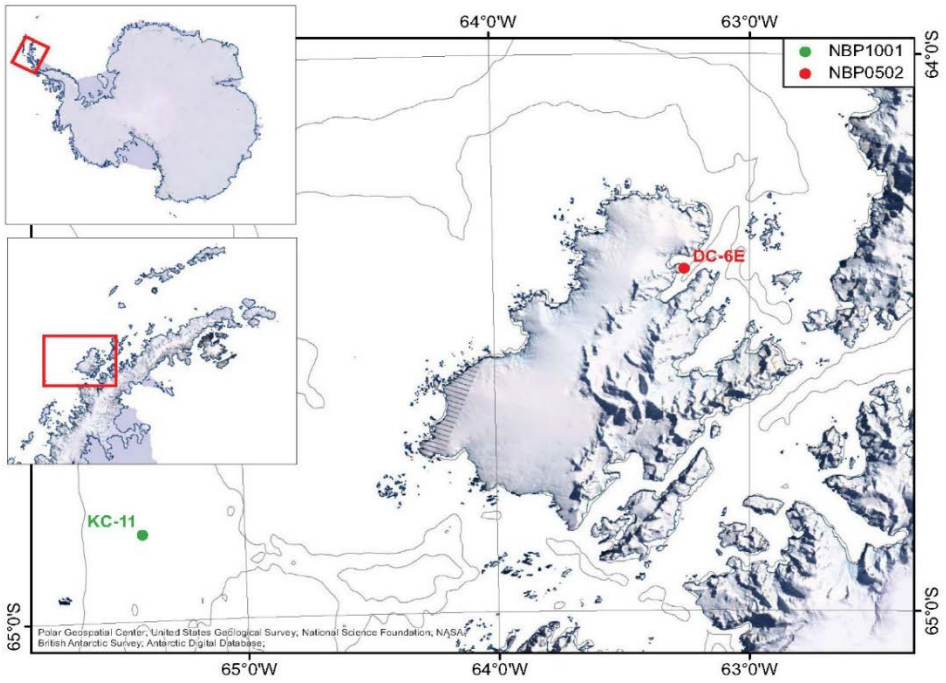

Figure 2.1. Anvers Island off the Eastern Antarctic Peninsula. Also shown are the locations of cores NBP-05-02 DC-6E (2005) in red in Lapeyrère Bay, and previously dated NBP1001 KC-11 (2010; Rosenheim et al., 2013b) in green in Hugo Trough. Bathymetric contour interval = 500 m. Background image is from Landsat Image Mosaic of Antarctica (LIMA).

mountainous peninsula, during and after the LGM (Domack et al., 2006; Lavoie et al., 2015; Leventer et al., 2006). As ice retreated from AP bays and fjords, tidewater glaciers formed. Deep troughs and basins along the inner shelf of the peninsula were caused by glacial scouring, marking the retreat of grounding lines where ice makes contact with the seafloor. Marine geophysical data have allowed extensive and detailed mapping of the past extent of ice around Antarctica (e.g. Domack et al., 2006; Livingstone et al., 2012; Wellner et al., 2001). However, temporal reconstructions of ice sheet distribution during and after the LGM using sedimentary evidence on the continental margin suffer from lack of reliable chronologies in sediment cores (Anderson et al., 2002; Bentley et al., 2014; Heroy and Anderson, 2005; Nakada et al., 2000).

As critical as marine sediment chronology around Antarctica's continental shelf is to understand the timing and pace of ice retreat following the LGM, it is also problematic. Foraminiferal carbonate radiocarbon (^{14}C) dates are usually presumed to be representative of the age of the sediment deposition, but most of these sediments lack enough preserved calcareous material for thorough carbonate ^{14}C dating. As a result, the bulk acid insoluble organic (AIO) carbon fraction has been used for determining ages of sediments (Andrews et al., 1999; Carlson and Clark, 2012; Mackintosh et al., 2014). Bulk AIO ^{14}C dates reflect a mixture of carbon from both autochthonous organic carbon that rained out from the water column at the time of deposition, and ancient detrital material that was dumped or distributed by ice shelves and icebergs, yielding an average age of all these sources. When applied to core tops, bulk AIO ^{14}C dates can be considerably older than the local reservoir age (Gordon and Harkness, 1992). In down-core samples, ages are usually corrected by subtracting the age at the sediment/water interface from subsequent dated samples as prescribed by Andrews et al. (1999). Reliable age models consisting of bulk AIO ^{14}C reservoir-corrected dates using this constant offset approach are therefore dependent upon a constant near-modern ratio in the supply of allochthonous

organic material from multiple sources down-core. These assumptions may often be too loosely applied, which can result in inaccurate ages (Carlson and Clark, 2012; Milliken et al., 2009; Rosenheim et al., 2013b).

Ramped PyrOx ^{14}C analyses (Rosenheim et al., 2008) can address some of the problems associated with AIO ^{14}C dating methods. If the organic material in Antarctic margin sediments can be more accurately analyzed for radiocarbon, then we are no longer dependent on the presence of rarely preserved calcareous material. Without this dependence, improved chronologies are possible throughout the Antarctic margins, potentially correlating important sedimentary evidence of ice retreat on a regional to continental scale. Ramped PyrOx ^{14}C dating allows for the separation of the bulk organic carbon and provision of at least a maximum age constraint that is younger than the bulk AIO age (Rosenheim et al., 2008; Rosenheim et al., 2013a). The partitioning of samples into several components produces a spectrum of radiocarbon ages, ranging from youngest to oldest with increasing pyrolysis temperature. This allows for the actual ages of the sediment horizons to be better resolved by separating the thermochemically stable detrital material which is generally older (Rosenheim et al., 2008; Rosenheim et al., 2013b). This method has demonstrated both the geological uncertainty of ^{14}C dates from AIO (Rosenheim et al., 2008) and the uncertainty that can result from assuming a constant surface age offset down-core (Rosenheim et al., 2013b).

To date, the Ramped PyrOx method has only been indirectly related to carbonate ^{14}C dates at different core depths, due in part to the scarcity of foraminifera and other carbonates in these sediments. To evaluate the reliability of Ramped PyrOx analyses in areas where carbonates are insufficiently present for ^{14}C dating, we compare them directly with carbonate ages throughout a single core. We provide both chronologies on a core taken from Lapeyrère Bay in Anvers Island (Figure 2.1), testing the assumption that Ramped PyrOx ^{14}C dating can

produce an equally dependable chronology to carbonate ^{14}C ages. By applying the resultant chronology to lithological changes down-core, we can deduce glacial retreat of Lapeyrère Bay ice sheets.

2.4 Methods

2.4.1 Physical Setting and Sediments

Lapeyrère Bay is a narrow fjord on the east side of Anvers Island, off the AP's Danco Coast. Anvers Island is mostly composed of granites and is almost entirely covered by an ice cap that thickens inland from the coast (Figure 2.1; Rundle, 1973). The eastern side of Anvers Island is characterized by mountains, the highest of which is Mt Français (2760 m). This mountain system is home to several valley glaciers, of which the Iliad Glacier is most prominent. The Iliad Glacier flows northward from Mt. Français to Lapeyrère Bay, and is partly responsible for the draining of the ice cap of Anvers Island (Domack and Ishman, 1993; Griffith and Anderson, 1989; Rundle, 1973). Additionally, small cirque glaciers and two extensive headland glaciers around the perimeter serve as secondary drainage systems (Griffith and Anderson, 1989).

2.4.2 Core Collection

Several sediment cores were collected aboard the *R/V Nathaniel B. Palmer* during the 2005 USAP expedition NBP-0502, and subsequently described as part of the Shallow Scientific Drilling on The Antarctic Continental Margin (SHALDRIL) program. Core 6E is a push and rotary-drilled core taken from the inner basin glacial outwash fan of Lapeyrère Bay at a depth of 382 m. The hole was drilled with a push-core tool to a sub-bottom depth of 20.3 meters below sea-

floor (mbsf). An additional 13 cm of granite were collected at the bottom of this core. The core was divided into sections from which samples were taken according to Table 2.1.

2.4.3 Chronology

Sediment samples were dried and pulverized using a mortar and pestle and then acid treated with 2N HCl for 24 hr to decarbonate them. The samples were centrifuged and rinsed in DI water until the pH of the supernatant was normalized at ~7. Each sample was then dried in pre-combusted (525°C, 2 hr) aluminum pans at 60°C. The dry samples were stored in pre-combusted (525°C, 2 hr) vials until they could be analyzed. A small amount (5–10 mg) from each sample was analyzed using an Elementar Vario Micro-Cube elemental analyzer (EA) to measure the total organic carbon (%TOC). A larger amount of the samples (100–300 mg) was then weighed into pre-combusted (900°C, 4 hr) quartz reactor inserts between plugs of pre-combusted (900°C, 4 hr) quartz wool. Ramped PyrOx ^{14}C analyses were conducted using the methods previously described by Rosenheim et al. (2008). Sample CO_2 gas was split and collected at intervals of ~5–35 µmol (intervals were determined based on sample size), cryogenically separated from other gases using a series of liquid nitrogen (–195°C) and liquid nitrogen–cooled isopropanol (approximately −70°C) traps, and sealed into pre-combusted (525°C, 2 hr), evacuated 6-mm Pyrex tubes with pre-combusted (525°C, 2 hr) copper oxide and granulated silver. The sealed tubes were then re-combusted (525°C, 2 hr) to remove possible contamination that could affect graphitization (e.g. sulfides). Each CO_2 sample was graphitized by Fe-H_2 reduction techniques, packed into aluminum targets, and ionized using a Cs^+ sputter ion source for determination of $^{14}C/^{12}C$ ratios by Accelerator Mass Spectrometer (AMS) with ancillary $\delta^{13}C$ measurements made by stable isotope mass spectrometer at the National Ocean Sciences Accelerator Mass Spectrometry (NOSAMS) facility. Samples were split

at lower temperatures than in previous studies to minimize the amount of older CO_2 evolved into the earliest temperature interval. Bulk AIO ^{14}C dates can be calculated as the weighted arithmetic mean of the ages comprising the spectrum (Rosenheim et al., 2008; Rosenheim et al., 2013a). During gradual temperature increase to volatilize particulate organic carbon in the bulk AIO material, the less thermochemically stable components volatilize at lower temperatures than the more refractory forms of carbon. The diagenetic stability of organic carbon within a sediment sample is related to the thermochemical stability of that sample, and in many depositional environments, thermochemical stability is positively correlated with age (Gaglioti et al., 2014; Rosenheim and Galy, 2012; Rosenheim et al., 2013a; Rosenheim et al., 2013b; Schreiner et al., 2014; Williams et al., 2015) except in sediment contaminated with volatile petroleum residues that are devoid of ^{14}C (Pendergraft et al., 2013; Pendergraft and Rosenheim, 2014). The percent of total organic carbon was calculated both by analysis through the EA and during Ramped PyrOx analysis by using the mass and the total amount of CO_2 as in Williams et al. (2014) and Rosenheim et al. (2013a).

Carbonate ages were acquired for the same samples by wet-sieving with a 63-μm sieve to isolate fine terrigenous grains, foraminifera tests, and shell fragments. Sieved material was dried in an oven at ~50°C. A minimum of 1 mg of carbonate was collected and sent to University of California at Irvine to be processed for ^{14}C AMS. All samples analyzed for radiocarbon, whether by NOSAMS or UC Irvine, were graphitized and ionized using a Cs^+ sputter ion source to determine $^{14}C/^{12}C$ ratios by AMS. To apply the reservoir correction, we employ the reservoir age of 1160 ± 51 years (Milliken et al., 2009) from an articulated mollusk using the equations:

$$A_{True} = A_M + A_R \qquad \text{Eq. 2.1}$$

$$\sigma^2_{A_{True}} = \sum \sigma_i^2 \left(\frac{dx_i}{d_y}\right) = \sigma^2_{A_M} + \sigma^2_R$$

or

$$\sigma_{A_{True}} = \sqrt{\sigma^2_{A_M} + \sigma^2_{A_R}} \qquad \text{Eq. 2.2}$$

where A_{True} is corrected for reservoir age, A_M is the measured age, and A_R is the age of the reservoir. The samples summarized in this work were analyzed well before blank contamination was characterized for the Ramped PyrOx system; therefore, no blank correction is applied to these ages (Fernandez et al., 2014). If the current blank contamination correction was applied to ages derived from these runs, we would expect these ages to stay within a few decades of those in Table 2.2 with higher uncertainty because of propagation of uncertainty in the mass of the blank during the time of these analyses. Repeat bulk AIO and Ramped PyrOx ^{14}C analyses were not possible due to insufficient sample material and limited resources.

2.5 Results

2.5.1 Lithology

The upper 15.5 m of the core has been interpreted as a glacial outwash fan (Mead, 2012) and consists of very dark greenish gray homogeneous mud with occasional stringers or layers of sand, similar to diatomaceous sediments found in the Palmer Deep (Leventer et al., 2002). It has an intermediate biogenic component, frequent scattered pebbles, and ice rafted debris (IRD), which become larger and more common down-core. The lower 4.8-m facies comprises sandy mud with a coarse sand component dispersed throughout, low biogenic

component and common drop stones scattered throughout, and has been interpreted as diamicton deposited in proximal glacial marine conditions (Mead, 2012).

There is a bias toward higher %TOC in RP samples than in EA samples (Table 2.1), which likely results from very low levels of %TOC, which are barely distinguishable from background in small EA sample analysis. Because RP uses larger amounts of sediment, these determinations of %TOC are more accurate.

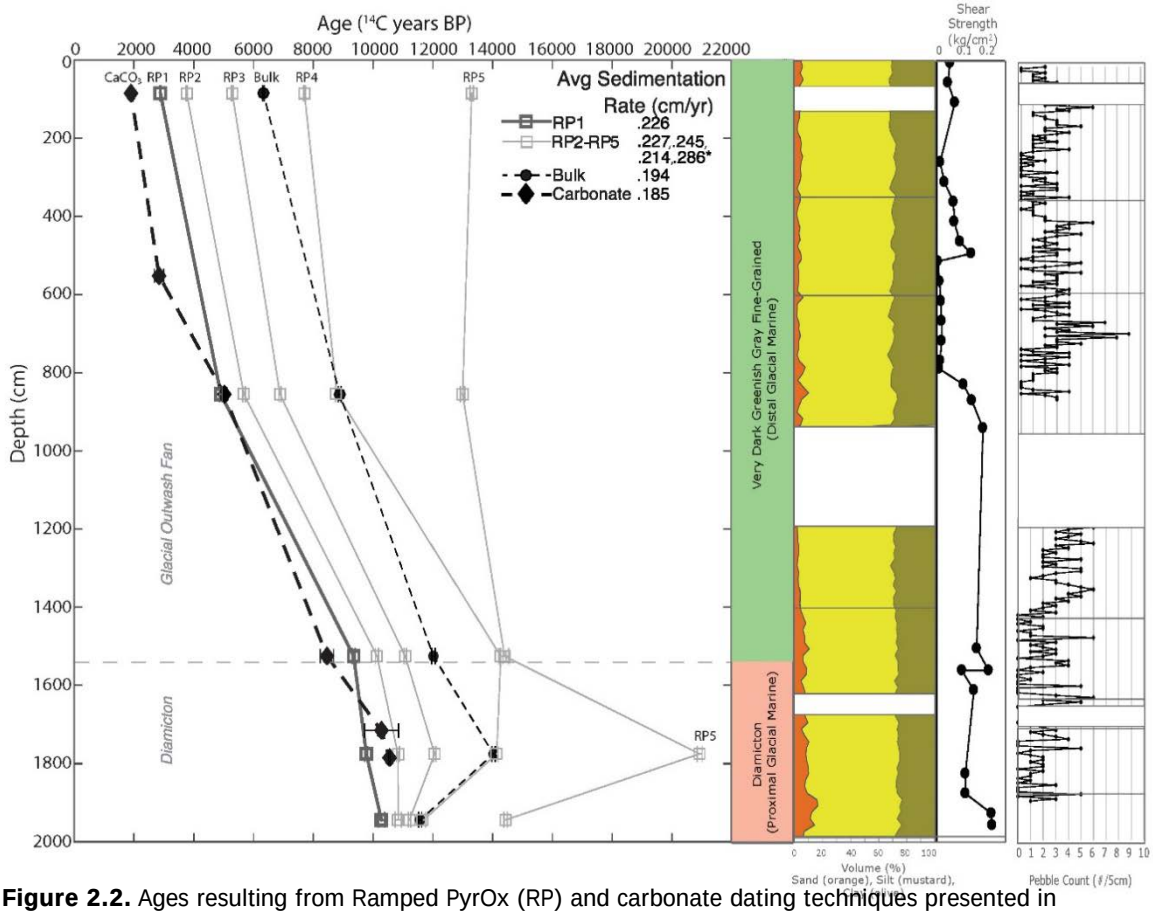

Figure 2.2. Ages resulting from Ramped PyrOx (RP) and carbonate dating techniques presented in conventional radiocarbon years (uncorrected for reservoir age, blank contamination, and uncalibrated). Horizontal gray dashed line indicates the approximate facies change. Carbonate ages and low-temperature Ramped PyrOx ages (RP-1) increase down-core. Calculated bulk AIO ages increase down-core at a relatively constant rate except for one pulse of an old, diagenetically stable component at 1774 cm depth in the core. Error bars indicate 1σ uncertainty reported in Table 2.2. Average sedimentation rates are relatively consistent regardless of the dating technique used. Core lithology shown is based on core description, grain size data, and x-ray analysis. Shear strength was measured using a hand-held Torvane. Gaps in graphic lithology represent gaps in recovered core material.

** Excluding the pulse of old material, average sedimentation rate from high-temperature Ramped PyrOx ages is*

2.5.2 Radiocarbon chronologies

The radiocarbon ages from both carbonates and Ramped PyrOx were corrected for isotopic fractionation and are presented in raw radiocarbon years with no reservoir correction (^{14}C BP), according to the convention established by Stuiver and Polach (1977) (Table 2.2). For consistency, ages are discussed in conventional radiocarbon years and depth intervals are specified by their cumulative depths unless otherwise noted. Sediment ages based on carbonate radiocarbon dates increase at varying rates down-core (Figure 2.2). Based on the rate of change in the carbonate dates, it is clear that sedimentation rates increased from the base to the top of the core. The analytical uncertainty in the carbonate dates generally increases from ±~30 to 570 toward the bottom of the core, though not monotonically.

Table 2.1. Samples taken from core NBP-0502-6E.

Core	Section	Section Depth Interval (cm)	Sample Name	Cumulative Depth-Top (cm)	Cumulative Depth-Bottom (cm)	%TOC (EA)	%TOC (RP)
NBP-0502-6E	1E	84-86	NBP0502 6E 1E 1 84-86	84	86	0.13	0.27
NBP-0502-6E	3E	52 – 54	NBP0502 6E 3E 1 52-54	552	554		
NBP-0502-6E	4E	104-106	NBP0502 6E 4E 1 104-106	854	856	0.24	0.60
NBP-0502-6E	7E	24-26	NBP0502 6E 7E 1 24-26	1524	1526	0.23	0.36
NBP-0502-6E	7E	215-217	NBP0502 6E 7E 2 215-217	1715	1717		
NBP-0502-6E	8E	24-26	NBP0502 6E 8E 1 24-26	1774	1776	0.16	0.37
NBP-0502-6E	8E	31-39	NBP0502 6E 8E 1 31-39	1781	1789		
NBP-0502-6E	8E	193-195	NBP0502 6E 8E 2 193-195	1943	1945	0.29	0.50

RP: Ramped PyrOx; EA: elemental analyzer.

Five fractions were collected sequentially for each sample, each of which was dated separately. Similar to the corresponding carbonate dates, the lowest temperature fractions (RP-1) show an increasing trend in age with depth through the entire core. The mid-temperature fractions (second, third, and fourth splits, or RP-2, RP-3, and RP-4, respectively) all show similar trends, where age increases with depth until 1774 cm, below which they show age reversals. At

the highest temperature fraction (RP-5), ages remain relatively constant with depth until 1774 cm depth, where the trend deviates strongly into a much older end-member, before returning to the previous nearly constant age. Bulk AIO dates, calculated using the weighted arithmetic mean of the full spectra of Ramped PyrOx ^{14}C ages, generally increase down-core until, similarly to splits 3, 4, and 5, an age reversal occurs at 1774 cm depth.

The difference between the highest and lowest temperature Ramped PyrOx ^{14}C dates is generally smaller down-core. The sample at 1774 cm depth is the only exception to this trend

Table 2.2. Radiocarbon ages from multiple dating techniques for Lapeyrère Bay samples. Sample designation includes cruise_site_section_sample_depth within section. Ages are reported as conventional radiocarbon ages without reservoir age correction, blank correction, or calibration to calendar years. Uncertainty in ages are reported as 1σ, and are based on analytical error from the total ^{14}C counts on AMS measurements made at NOSAMS.

Sample	Cumulative Depth (cm)	Type	Temperature Interval	CO_2 (µmol)	$\delta^{13}C$ (‰)	±	Fm	± (1σ)	Age (^{14}C y BP)	± (1σ)
NBP0502 6E 1E 1 84-86 cm	84 - 85	RP-1	Ambient - 348	10.7	-25.35	0.1	0.6978	0.0018	2890	21
		RP-2	348 - 407	10.5	-21.66	0.1	0.6303	0.0029	3708	37
		RP-3	407 - 477	20.5	-18.97	0.1	0.5241	0.0015	5190	23
		RP-4	477 - 543	25.7	-16.17	0.1	0.3903	0.0013	7558	27
		RP-5	543 - 678	14.7	-12.74	0.1	0.1958	0.0012	13099	49
NBP0502 6E 4E 1 104-106 cm	854 - 856	RP-1	Ambient - 349	4.29	-24.15	0.1	0.5438	0.0031	4893	46
		RP-2	349 - 406	5.58	-21.23	0.1	0.4971	0.0025	5615	40
		RP-3	406 - 454	7.42	-19.47	0.1	0.4292	0.0021	6795	39
		RP-4	454 - 514	5.47	-18.09	0.1	0.3394	0.0024	8680	57
		RP-5	514 - 772	19.2	-14.08	0.1	0.2028	0.0018	12817	71
NBP0502 6E 7E 1 24-26 cm	1524 - 1526	RP-1	Ambient - 359	8.4	-25.45	0.1	0.3119	0.0021	9359	54
		RP-2	359 - 419	11.4	-21.82	0.1	0.2851	0.0016	10081	45
		RP-3	419 - 491	18.7	-20.05	0.1	0.2545	0.0013	10993	41
		RP-4	491 - 597	30.2	-16.92	0.1	0.1720	0.0015	14140	70
		RP-5	597 - 725	5.2	-18.36	0.1	0.1688	0.0029	14291	137
NBP0502 6E 8E 1 24-26 cm	1774 - 1776	RP-1	Ambient - 357	12.7	-25.83	0.1	0.2957	0.0019	9787	51
		RP-2	357 - 413	13.4	-22.56	0.1	0.2610	0.0020	10790	61
		RP-3	413 - 484	21.2	-20.41	0.1	0.2250	0.0012	11982	43
		RP-4	484 - 553	25.2	-18.24	0.1	0.1745	0.0010	14024	46
		RP-5	553 - 887	36.7	-12.19	0.1	0.0759	0.0008	20712	84
NBP0502 6E 8E 2 193-195 cm	1943 - 1945	RP-1	Ambient - 341	13.1	-25.67	0.1	0.2777	0.0038	10292	109
		RP-2	341 - 395	13.9	-23.07	0.1	0.2603	0.0016	10812	49
		RP-3	395 - 474	22.2	-21.35	0.1	0.2494	0.0011	11155	35
		RP-4	474 - 550	28.2	-19.39	0.1	0.2360	0.0017	11599	58
		RP-5	550 - 660	14.4	-18.59	0.1	0.1680	0.0011	14329	52
NBP0502 6E 1E 1 84-86 cm	84 - 85	Bulk		82.1	-18.2	0.9	0.4545	0.0016	6334	28
NBP0502 6E 4E 1 104-106 cm	854 - 856	Bulk		41.9	-17.5	0.9	0.3306	0.0020	8892	48
NBP0502 6E 7E 1 24-26 cm	1524 - 1526	Bulk		73.9	-19.5	0.9	0.2238	0.0016	12026	56
NBP0502 6E 8E 1 24-26 cm	1774 - 1776	Bulk		109.2	-18	0.9	0.1742	0.0011	14040	52
NBP0502 6E 8E 2 193-195 cm	1943 - 1945	Bulk		91.8	-21.2	0.9	0.2365	0.0014	11583	49
NBP0502 6E 1E 1 84-86 cm	84 - 85	Carbonate					0.7894	0.0030	1900	30
NBP0502 6E 3E 1 52-54 cm	552 - 554	Carbonate					0.7022	0.0141	2840	160
NBP0502 6E 4E 1 104-106 cm	854 - 856	Carbonate					0.5350	0.0023	5025	35
NBP0502 6E 7E 1 24-26 cm	1524 - 1526	Carbonate					0.3488	0.0097	8460	220
NBP0502 6E 7E 2 215-217 cm	1715 - 1717	Carbonate					0.2781	0.0205	10280	570
NBP0502 6E 8E 1 31-39 cm	1781 – 1789	Carbonate					0.2691	0.0011	10550	30

and has the largest difference between the two thermochemical endmembers. The variable difference between the young and old endmembers indicates changes in the proportions of pre-aged organic matter down-core; however, in this core, the trend is different than in a core (NBP-1001 KC-11) from the Hugo Island Trough (Rosenheim et al., 2013b) where the age spectra widen with core depth. Thermographs for each sample show down-core variability (Figure 2.3) which is larger than that observed in the Hugo Island Trough. The sample at 1774 cm depth shows two pronounced secondary peaks, one at high temperature (>800°C, Figure 2.3, green oval), and the overall shape is considerably wider than other samples. The secondary peaks largely disappear at the 1944 cm depth.

Carbonate and Ramped PyrOx dates both show similar ages at matching depth intervals. In fact, at several depth intervals, RP-1 dates are younger than corresponding carbonate ^{14}C ages. At 854 cm in the core, RP-1 is only slightly younger than the corresponding carbonate age, though within error. At 1774 and 1944 cm, RP-1 ages are lower than the carbonate age at 1715 cm (within error). Contrarily, bulk AIO ages are always at least 1200 years older than either the Ramped PyrOx or the carbonate ages at concordant depths. Interestingly, where Ramped PyrOx ages get younger than the carbonate dates (~1775 cm), bulk AIO ages diverge further from the carbonate and RP-1 ages.

2.6 Discussion

Sediments in this region are dominated by terrigenous content, which is deposited through snowmelt runoff, glacial melt, subglacial plumes, calved icebergs, and aeolian inputs (Ashley and Smith, 2000; Gustavson and Boothroyd, 1987; Lønne, 1995). Fine-grained sediment arrives at the seafloor via fluvial inputs of snowmelt and glacial meltwater. Meltwater from glaciers can also erode subglacial till and create subglacial plumes, which transport

sediments and supply them to marine deposits (Domack and Williams, 1990). Calved icebergs serve as a rafting mechanism for debris. As icebergs detach from glaciers, they are removed from their source by currents and melt, releasing contained sediment, which sinks to the seafloor. Linear fjords such as Lapeyrère Bay are geographically ideal for ice rafting as the amount of dumping and debris-fall that occurs because of ice rafting is greatest at the calving line (Domack and Ishman, 1993).

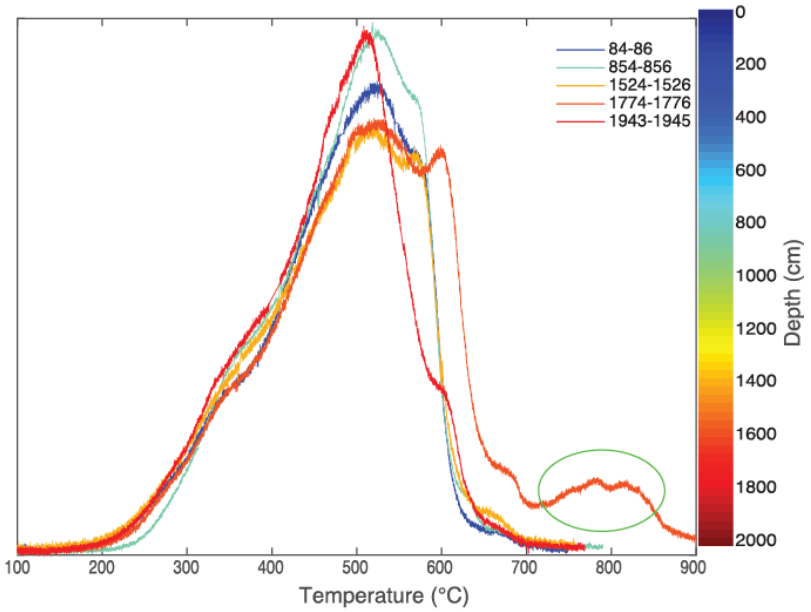

Figure 2.3. Thermographs display CO_2 evolution for each sample analyzed through Ramped PyrOx. An increase of CO_2 evolved at high temperatures for the sample at 1774 cm depth (green oval) is responsible for the older ages observed in RP5 seen in Figure 2.2.

Chronologies resulting from ^{14}C analysis of carbonates and Ramped PyrOx ^{14}C are consistent with changes in lithology (Figure 2.2). Sediment facies change from sediment deposited by a glacial outwash fan in the upper ~15.5 m of the core, probably mostly originating in the nearby Iliad Glacier, to a diamicton unit in the lower ~4.8 m. All chronologies, including calculated bulk AIO dates and Ramped PyrOx fractions of higher temperatures, show relatively consistent trends in the upper section related to sediments from the glacial outwash fan, but diverge in the lower section where the diamicton becomes dominant. Perhaps most notably, a pulse of old, thermochemically stable material, not found in the other samples, is apparent in this layer at the high-temperature fraction. This pulse causes an age reversal in bulk AIO ^{14}C ages that both low-temperature RP and foraminiferal ^{14}C ages suggest is false, and

likely occurs due to varying lithology of the core. Variability in Ramped PyrOx thermographs down-core is higher in core NBP-0502 6E than in a previously sampled and analyzed core (NBP-1001 KC-11) from the Hugo Island Trough near Anvers Island where Lapeyrère Bay is found (Figure 2.1; Rosenheim et al., 2013b). Core NBP-1001 KC-11 spans the last 12,000 years in an open-shelf environment and is lithologically consistent (Rosenheim et al., 2013b), while core NBP-0502 6E documents a change from proximal glacial marine sedimentation to glacial outwash. The base of the core is interpreted as the LGM subglacial contact.

Age distributions coupled with CO_2 evolution data from Ramped PyrOx analyses provide insights into the various endmembers present within different samples. Differences between low- and high-temperature Ramped PyrOx ^{14}C dates generally decrease down-core, with the exception of the pulse of thermochemically stable material at 1774 cm (~9800 ^{14}C yr BP) where the difference is the highest of all reported ages (Figure 2.2). This is the same sample that demonstrated continued pyrolytic decomposition at higher temperatures than all other core depths (Figure 2.3). In Antarctic sediments, the most thermochemically stable components are usually representative of older allochthonous carbon, supporting the hypothesis that thermochemical stability should relate to diagenetic stability (Rosenheim et al., 2008; Rosenheim et al., 2013b). Because the maximum in ages corresponds with the highest temperature fraction, we interpret it as a pulse of older material deposited during a short period of time and likely related to the changing lithology of the core. Whereas that core depth illustrates an abrupt change to AIO ages related to changing sediment input, the narrowing age spectra down-core also indicate more continuously changing proportions of different components in each sample and in a different direction than past work (Rosenheim et al., 2013b).

The Ramped PyrOx ^{14}C data from this core demonstrate an improvement over bulk AIO dates by illustrating the potentially false interpretation of an age reversal which is not present in the carbonate or Ramped PyrOx chronologies (Figure 2.2). The occurrence of this false age reversal in bulk AIO dates, coupled with the previously described change in variability across the sediment facies boundary, indicates the effect that changes in lithology can have on ^{14}C ages of AIO. Applying Ramped PyrOx where changing sediment facies or large proportions of diagenetically stable and old ^{14}C are present can remedy these problems by separating the 'contaminant' old carbon from the autochthonous carbon that can persist from the same source (water column productivity) even when terrigenous sediments are present.

The ages of the high-temperature fraction do not increase appreciably with depth (RP-5, Figure 2.2; 14,000 ^{14}C years), with the exception of the sample registering more high-temperature pyrolytic decomposition. The nearly constant ages of RP-5 (Figure 2.2) at all core depths is deceptively simple and potentially misleading. It would be easy to interpret this pattern as a constant supply of material of ~14,000 years in age; however, this is likely a misrepresentation of the true nature of these ages. The highest temperature fraction of Ramped PyrOx is a representation of the average age of detrital material

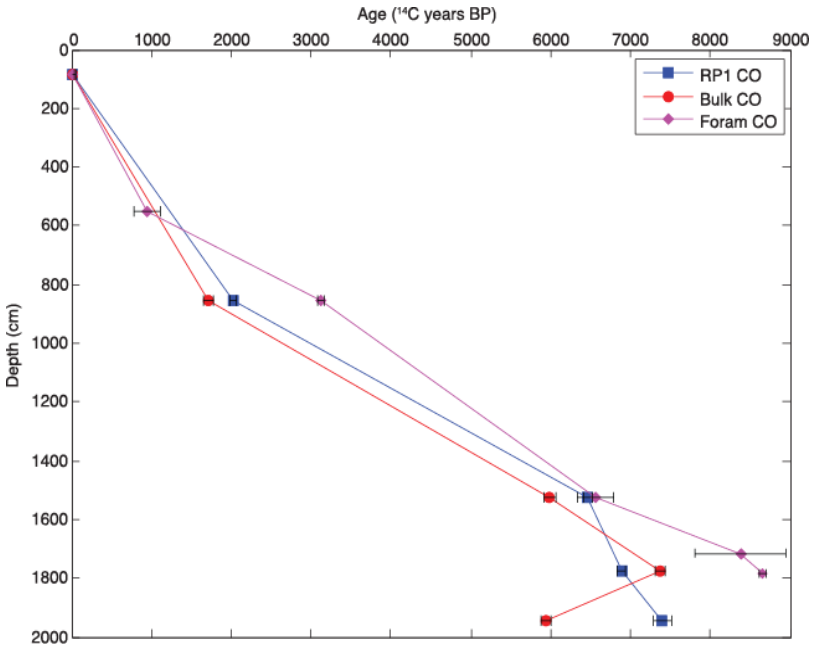

Figure 2.4. Carbonate, low-temperature Ramped PyrOx, and calculated bulk AIO in radiocarbon years with a constant core-top ^{14}C age offset. Bulk ages show similar rate of change to Ramped PyrOx and carbonate dates, but appear to demonstrate a false age reversal from 1774 to 1943 cm depths. Analytical uncertainty is shown for all ages. However, this is not likely to be an accurate representation of the 'geologic' uncertainty.

transported to the site of the core with a minimal contribution from stabilized material from the most reactive fractions (Williams et al., 2014). If the proportions of components in this most thermochemically stable fraction remained constant during deposition, the age of the fraction would likely still vary because of changes in the ages of the admixed detrital AIO.

In this study, smaller temperature ranges were integrated at the beginning of the reaction than in previous studies (e.g. Rosenheim et al., 2008; Rosenheim and Galy, 2012; Rosenheim et al., 2013a; Rosenheim et al., 2013b) to minimize the admixture of older, pre-aged material into the first fraction. This resulted in closer constraint of RP ^{14}C ages and carbonate ^{14}C ages (Figure 2.4). Although chronologies from carbonate ages are generally thought to be more accurate than AIO dates, our data suggest Ramped PyrOx can yield equally accurate chronologies as dating of foraminifers and other carbonates. A comparison of Ramped PyrOx and carbonate dates at equal depth intervals yields a root mean squared (RMS) residual error of 776 ^{14}C years with a bias toward Ramped PyrOx ages being older. By contrast, a comparison of carbonate dates with bulk AIO dates yields a much higher RMS value of 3972 ^{14}C years, implying a much stronger bias toward older bulk AIO ages. It must be stressed that none of the ages that Ramped PyrOx yields for any given core depth can be considered an absolute age without supporting evidence. For example, unless the first and second temperature fractions to pyrolyze exhibit equal ages (age plateaus), the lowest temperature fraction of the Ramped PyrOx age spectrum typically represents a maximum age constraint resulting from a mixture of organic carbon with potentially disparate ages (Rosenheim et al., 2008). Past studies which sampled roughly equal temperature intervals have suggested consistently older maximum age constraints from low-temperature Ramped PyrOx ^{14}C than carbonate ^{14}C ages (Rosenheim et al., 2008). In this past example, comparisons of ages were not from the same intervals because of difficulties in finding sufficient $CaCO_3$ in foraminiferal tests for dating. Here, the very

close – and in some cases younger (more accurate) – low-temperature Ramped PyrOx dates, compared with carbonate dates (Figure 2.2), provide evidence that the RP method effectively removes contaminant ^{14}C and produces ages that can be considered "absolute". In other words, the similarity of two independent chronologies lends support to their accuracy. Although it is evident that smaller low-temperature intervals can approach the accuracy of carbonate dates, the regional and lithologic heterogeneity between samples does not allow for the establishment of the 'ideal' temperature of first separation. Furthermore, smaller samples from the Ramped PyrOx method are more susceptible to blank contamination which can affect the precision of Ramped PyrOx ages (Fernandez et al., 2014).

A local reservoir age correction can be applied differently to ages generated from Ramped PyrOx or bulk AIO ^{14}C dating. There is limited knowledge of the changes in the radiocarbon reservoir age through time, but the common technique for correcting for reservoir effects assumes constant ΔR, which may not be the case (Domack et al., 2005; Ohkouchi and Eglinton, 2008). The reservoir correction also inherently assumes all components of a sample have the same age. But as previously illustrated, the age distributions from Ramped PyrOx analyses show this is inaccurate (Rosenheim et al., 2013b). Whereas RP and bulk AIO ages have been shown to be mixtures of different components, the same can be argued for carbonate dates. Individual carbonate microfossils may exhibit any number of ages, representative of different reservoir ages at the time of deposition, which can potentially introduce biased dates. Variable reservoir ages are the result of complex water mass circulation patterns in the Antarctic margins. However, because Ramped PyrOx and carbonate dates are so similar here, the offset created by the reservoir correction on the whole age can be inferred to be equal. Thus, when comparing ages yielded by different methods in this case, the reservoir correction applied should be equal for all raw ages, regardless of the method used to attain

them, and the associated uncertainties should be accounted for. Subsequently, calibration of the ages to calendar years would progress in the same way for both data sets.

Similar to that shown by Rosenheim et al. (2013b), our data suggest that a constant age offset can be an over-simplification when reconciling old core tops with samples down-core, and even more so across changing lithologies. By applying a constant age offset to each chronology from this study, which shows relatively constant accumulation rates (Figure 2.4), it is evident that the approach has its limitations. Applying a constant age offset is simple and has produced consistent results in several cases; however, the resulting ages are not always consistent with either carbonate or Ramped PyrOx ^{14}C ages (Rosenheim et al., 2013b). A constant age offset is meant to correct the effects of bioturbation, reservoir age, and old contaminant ^{14}C for bulk AIO ages. This correction assumes that the sum of these effects is constant, although it is likely that they vary through time. Moreover, when applied to carbonate or Ramped PyrOx dates, a constant offset does not correct for the same effects. Contaminant or detrital ^{14}C sources have no effect on foraminifera or carbonate ages. Ramped PyrOx removes some of those contaminants and reduces the impact of others, thus a core-top constant offset applied to carbonate or Ramped PyrOx ages mainly corrects for bioturbation and reservoir effects. In some cases, the constant offset may be successful for the wrong reasons. Regardless of which chronology method is used, assuming constant age offset implies that geologic effects, which are shown to vary, would have to be constant as well (Berger and Johnson, 1978; Ohkouchi and Eglinton, 2008; Rosenheim et al., 2013b). In this core, the constant offset approach is most troublesome at the base where it preserves the bulk AIO age reversal and then produces a bulk AIO age that is younger than the RP low-temperature fraction.

2.7 Conclusions

More so than in previous work, we have demonstrated that the Ramped PyrOx method of ^{14}C dating is an accurate and reliable alternative to carbonate ^{14}C dating in sediments where carbonates may be lacking. The use of smaller low-temperature fractions is an improvement on the Ramped PyrOx method, which reduces uncertainty and results in absolute ages which are comparable with carbonate dates. When used in conjunction with foraminiferal or other carbonate dates and a thorough understanding of the sedimentology, Ramped PyrOx can also provide useful additional information about sources of organic matter to the sediment.

Age reversals that sometimes occur in bulk AIO ^{14}C dates result from changes in the proportions of older contaminant ^{14}C sources and can be eliminated by the application of Ramped PyrOx. These contaminants can also cause much older ages in bulk AIO dates, relative to the more accurate carbonate ^{14}C ages, and are demonstrated to be greatly reduced by Ramped PyrOx.

Based on the data collected here, and previous research using Ramped PyrOx, we have compiled a list of recommendations for the applications of Ramped PyrOx to produce robust chronologies:

- We have demonstrated that use of smaller low-temperature intervals rectifies Ramped PyrOx chronologies, thereby demonstrating that Ramped PyrOx ^{14}C ages are not necessarily maximum ages (Rosenheim et al., 2008). The use of smaller splits, however, necessarily results in higher analytical uncertainty which can increase when blank corrections are eventually applied.
- When low-temperature Ramped PyrOx ^{14}C ages are similar to foraminiferal ^{14}C ages, the same reservoir age correction should be applied.

- A constant age offset applied to the lowest temperature Ramped PyrOx ages may oversimplify the chronology of a core, especially across changing lithologies, and should be applied only with caution.

2.8 Organic carbon in Lapeyrère Bay

The presence of organic carbon in the sediment depends entirely on primary productivity in surface waters. The proportion of organic matter in the sediment increases distally from the glacier front, which may be a result of dilution by meltwater carrying glacial sediment poor in OC (Ashley and Smith, 2000). Bottom sediments from Lapeyrère Bay exhibit increasing total organic carbon (TOC) with distance from the fjord head (Domack and Ishman, 1993).

2.9 Analysis of $\delta^{13}C$ measurements

To shed further light into the spurious AIO ^{14}C ages in this study (Figure 2.2, Table 2.2), it helps to examine $\delta^{13}C$ values corresponding to their respective Ramped PyrOx splits. Because the Ramped PyrOx and AIO approaches both analyze organic carbon pretreated for the removal of carbonates, we would expect $\delta^{13}C$ values in this carbon to be isotopically lighter than that from carbonates, with values ranging between -26 and -12 ‰ for organic carbon and ~0 to 1 ‰ for carbonates. Values yielded from Ramped PyrOx splits are consistent with values within the expected range of $\delta^{13}C$ and tend toward heavier values with increasing temperature. Our results show that two of the five highest-temperature splits have significantly heavier $\delta^{13}C$ values than the rest (< -13 ‰) (Table 2.2). Carbonate material combusts at temperatures above 550° C and often shows distinctive peaks in pCO_2 evolution that overlap with those of organic carbon (Salonen, 1979), but this may not always be the case. Recent work analyzing samples not pretreated for the removal of carbonates showed that these distinctive peaks are

not always visible. However, the incorporation of carbonates in an organic carbon sample is always reflected by heavier isotopic compositions, indicating a mixture of carbonates and organic carbon in the sample (Reese et al, unpublished). Although the heavy $\delta^{13}C$ values of high-temperature Ramped PyrOx splits are within the expected range for organic carbon, the heaviest isotopic compositions found in two high-temperature splits could indicate some pre-aged carbonate (perhaps in the form of dolomite or siderite (Swart, 2015)) is still incorporated into these samples by diluting an otherwise light isotopic composition with isotopically heavy carbonates. The available thermographs show some distinct high-temperature peaks in the pCO_2 evolution of some samples, but these do not appear to be correlated with heavier isotopic compositions. As these samples were treated to remove carbonates, it is likely that if pre-aged carbonate is being incorporated, it is only in small quantities that are not demonstrated in the pCO_2 evolution.

An alternate and more likely explanation for heavier isotopic compositions in some high-temperature splits is in the relative mixtures of different sources of organic carbon in these samples. The bulk $\delta^{13}C$ in marine settings typically reflects a range of organic carbon values consistent with C3 (~-23 ‰) and C4 (~-12 ‰) terrestrial plants. As all $\delta^{13}C$ values for the samples analyzed fall within this range, it is possible that splits with lighter values indicate that the main source of organic carbon is from C3 plants, while those with heavier values suggest C4 plants might be the main constituent for organic carbon.

2.10 Carbonate ^{14}C dating

Carbonate ^{14}C dates were analyzed for comparison with Ramped PyrOx ^{14}C ages. Although foraminiferal assemblages were not analyzed in detail for this study, it is important to note that planktonic species produce significantly younger ages than benthic species (e.g.

Wychech et al., 2016; Barker et al., 2010). Foraminifera identified in core NBP0502 6E were mostly planktonic and largely intact, including species *Fursenkoina fusiformis* and *Stainforthia corplanata*, but were sampled as mixed foraminiferal samples (Mead, 2012). Other species in these samples were not identified. Only whole foraminifers and occasional shell fragments were picked for ^{14}C dating. The carbonate ^{14}C dates in this study likely incorporate some amount of reworking, which would account for the occasionally older ages than Ramped PyrOx ^{14}C.

Although carbonate ^{14}C ages are typically the most sought-after type of ^{14}C dates for Quaternary research, it is important to understand that it is by no means a perfect proxy. The paucity of foraminiferal carbonates may certainly be a limitation for Antarctic sediments, not only for ^{14}C dating, but also for $\delta^{18}O$ measurements, which can be a useful tool for reconstructing temperature records. More widespread problems with these measurements include the effects from diagenesis, reworking, vital effects, and reservoir effects. For example, ^{14}C ages from translucent and opaque foraminiferal shells have been shown to result in differences as large as 8 kyrs (Wycech et al., 2016). Effective identification and caution with species assemblages used for ^{14}C dating is important for maintaining the highest quality dates. Where possible, only monospecific, pristine shells should be used to avoid uncertainties in the dating.

CHAPTER 3:

SUB-ICE SHELF SEDIMENT GEOCHRONOLOGY UTILIZING NOVEL RADIOCARBON METHODOLOGY FOR HIGHLY DETRITAL SEDIMENTS

3.1 Note to Reader

This chapter includes materials previously published in *Geochemistry, Geophysics, Geosystems*; Volume: 18; Issue: 4; Pages: 1404-1418; doi: 10.1002/2016GC006578; Copyright © 2017 (American Geophysical Union).

Reprinted by permission of AGU Publications (see Appendix A).

Authors: Cristina Subt[1], Ho Il Yoon[2], Kyu-Cheul Yoo[2], Jae Il Lee[2], Amy Leventer[3], Eugene W. Domack[1], Brad E. Rosenheim[1]

[1]College of Marine Science, University of South Florida, USA

[2]Korea Polar Research Institute, Incheon, Republic of Korea

[3]Department of Geology, Colgate University, USA

C. Subt (first author) generated all Ramped PyrOx data, compiled and analyzed ^{14}C data, and prepared the manuscript. H.I. Yoon, K.C. Yoo and J.I. Lee provided samples and generated bulk AIO data. A. Leventer generated diatom abundance data. E. Domack assisted with lithology descriptions and provided insights into their origin. B. Rosenheim provided direction in the experimental design and successful completion of the project. All co-authors also provided useful input, discussions and editing for the manuscript.

3.2 Abstract

Sub-ice shelf sediments near Larsen C ice shelf (LIS-C) show fine-scale rhythmic laminations that could provide a near continuous seasonal-resolution record of regional ice mass changes. Despite the great potential of these sediments, a dependable Late Quaternary chronology is difficult to generate, rendering the record incomplete. As with many marginal Antarctic sediments, in the absence of preserved carbonate microfossils, the reliability of radiocarbon chronologies depends on presence of high proportions of autochthonous organic carbon with minimized detrital organic carbon. Consequently, acid insoluble organic (AIO) ^{14}C dating works best where high productivity drives high sediment accumulation rates, but can be problematic in condensed sequences with high proportions of detrital organic carbon. Ramped PyrOx ^{14}C dating has progressively been shown to improve upon AIO ^{14}C dates, to the point of matching foraminiferal carbonate ^{14}C dates, through differential thermochemical degradation of organic components within samples. But in highly detrital sediments, proportions of contemporaneously deposited material are too low to fully separate autochthonous organic carbon from detrital carbon in samples large enough to ^{14}C date. We introduce two modifications of the Ramped PyrOx ^{14}C approach applied to highly detrital sediments near LIS-C to maximize accuracy by utilizing ultra-small fractions of the highly detrital AIO material. With minimization of the uncertainty cost, these techniques allow us to generate chronologies for cores that would otherwise go undated, pushing the limits of radiocarbon dating to regions and facies with high proportions of preaged detritus. Wider use of these techniques will enable more coordinated a priori coring efforts to constrain regional glacial responses to rapid warming where sediments had previously been thought too difficult to date.

3.3 Introduction

An accurate reconstruction of past Earth conditions requires an archive that is not only datable, but that offers the ability to compile dates into a meaningful chronology that can be regionally correlated to preexisting age models. Sedimentary archives are fundamentally detrital in nature, and in sediments where high proportions of detritus include the material from which ages are sought, dating can become ambiguous. Antarctic glacial marine sediments have long been considered among the most problematic to date due to a lack of preserved foraminifera (Andrews et al., 1999; Domack et al., 1989; Licht et al., 1998; Mackintosh et al., 2014). Hence, acid insoluble organic (AIO) radiocarbon (^{14}C) is often used for Antarctic sediments with the hope that authigenic algal-derived organic matter from the water column above (henceforth referred to as ‘‘syndepositionally-aged’’) dilutes any pre-aged detritus transported from continental rocks or sediments that would be dated in conjunction with the authigenic material. But AIO ^{14}C ages have often been found to incorporate pre-aged reworked carbon (Andrews et al., 1999; Leventer et al., 2006; Mackintosh et al., 2011; Rosenheim et al., 2008; Rosenheim et al., 2013b; Subt et al., 2016). In ‘‘highly detrital’’ sediments, the portion of syndepositionally-aged carbon is exceedingly small, creating further difficulties in achieving accurate ages. The potential of sedimentary research in Antarctica is maximized if the effects of detrital organic carbon in AIO are reduced, increasing accuracy of AIO dates. Doing so can expand Antarctic research not only into improved deglacial chronology, but also into broadened exploration of regions where typical dating methods have been impractical or ineffectual.

Although dating AIO material can be problematic, proper application to well-understood stratigraphy and depositional settings has improved our understanding of Antarctic deglaciation. Advances in using stratigraphic information to ensure more accurate ^{14}C using the AIO carbon have expanded our ability to date sediments without carbonate material (Domack et al., 1999a;

Domack et al., 1989). AIO ^{14}C dating has allowed for advancements such as an unsurpassed chronology of 43 dates in ~44 m of Holocene sediment in the Palmer Deep (Domack et al., 2001), constraints on Antarctic Peninsula and Ross Sea Ice Sheet retreat during the Last Glacial Maximum (LGM) (Heroy and Anderson, 2007; McKay et al., 2008), and can provide limiting ages for grounding line retreat (e.g. Domack et al., 2005; Leventer et al., 2006; Mackintosh et al., 2011; Rebesco et al., 2014). Traditionally, AIO material in sediments has been used in conjunction with constant age offsets, whereby a core-top age is subtracted from all subsequent downcore ages, as an alternative to the more trusted carbonate ^{14}C ages (Andrews et al., 1999; Domack et al., 1999b; Mackintosh et al., 2011). The subtraction of a constant ^{14}C age downcore, however, can result in nonlinear isotopic bias, and is dependent on the constancy of the proportions of ancient carbon and syndepositionally-aged carbon, which is unlikely given the ephemeral nature of ice flows (Andrews et al., 1999; Michalchuk et al., 2009; Pudsey et al., 1994; Rosenheim et al., 2013b; Subt et al., 2016), and on the uncertain assumption that the reservoir age has remained the same through time (Carlson and Clark, 2012; Stuiver et al., 1986a). Thus, despite refinements in ^{14}C dating, Antarctic sediment cores can often lack accurate chronologies.

Methodological improvements in separating pools of organic carbon within the sediment have been made by employing compound-specific/compound-class diatom-bound ^{14}C dating (Eglinton et al., 1996; Eglinton et al., 1997; Ingalls et al., 2004; Ohkouchi and Eglinton, 2006; Ohkouchi and Eglinton, 2008; Ohkouchi et al., 2003; Pearson et al., 1998; Yamane et al., 2014). This technique involves the chemical extraction of specific compounds (biomarkers) associated with organism-specific processes. Early work utilizing this technique had difficulties with the large amounts of material required for ^{14}C analysis (Ingalls and Pearson, 2005). Compound-specific ^{14}C dating has since been developed more recently for sediments that

contain greater quantities of the necessary pools of carbon. However, recent work in the Ross Sea (Yokoyama et al., 2016) and the Wilkes Land Coast (Yamane et al., 2014) illustrates large uncertainties that result from applying compound-specific ^{14}C dating to hemipelagic sediments. Moreover, this approach requires large amounts of sediment for extraction to produce an accurate chronology.

Ramped PyrOx ^{14}C dating has also offered recent advances in separating of pools of organic carbon through thermochemical degradation (Rosenheim et al., 2008; Rosenheim et al., 2013b; Subt et al., 2016). In Ramped PyrOx, the least diagenetically stable component of the sediment is related to the least thermochemically stable (lowest temperature) and is thus concentrated in the first aliquot of CO_2 to be collected when temperature is increased linearly. Early work shows that high-resolution temperature intervals approached foraminiferal ages, but lower-resolution intervals did not offer as much an improvement (Rosenheim et al., 2008). Results suggested that contributions from different pools changed downcore and that constant age offsets were potentially erroneous (Rosenheim et al., 2013b). Further advancements have been made by using smaller aliquots at the beginning of the reaction to reduce the amount of older CO_2 incorporated into the aliquot (Subt et al., 2016). Smaller first aliquots have also been

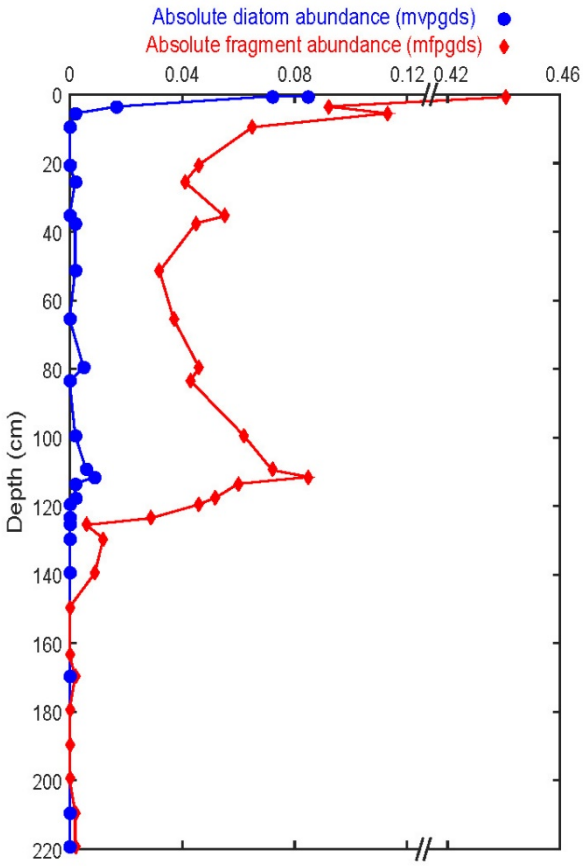

Figure 3.1. Diatom valve and fragment counts in core EAP13 GC16B. The nearly barren assemblage downcore except for samples within the top 5 cm, establishing the highly detrital nature of this core.

shown to improve the age to match the ^{14}C age from carbonate material (Subt et al., 2016). Ramped PyrOx dating is not without complication, especially for highly detrital sediments. If the amount of autochthonous, syndepositionally-aged carbon in a sample is too small, it may be overwhelmed by blank contamination (Fernandez et al., 2014; Santos et al., 2010) or overwritten by older, pre-aged carbon in larger thermochemically separated samples. It should also be noted that both compound-specific and Ramped PyrOx dating may still yield an average age from a mixture of components.

Although many incremental advances have been made to improve the accuracy and precision of dates from highly detrital samples, much of the research conducted in Antarctic marine sediments is still highly dependent on the ability to retrieve high-resolution sediment cores with sufficient carbonate material for dating. Alternative ^{14}C dating approaches are needed to reduce uncertainty of more accurate ^{14}C dates from highly detrital sub-ice shelf sediments. Here, we generate a reliable and meaningful chronology for a sediment core proximal to the grounding line of the Larsen C ice shelf (LIS-C, Figure 3.1), offering a major advance involving a manipulation of the Ramped PyrOx approach to minimize precision costs of previous incremental advances (Rosenheim et al., 2008; Rosenheim et al., 2013b; Subt et al., 2016). We present two innovations to the Ramped PyrOx approach that allow us to look beyond the last deglaciation and to address more condensed sediment sequences over the Holocene that are difficult to date due to a greater mixture of detrital material (Figures 3.1 and 3.2). In one technique, we apply multiple identical Ramped PyrOx analyses and combine ultra-small low-temperature aliquots of CO_2 of the same sample (Composite technique). In the other techinque, we combine ultra-small low-temperature CO_2 aliquots with a surrogate of known age and quantity (Isotope Dilution technique). By developing these alternate techniques and

improving AIO ^{14}C dating, future research may be able to delve deeper into regions, time periods and lithofacies that have precluded dating and adequate understanding.

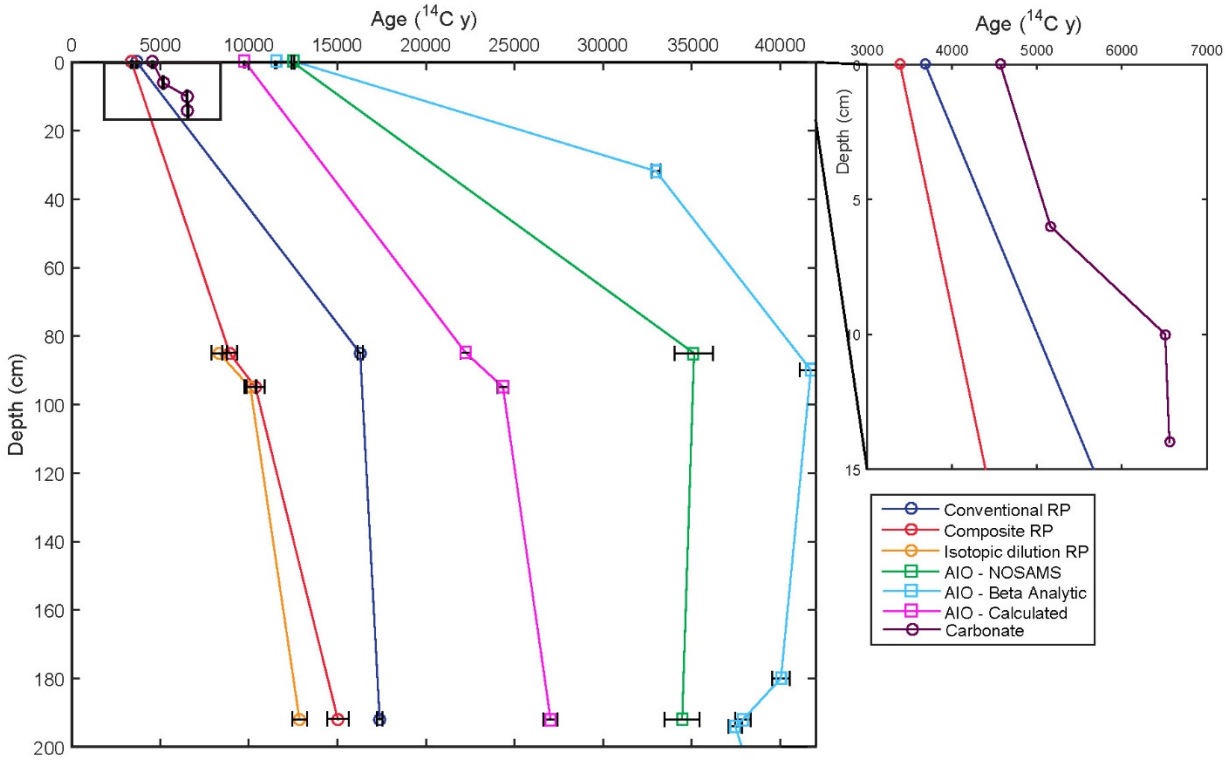

Figure 3.2. Comparison of Larsen C age models using conventional, composite, and isotope dilution Ramped PyrOx techniques as well as measured and calculated AIO ages. Note an additional Beta Analytic data point extends beyond the depth range shown in this figure. Error bars indicate 1σ uncertainty reported in Table 3.2. The complete data can be found in Tables 1 and 2.

3.4 Methods

3.4.1 Site Locations

This study examines marine sediments from near the LIS-C on the Antarctic Peninsula (Figure 3.3), one of the most sensitive regions to recent climate change (Vaughan et al., 2001). Thus, it is important to determine whether the strong climate sensitivity of the LIS-C is purely the result of anthropogenic warming, or if past climate variability has shown similar trends.

Other parts of the Larsen Ice Sheet (LIS-B in 2002 and LIS-A in 1992) have disintegrated rapidly in recent years, garnering public attention and spurring advancement of research concerning Antarctic glacial advance and retreat (Brachfeld et al., 2003). LIS-C is the largest and most stable ice shelf of this system, and ice conditions in 2013 allowed a close approach of the R/V Araon to the ice shelf edge. Sediment cores were taken that were largely considered sub ice shelf in nature (see below). Interpretation of sediment transport process and biogeochemistry in these setting is not only interesting from the standpoint of modern ice shelf environments, but also may relate, as an analog environment, to ocean sedimentation from the Cryogenian.

3.4.2 Core Description

Several cores were collected along the East Antarctic Peninsula in 2013 on-board the R/V Araon by the Korea Polar Research Institute (KOPRI). Gravity core 16B (EAP13 GC16B: 660 3.89832' S, 600 27.69212' W) was taken near the northern region of the LIS-C (Figure 3.3). It was taken from a water depth of 324 m and is 238

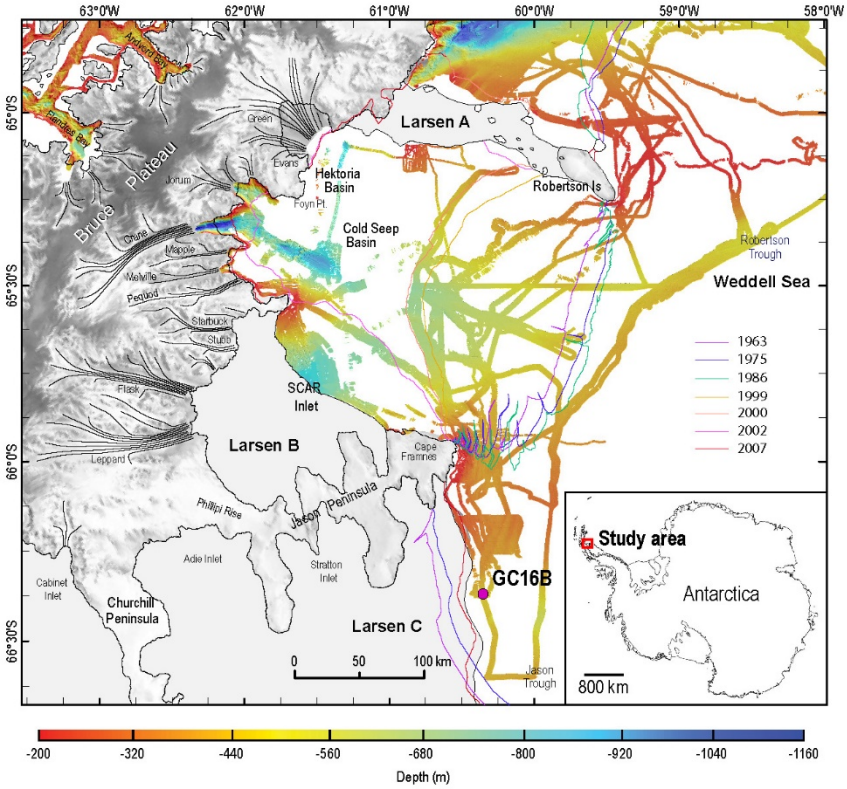

Figure 3.3. Map of the study region near the Larsen C on the eastern Antarctic Peninsula with swath bathymetry data and bedforms of the region indicated with arrows. The purple circle indicates the location of core EAP13 GC16B and its accompanying box core, EAP13 BC16A. Adapted from Lavoie et al. [2015].

cm long. This location is rather unique in that it has remained under a disintegrating ice sheet adjacent to the LIS-C, which retreated from this site in the past century (Ferrigno et al., 2008). Figure 3.4 describes this core graphically, but we offer this brief textual description for reference. This core consists of four lithologic units: the upper 21 cm of the core is characterized by sandy diamicton, rich in calcareous microfauna. The interval from 21 to 90 cm is characterized by finely laminated, sandy-clayey silt. From 90 to 194 cm, the mud consists of slightly sandy, silty clay. Below 194 cm, a structureless diamicton constitutes the basal unit of the stratigraphy. The mud intervals (from 21 to 194) are characterized by a systematic bundling of fine laminations that consist of alternating (rhythmic) intervals of thick and thin couplets (of silt and clay). Generally, intervals of thinner couplets are thicker and more variable than the thicker couplet intervals. Horizontal laminations dominate the lower third of the mud interval, but then are interspersed with inclined bedding, likely indicative of migrating bed forms with amplitudes of approximately 20–30 cm. Reversals in the direction of inclined bedding are evident in several intervals. There are finer-scale higher-frequency alternations within the lamination bundles but these are deserving of a much more detailed analysis than appropriate to this paper and will be discussed in a subsequent publication. Notably lacking within the mud facies are any signs of unsorted, coarse sand, or gravel. Also of note are five disconformable horizons whereby the inclined laminations are abruptly truncated, but notable without any coarse lag or irregular erosive surface (these are indicated as surfaces D-1 through D-5 in Figure 3.4). Hence, this core is unique in that most sub-ice shelf muds consist of non-rhythmic laminations typically interspersed with coarse grains of ice-rafted origin (Domack et al., 2005; Rebesco et al., 2014). The fine-scale systematic (rhythmic) laminations in this core could provide annual and even seasonal (varved) time increments on a near-continuous basis. Therefore, core EAP13 GC16B has great potential as a precise and accurate chronometer for ice

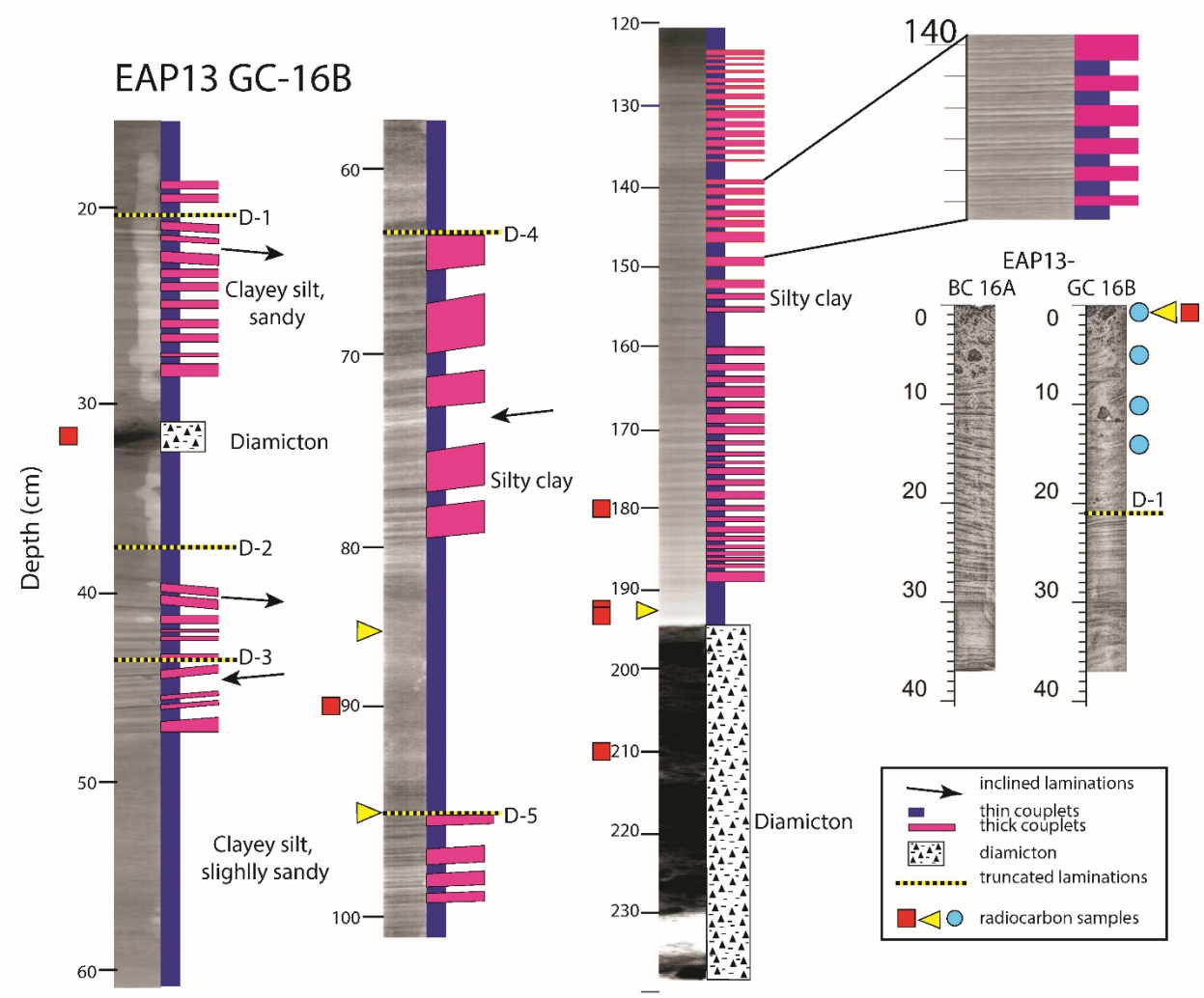

Figure 3.4. Stratigraphic column for EAP13 GC16B. Blue circles indicate carbonate, red squares indicate preliminary AIO measurements, and yellow triangles indicate RP radiocarbon dates.

mass changes associated with the LIS-C. Yet, due to its overwhelming detrital nature, there is a challenge in developing a fixed absolute time for what is now a "floating record" of potential glacial marine varves.

Twelve sediment samples were taken from this core for ^{14}C analysis (Figure 3.4). Only four samples near the top of the core contained sufficient well-preserved foraminiferal tests for carbonate ^{14}C analysis.

3.4.3 Carbonate ^{14}C analysis

Four samples were taken within the top 14 cm of the core from which sufficient foraminifera were retrievable for ^{14}C analysis. All samples were benthic, monospecific *Globacassidulina biora* in pristine condition, but the assemblage in general was diverse, well-preserved, and abundant. Not enough material was present for repeated analyses, thus precision is based on analytical uncertainty alone.

3.4.4 AIO ^{14}C chronologies

Table 3.1. Sample preliminary data for core EAP13 GC16B, including AIO ages analyzed at Beta Analytic. f_{SA} refers to the calculated fraction of estimated syndepositionally-aged carbon in the sample and was calculated using preliminary AIO ^{14}C measurements and assuming a two-endmember mixing model. T_1 is the temperature at which syndepositionally-aged material was estimated to combust.

Depth (cm)	%TOC	AIO Age (^{14}C y)	±	f_{SA}	T_1 (°C)
0	0.315	12500	50	0.2575	288
0		11470	50		
32		32960	240		
85	0.675			0.0132	270
90		41720	620		
95	0.420			0.0141	279
180		40030	510		
192	0.795	37880	430	0.0400	338
194		37440	380		
210		39460	440		

Typically, AIO ^{14}C dates produce older ages because they incorporate some amount of pre-aged material in the sediment. Preliminary AIO ^{14}C measurements have been analyzed by Beta Analytic Radiocarbon Dating Laboratory (Figure 3.2). Freeze-dried bulk sediments were dispersed and subjected to 2.5 N HCl at 90 °C for a minimum of 1.5 hours and rinsed in deionized water at 70 °C until neutrality was reached to remove carbonate components prior to AMS dating. These analyses were pursued to inform decisions of the available contemporaneously-deposited ^{14}C in each sample analyzed by alternate Ramped PyrOx techniques, as described below. All Ramped PyrOx aliquots analyzed by the three techniques

described below were sent to the National Ocean Sciences Accelerator Mass Spectrometry (NOSAMS) facility for $^{14}C/^{12}C$ ratio determination. High precision measurements were applied for lowest-temperature Ramped PyrOx (RP1) ages. As preliminary AIO ages were analyzed by Beta Analytic, a second set of AIO sediment samples were also analyzed at NOSAMS to avoid inter-laboratory differences and to match the core-depths with those used for Ramped PyrOx analyses. For comparison, AIO ^{14}C ages were also calculated from the weighted arithmetic mean of the spectrum of Ramped PyrOx ages, as they have previously been found to match measured AIO ^{14}C ages (Rosenheim et al., 2013b).

3.4.4.1 Conventional Ramped PyrOx ^{14}C analysis. All sediment samples were processed at the University of South Florida College of Marine Science. Each sample was dried and homogenized, then pretreated with 1N HCl for ~2 h to remove carbonate material. The samples were centrifuged and rinsed in deionized water until the pH of the supernatant was normalized at 7.0. The samples were dried and stored in pre-combusted (525°C, 2 h) glass vials until analysis. Individual Ramped PyrOx analyses were based on the methods described by Rosenheim et al. (2008), wherein sediment was weighed out (~100 µmol C based on %TOC measurements) into pre-combusted (900°C, 2 h) quartz flow-through reactor inserts in between plugs of pre-combusted (525°C, 2 h) quartz wool. The quartz reactor was inserted into the top portion of the combustion chamber, and was continuously purged with 35 mL/min of ultra-high purity (UHP) He, while the combustion chamber was continuously purged with 4 mL/min of (UHP) O_2 in 7 mL/min of (UHP) He to prevent back-flow of O_2 into the reactor (Figure 3.5). The reactor resides within two tubular furnaces, where the top furnace (pyrolysis furnace) is ramped up in temperature by 5°C/min and the bottom furnace (oxidation furnace) is kept at a constant temperature of 800°C throughout the pyrolysis reaction. Pyrolysates entrained in He and flowing downstream were converted to CO_2 in the combustion furnace on CuO wire. An infrared

CO_2 detector (Sable Systems Ca-10) measured the CO_2 concentration in the mixture of gases as it flowed to one of two 8-loop borosilicate glass cryogenic traps partially immersed in liquid N_2. Remotely controlled pneumatic valves (Luwers) toggled in a way that enabled one trap to accumulate incoming condensable products from the He carrier gas at atmospheric pressure while the other was connected to allow expansion into a vacuum separations line for cryogenic purification of CO_2 with liquid nitrogen and n-propanol cooled to solid-liquid phase transition with liquid nitrogen. Purified CO_2 aliquots were collected and flame-sealed into evacuated pre-combusted (525°C, 2 h) Pyrex tubes with pre-combusted copper oxide and silver wire (Figure 3.5).

To provide a baseline by which two novel techniques could be compared, Ramped PyrOx analyses were performed with little change to the originally established approach (Rosenheim et al., 2008). Subsequent work by Rosenheim et al. (2013b) and Subt et al. (2016) showed that smaller low-temperature aliquots could improve the dates considerably. Thus, for this study, we collected the two lowest-temperature aliquots (RP1 and RP2) at sizes of 10–15 μmol, and the subsequent three CO_2 aliquots (RP3, RP4, and RP5; see Appendix Table B1) at approximately 23–27 μmol, roughly equally splitting the remaining carbon.

It is important to note that blank contamination (unavoidable admixture of contaminant CO_2 into the sample during any analysis) from Ramped PyrOx analysis should be accounted for in all samples analyzed. The blank contamination for each sample was calculated using equations based on the derivation of blank correction by Santos et al. (2007):

$$\delta_U = \delta_M + \delta_M\left(\frac{m_{dead}}{m_U}\right) + \delta_M\left(\frac{m_{mod}}{m_U}\right) - \delta_{mod}\left(\frac{m_{mod}}{m_U}\right) \quad \text{Eq. 3.1}$$

$$\sigma^2_{\delta_U} = \sigma^2_{\delta_M}\left(1 + \frac{m_{dead}+m_{mod}}{m_U}\right)^2 + \sigma^2_{m_{dead}}\left(\frac{\delta_M}{m_U}\right)^2 + \sigma^2_{m_{mod}}\left(\frac{\delta_M-\delta_{mod}}{m_U}\right)^2 + \sigma^2_{m_U}\left(\frac{\delta_{mod}m_{mod}-\delta_M m_{dead}-\delta_M m_{mod}}{m_U^2}\right) \quad \text{Eq. 3.2}$$

where δ is the fraction modern (Fm) value, as described by Stuiver and Polach (1977), σ is uncertainty, m is the mass, and subscripts U and M are the unknown and the measured values of the sample, respectively, and subscripts *dead* and *mod* are ^{14}C-free blank and modern blank, respectively (see Appendix Text C1). Recent studies on modern and dead blank contamination in the Ramped PyrOx system suggests m_{mod} is time-dependent, while the m_{dead} remains the same over time and is independent of the pyrolysis system (Fernandez et al., 2014). The total modern carbon in one Ramped PyrOx analysis is 2.8 ± 0.6 µg (all errors reported are 1σ). A proportion of this amount was assigned as the modern blank contamination for each temperature interval based on the collection time of each aliquot. m_{dead} has a constant mass of 1.4 ± 0.8 µg and is not time-integrated, thus all 1.4 µg must be applied to each aliquot from a Ramped PyrOx run.

To surpass the limitations of the Ramped PyrOx method in analyzing ultra-small fractions of young material in highly detrital sediments (Figure 3.6), we have developed two techniques to minimize the costs in precision while improving accuracy. For both techniques, the preexisting AIO ^{14}C ages were used to estimate the proportion of material assumed to be syndepositionally-aged (f_{SA}, as shown in Figure 3.6) by assuming a two end-member mixing model and a linear accumulation rate (see Appendix B2). Initial sample Ramped PyrOx analyses were also conducted to determine the CO_2 evolution as well as the percent of total organic carbon (%TOC) in each sample (Table 3.1). Decomposition rates of organic carbon and preliminary AIO ^{14}C dates were used to calculate the temperature at which the estimated amount of syndepositionally-aged material combusts (T_1; see Appendix B2). We inherently assume in this approach that no pre-aged organic carbon would decompose until all autochthonous organic carbon had pyrolyzed—this is a necessary oversimplification that enables our preliminary estimate of the sampling temperature.

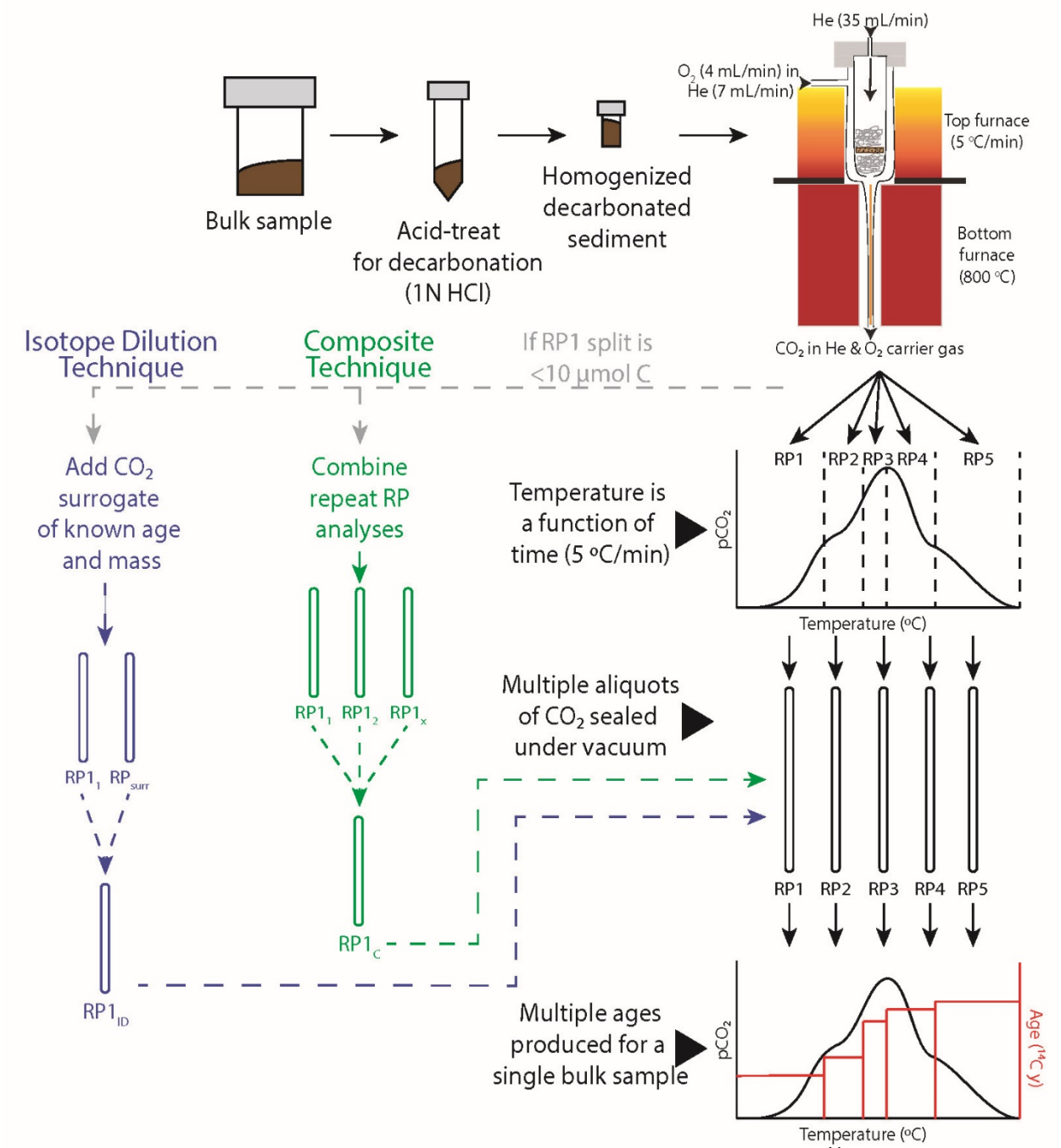

Figure 3.5. Schematic demonstrating steps involved in pretreatment and Ramped PyrOx ^{14}C analysis. Samples are homogenized and treated with 1N HCl for ~2 h for decarbonation. Samples are pyrolyzed at a rate of 5°C/min in the top furnace of the combustion chamber and carried by He to the bottom furnace, which is held constant at 800°C, and combined with O_2 gas where products of the pyrolysis reaction are subsequently oxidized. CO_2 resulting from this process accumulates gradually and separated at selected time intervals. Subsamples are purified in a vacuum line before being collected and flame-sealed in individual pyrex tubes where aliquots are numbered sequentially based on T_1 (e.g., RP1 is lowest-temperature aliquot and Ramped PyrOx is highest-temperature). Each CO_2 aliquot is individually analyzed for Ramped PyrOx. In conventional Ramped PyrOx analyses (black), lowest-temperature aliquots contain between 10 and 15 µmol of CO_2. If <10 µmol are desired, then alternate techniques may be appropriate: Composite Ramped PyrOx (green) analyses consist of combining the lowest-temperature aliquots from multiple identical analyses of the same sample. Isotope dilution Ramped PyrOx (blue) analyses consist of combining the lowest-temperature aliquot with a CO_2 surrogate of known age and mass.

3.4.4.2 Composite Ramped PyrOx ^{14}C analysis. Of the four LIS-C samples collected for Ramped PyrOx ^{14}C dating, three (85, 95, and 192 cm core depths) had very small f_{SA}; thus the "conventional" 10 µmol RP1 would have incorporated too much pre-aged detrital material. For these samples, a composite of analyses was performed where equivalent masses were analyzed each time (100 µmol C, as determined by %TOC). RP1 was collected at the same temperature (T_1; Table 3.1) each time, and the number of analyses was determined by f_{SA} (Figure 3.5). An additional two aliquots were collected for a portion of the analyses, where RP2 was ~10–15 µmol and RP3 included the remaining material. To reduce analytical error associated with AMS measurements of small samples, RP1 aliquots of the same sample were combined ($RP1_C$, Figure 3.5); 10 µmol was decided to be a sufficiently large sample to produce an acceptably small analytical uncertainty (<10%) based on previous analyses made with the Ramped PyrOx approach (Figure 3.6) and minimize the number of composite runs that needed to be combined (each with its own blank contamination). Because the amount of carbon in each sample is collected in a relatively short amount of time, the time-dependent modern blank contamination is not very large (Fernandez et al., 2014). However, the resulting modern blank contamination from mixing multiple aliquots becomes cumulative. In the case of composite aliquots, m_{mod} was calculated by taking into account the cumulative, time-integrated proportion of each individual CO_2 aliquot. Additionally, m_{dead} was used as determined by Fernandez et al. (2014) because only the composite sample was recombusted and subject to the likely source of ^{14}C-free blank contaminants. Due to the complexity of this approach and limited sample sizes, replicate composite and isotope dilution analyses were not conducted, however, thermographs of replicate analyses of each sample were compared to determine the reproducibility of sample analyses.

3.4.4.3 Isotope Dilution Ramped PyrOx ^{14}C analysis. An isotope dilution technique was applied to equal-sized low-temperature aliquots of the same samples as the composite technique for comparison of an independent technique using the Ramped PyrOx approach. Multiple analyses (composite analyses) were also required for this technique, but the number was reduced by adding an amount of a diluent, which may be any substance of well-constrained ^{14}C content. We used NBS Oxalic Acid I (Ox-I) as the surrogate for this technique because it is a modern standard that generally decomposes at lower temperatures than the estimated T_1 for each sample. Multiple analyses were conducted using the same parameters as those in the composite technique and were combined with individual samples of Ox-I to create a single ~10 µmol aliquot ($RP1_{ID}$, Figure 3.5). For each isotope dilution, resulting ages needed to be corrected for the addition of a diluent to calculate the age of the sample using the following equations:

$$\delta_{U-ID} = \frac{\delta_S - \delta_U - f\delta_s}{-f} \quad \text{Eq. 3.3}$$

$$\sigma^2_{\delta_{U-ID}} = \sigma^2_f(\frac{\delta_S - \delta_U}{f^2})^2 + \sigma^2_{\delta_S}(1 - \frac{1}{f})^2 + \sigma^2_{\delta_U}(\frac{1}{f})^2 \quad \text{Eq. 3.4}$$

where subscripts *U-ID* and *S* are the isotope dilution-corrected unknown and the diluent respectively, and *f* is the proportion of the unknown relative to the mixture of diluent and unknown (see Appendix Text C3). It should be noted that these equations utilize the blank-corrected unknown (δ_U, $\sigma_{\delta U}$), thus the blank correction must be applied first before correcting for the addition of a surrogate. This blank correction was applied in the same manner as was done for the composite technique.

In this study, the diluent was prepared using Ramped PyrOx analyses in the same manner as the samples for consistency. Doing so adds slightly to the blank contamination previously described, but the time of decomposition of Ox-I is only minutes and not much blank

will accumulate over that time. In the future, this blank contamination could be reduced by using closed-tube combustion to extract CO_2 from the diluent.

Determining how much isotopic diluent to add to composite Ramped PyrOx samples involves minimizing the number of times that the sample needs to be composited while maximizing precision. By reducing the number of analyses per sample, we also reduced the amount of time spent on the technique (preparing and compositing multiple runs), thereby decreasing the mass of sample required. However, reducing the number of analyses increases the amount of Ox-I relative to the sample and incurs an increased cost in precision.

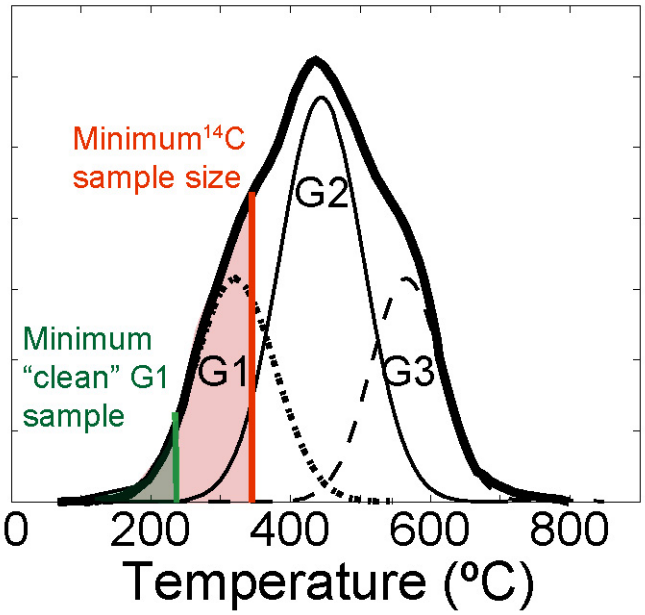

Figure 3.6. Idealized thermograph illustrating the evolution of pCO_2 as temperature is raised at a constant rate in a situation where the amount of autochthonous OC may be smaller than a measurable ^{14}C sample. Gaussian modeling has been implemented (G1–G3) to represent the mixture of multiple organic components incorporated in the bulk organic sample [Rosenheim et al., 2013]. The minimum "clean" sample denotes where the lowest-temperature aliquot can be taken to collect G1 component without a mixture of the G2 component.

3.5 Results

The CO_2 evolution (thermographs) of all four samples shows interesting trends that relate to diagenetic and thermochemical stability of each sample (Figure 3.7). Thermographs in Figure 3.7 have undergone a simple temperature offset to match maximum temperature peaks. This is to correct for potential technical issues independent of sediment properties, such as movements of the thermocouples from sample loading between analyses, causing the thermographs to shift along the temperature ramp. Because the targeted temperature intervals

Table 3.2. Radiocarbon ages from multiple dating techniques for Larsen C samples. Ages are reported in blank-corrected ^{14}C years BP and have been calibrated to calendar years BP using Calib 7.1 Marine13 calibration curve with $\Delta R = 880 \pm 30$ based on epibenthic foraminifera obtained from the Larsen B embayment (Domack et al., 2005). Total masses of carbon used for ^{14}C analysis are included for all Ramped PyrOx analyses. Isotope dilution Fm values and ^{14}C ages have been corrected for the addition of a surrogate using equations 3 and 4. AIO Sediment refers to treated samples analyzed by NOSAMS.

Depth (cm)	Type	Mass (µmol of C)	$\delta^{13}C$ (‰)	Fm	± (1σ)	Age (^{14}C yrs BP)	± (1σ)	Calibrated Age (yrs BP)	± (1σ)
0	AIO Sediment		-25.93	0.2112	0.0016	12490	50	N/A	
85	AIO Sediment		-25.06	0.0126	0.0017	35000	1100	N/A	
192	AIO Sediment		-25.46	0.0137	0.0017	34500	1000	N/A	
0	AIO Calculated			0.2990	0.0012	9695	35	N/A	
85	AIO Calculated			0.0631	0.0023	22200	290	N/A	
95	AIO Calculated			0.0485	0.0019	24310	310	N/A	
192	AIO Calculated			0.0348	0.0017	27000	400	N/A	
0	Conventional RP1	14.820	-25.64	0.6320	0.0035	3685	40	620	90
0	Conventional RP1	12.315	-24.86	0.6558	0.0043	3390	50	250	80
0	Conventional RP5	6.882	-20.78	0.0173	0.0048	33000	2200	N/A	
85	Conventional RP1	11.982	-27.11	0.1316	0.0023	16300	140	16300	180
85	Conventional RP5	18.318	-23.63	0.0060	0.0016	41000	2100	N/A	
192	Conventional RP1	13.011	-27.22	0.1148	0.0022	17387	150	17500	200
192	Conventional RP5	11.996	-23.45	0.0114	0.0024	36000	1700	N/A	
85	Composite RP1	9.870	-24.75	0.3295	0.0177	8900	430	6600	490
95	Composite RP1	11.370	-25.6	0.2747	0.0171	10400	500	8400	650
192	Composite RP1	8.520	-29.08	0.1540	0.0118	15000	610	14700	860
85	Isotope Dilution RP1	10.190	-21.95	0.3546	0.0187	8300	420	6000	420
95	Isotope Dilution RP1	9.790	-24.43	0.2849	0.0118	10000	330	8000	410
192	Isotope Dilution RP1	11.850	-24.77	0.2017	0.0105	12900	420	11500	470
0	Foraminiferal Carbonate			0.5661	0.0028	4570	40	1660	70
6	Foraminiferal Carbonate			0.5261	0.0023	5160	35	2460	70
10	Foraminiferal Carbonate			0.4447	0.0017	6510	30	4080	70
14	Foraminiferal Carbonate			0.4419	0.0019	6560	35	4140	70

are so small, shifts on the order of a few degrees are significant relative to the slopes of the thermographs over these short intervals. Samples from 85, 95, and 192 cm depth intervals possess similar shapes, with only small variations in the height of main peaks. The first distinct peak occurs at ~390–400°C, and a second main peak occurs between ~480 and 500°C. In the core-top sample, the main peak occurs at ~370°C, the second smaller peak at ~500°C and they shift in relative proportion. CO_2 thermographs also showed some variability between analyses of the same sample (Figure 3.7). In samples at 85, 95, and 192 cm core depths, the combination of multiple runs provides us with the opportunity to visualize the replicability of thermograph shapes when the same sample is analyzed by Ramped PyrOx multiple times in the same

manner (Williams et al., 2014). Each run was normalized and integrated onto the same temperature scale for statistical comparison.

All ages are reported in Table 3.2 in both blank-corrected ^{14}C years and calibrated years BP (see Appendix Table B2). All following discussion refers to ages in uncalibrated ^{14}C years. However, the calibration of these ages does not change the overall findings. The Ramped PyrOx ^{14}C ages derived using composite and isotope dilution demonstrate a nearly constant sedimentation rate downcore (~69 yr/cm). The composite technique yielded ages between 8,900 and 15,000 ^{14}C years. The isotope dilution technique yields ages from 8,300 to 12,900 ^{14}C years. The offset between these ages increases downcore. The core-top sample required no alternate technique to yield an age of acceptable precision, but was dated twice using the conventional Ramped PyrOx technique and yielded ages of 3390 ± 50 (~12 µmol CO_2) and 3685

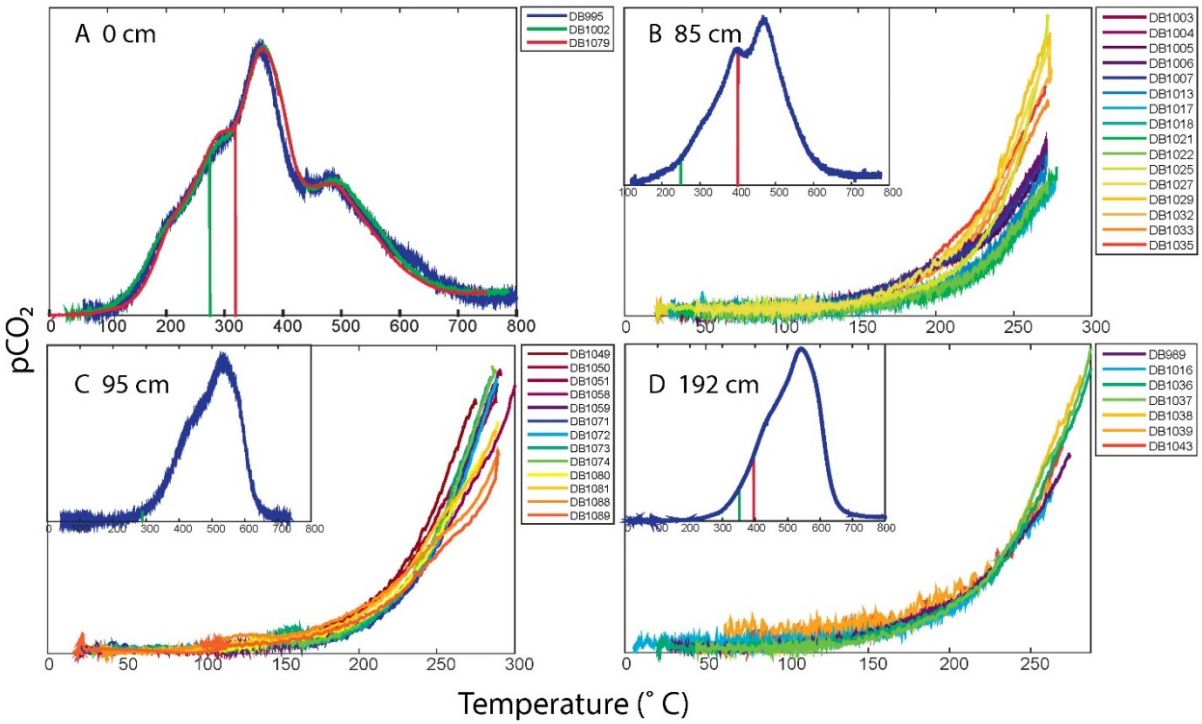

Figure 3.7. pCO_2 evolution along the temperature ramp for individual sample analyses (indicated in legends by laboratory run number) at core depths of (a) 0 cm, (b) 85 cm, (c) 95 cm, and (d) 192 cm. Insets in Figures 3.7b, 3.7c, and 3.7d are representative of a single full run and vertical lines show average temperatures where first aliquots were collected for Composite and Isotope Dilution (green) and Conventional (red) techniques. ^{14}C ages of the combined splits of each of these samples are reported in Table 3.2.

± 40 (~15 μmol CO_2) ^{14}C years. The analytical uncertainty of these ages increased downcore for all techniques used. The conventional Ramped PyrOx technique yields the lowest uncertainty, but oldest ages. The isotope dilution technique yields lower uncertainty for the samples analyzed (330–420 ^{14}C y) than the composite technique (430–610 ^{14}C y). Carbonates were only available to date within the first 15 cm of the core, so only the core-top sample can be compared to carbonate ages. Nevertheless, the Ramped PyrOx ages are younger by ~1050–1440 ^{14}C years than the corresponding carbonate ages (Table 3.2 and Figure 3.2).

3.6 Discussion

The results of our AIO ^{14}C dates measured by two different techniques and calculated from Ramped PyrOx determinations illustrate the ambiguity associated with dating a mixture of different-aged material. Acid insoluble organic matter was treated differently to remove carbonates prior to AIO dating due to the fact samples were originally sent to a commercial laboratory with a different protocol for removal of carbonates. Although only a ~10-^{14}C year difference was observed between core-top AIO ages, an offset of >3000 years was observed at 192 cm depth (Table 3.2). Previous research has found that calculated AIO ^{14}C dates based on the weighted arithmetic mean of Ramped PyrOx ^{14}C dates are similar to measured ^{14}C analyses of the measured AIO dates (Rosenheim et al., 2013b). Yet in this study, calculated AIO dates are consistently younger than measured values (Figure 3.2). The disparity between measured values can be attributed to interlaboratory differences, primarily in differing acid-treatment protocols. Moreover, in samples where the ^{14}C date is very old, such as AIO in these samples, small differences in the $^{14}C/^{12}C$ ratio measured by AMS, caused by process or sample heterogeneity, can cause large differences in the ^{14}C dates (see Appendix Figure B5). The more rigorous pretreatment protocols used at Beta Analytic may have removed more AIO material,

thus resulting in older preliminary AIO ^{14}C dates. By contrast, samples that underwent Ramped PyrOx analyses and used to calculate AIO ^{14}C dates were treated with a more dilute acid for a minimal amount of time. Thus, these analyses showed the best preservation of the most labile component. Such differences, illustrative of highly detrital sediment and brought forth by different acid treatments, are prominent in this study due to the age and detrital nature of the sediments.

Like AIO ^{14}C dates, thermographs can also be impacted by small differences in processing and analysis. We examined the replicability in the initiation of pyrolysis decomposition in the Ramped PyrOx system and found strong similarities between all samples, suggesting good low-temperature replicability (Figure 3.7). However, small differences are evident in all cases, which is most likely be explained by sample heterogeneity. Sample heterogeneity is mostly accounted for by the large number of identical runs for each sample, however it follows that samples with fewer runs may not account for small differences between splits as well. It is important to note that the data from pyrolysis initiation (Figures 3.7b–3.7d) are highly amplified compared to Figure 3.7a and previous publications showing reproducibility (Bianchi et al., 2015; Rosenheim and Galy, 2012; Rosenheim et al., 2013b; Williams et al., 2014). Thus, very small differences in the proportions of different components within a sample may result in visible thermograph variations. Other possible causes for thermograph variability, including movement of the thermocouples and changes in sample size, were avoided by, offsetting the temperature as described in the results and by analyzing equal masses of individual samples, respectively.

All three Ramped PyrOx techniques discussed in this study (conventional, composite, and isotope dilution) result in significantly younger dates than their associated AIO ^{14}C dates and thus offer substantial improvement on the AIO ^{14}C dating approach. Conventional Ramped

PyrOx ^{14}C dates are also significantly younger than carbonate dates at core-top samples by >1000 ^{14}C years. But this is likely caused by reworking and lag processes which serve to concentrate foraminifera of various dates across surfaces of little or no sedimentation (i.e. Domack et al., 2005; Domack et al., 1999a; Rebesco et al., 2014). In this core, these processes seemingly acted without leaving any visual clues (broken tests, opacity) that the tests had been reworked. The offset may also be influenced by inherent chemical differences between planktic algal material and benthic foraminifera. For example, Ohkouchi et al. (2002) and Uchida et al. (2005) demonstrated temporal offsets between the two proxies, despite large differences in study sites, water depth and sedimentation rates. In this study, there was no carbonate material further downcore with which to compare the AIO chronology, but a previous study by Subt et al. (2016) shows that the use of a smaller RP1 aliquot for a Ramped PyrOx analysis can yield similar dates to those derived from carbonate material. Here we demonstrate that in highly detrital sediments, the use of ultra-small aliquots of the most labile material in the composite Ramped PyrOx technique improves chronologies at depths where AIO ^{14}C is overwhelmed by pre-aged detrital material that produces dates clearly too old to be realistic (Figure 3.2).

Ramped PyrOx ^{14}C dates derived using alternate techniques (composite and isotope dilution Ramped PyrOx) showed significantly younger dates than not only AIO, but also conventional Ramped PyrOx ^{14}C dates. Nevertheless, there are relatively small differences between the composite and isotope dilution Ramped PyrOx ^{14}C dates. In order to estimate the amount of CO_2 to sample at the beginning of the pyrolysis reaction, we assumed that no pre-aged carbon would decompose until all autochthonous OC decomposed. However, there is no clear method to rule out the possibility that the material within each single aliquot is still a mixture incorporating some degree of pre-aged OC. By assuming a ^{14}C free endmember, we

minimize the sample size from the beginning of the decomposition reaction, thereby minimizing the potential for admixture of pre-aged OC. The fact that these two independent techniques produce relatively equal chronologies emphasizes their utility in approaching the true date of the sample by demonstrating that the fraction of pre-aged material sampled in each aliquot, if greater than zero, is likely not variable.

Interpretation of our determinations of the ^{14}C content of the extreme low-temperature end of our thermographs as calibrated radiocarbon ages depends upon our consideration of these aliquots as mixtures of autochthonous and pre-aged carbon. It is not meaningful to calibrate ages of mixtures of autochthonous and detrital OC, although we have learned quite a bit about Antarctic deglaciation from calibrated AIO ages, as calibration relies upon past variations in the amount of ^{14}C in the atmosphere (e.g. Domack et al., 2001). Considering the potential pitfalls of calibrating radiocarbon ages from samples that we cannot rule out as mixtures, along with our goal to chronicle the unique sediments from the LIS-C, we only apply radiocarbon calibration to carbonate and RP1 (Table 3.2). Such an approach is justified because the improvement of ages of independent ages strongly suggests minimization of the pre-aged OC in RP1. In other words, the improvement in ages demonstrates that the mixture of pre-aged detrital material in RP1 is substantially diluted. By comparison, carbonate ^{14}C ages show older core-top ages than Ramped PyrOx ^{14}C ages of equivalent depth, indicating that even carbonate ^{14}C ages can be either mixed with older forams or biased to some degree. Furthermore, it is important to note that dating of chemical separations of individual compounds (Ohkouchi and Eglinton, 2006; Ohkouchi and Eglinton, 2008; Yokoyama et al., 2016) does not guarantee zero admixture of older members of that compound class.

Given that both Ramped PyrOx techniques reported herein result in consistently improved chronologies, but that sufficient material does not usually exist to allow both, it

becomes necessary to choose between them in order to to maximize accuracy. Consideration of the AIO ^{14}C age of the sample and the hypothesized age or stratigraphic control of the deposit in question is important in informing this decision (see Appendix Text B4). If the difference between AIO ^{14}C ages and the stratigraphic control is large, then the target for dating becomes smaller. In such cases, a larger number of composited runs are required to accumulate sufficient CO_2 or ^{14}C analysis (see Appendix Figure B2). This number of runs, as well as the %TOC dictates the amount of sample required to accumulate sufficient ultra-small first aliquots from identical runs to minimize analytical error, as well as the amount of time needed to complete these runs (see Appendix Figure B3). Moreover, if considering the isotope dilution Ramped PyrOx technique, the availability of a well-measured surrogate of a known age is, of course, very important (see Appendix Figure B4).

One of the most important considerations for using these alternate techniques, and a guiding factor in deciding whether any one of them is even appropriate for a set of given samples, is the blank contamination associated with combining aliquots from multiple runs (see Appendix Text B4). Modern blank contamination from Ramped PyrOx is time-dependent (Fernandez et al., 2014), thus an aliquot collected over a short amount of time has less modern blank than an aliquot collected over a longer period. ^{14}C dead blank contamination results from recombustion reagents (Ag and CuO), and is therefore applied equally to each aliquot that is recombusted (Fernandez et al., 2014). This means that the overall blank contamination is more significant for an ultra-small aliquot than a larger aliquot. When multiple ultra-small aliquots are mixed as in the alternate techniques, the combined blank contamination can lead to much greater uncertainty. Recent improvements made on the Ramped PyrOx system have reduced the blank contamination to 2.8 ± 0.6 µg modern C and 1.4 ± 0.8 µg dead C (see Appendix Figure B6). This is a significant improvement over the amounts of blank contamination reported

by Fernandez et al. (2014), and consequently also provides an improvement on the precision of our Ramped PyrOx ^{14}C ages. By reducing the uncertainty from blank contamination, we are also able to combine a significantly larger sum of ultra-small aliquots required for our new techniques.

Assuming both composite and isotope dilution Ramped PyrOx can produce equally accurate ^{14}C ages and that the necessary resources are available for either technique, the main deciding factor becomes the precision, or the overall analytical uncertainty resulting from either technique. Uncertainties from both techniques increase with age of sample and with the number of runs composited. Both uncertainties are also subject to change depending on the difference between the ^{14}C age of the surrogate and the age of the lowest-temperature dated material. However, by using the isotope dilution technique, we effectively reduce the number of runs required to accumulate the necessary amount of CO_2, reducing the blank contamination and the analytical error. Nevertheless, the isotope dilution technique also requires the addition of a surrogate of known age and mass, which propagates additional uncertainty. When small proportions of the total OC are targeted, necessitating many composites, isotope dilution should

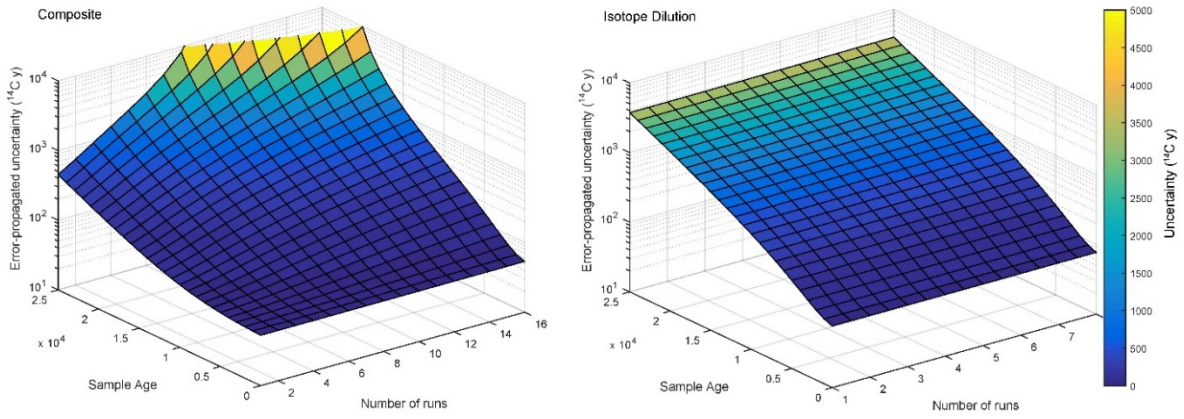

Figure 3.8. Uncertainty as a function of the number of runs required to accumulate sufficient CO_2 for precise ^{14}C dating. The fully corrected age of the sample is variable depending on the technique used for Ramped PyrOx. Above uncertainties are based on the assumption of f =50.7, δ_S = 1.039, and m_U = 120 mg C. Values for blank contamination are as reported in Methods section. For simplicity, an analytical uncertainty of 0.002. Note the z axis is shown in logarithmic scale.

likely be favored over composite Ramped PyrOx. Conversely, when the number of runs required is low (targeted proportion of initial OC is higher), the isotope dilution technique has higher uncertainty because of additional uncertainty propagation from isotope dilution and composite Ramped PyrOx should be chosen. This is particularly true for older samples (Figure 3.8). The position of the uncertainty crossover between composite or isotope dilution techniques depends on the number of runs required and how the age of the sample and shape of the thermograph confer to dictate the amount of surrogate used (Table 3.1).

It is important to note that the composite and isotope dilution techniques of Ramped PyrOx are for highly detrital sediment; not every sample analyzed using Ramped PyrOx may require these techniques. Many samples may not require multiple runs to accumulate sufficient CO_2 for ^{14}C dating, as in the case of the core-top sample in this suite of samples or previous work (Subt et al., 2016). Just as conventional Ramped PyrOx is an alternative when carbonates are not available and AIO ^{14}C dating may be problematic, the composite and isotope dilution techniques are an alternative when the projected amount of syndepositionally-aged material is too small to be captured in a conventional Ramped PyrOx aliquot (~10–15 μmol CO_2) without influence from the mixture of the age of ancient detritus.

The techniques developed for this study have greatly improved our ability to date highly detrital samples. Techniques such as isotope dilution are not new and unique to this work, and it is conceivable that we can use isotope dilution, for instance, at core intervals where there is some, but not enough, foraminiferal carbonate for a single date. However, similar calculations and logic to that found in Figure 3.8 would need to be carried out independently to assess the cost in precision of isotopic dilution for foraminiferal carbonate dates. By using these techniques, we may ultimately become capable of retrieving more accurate dates for Antarctic marginal marine sediments not only within periods of high productivity and reduced glacial

deposition, but within the glacial deposits where dating has so often been precluded. These techniques would also be applicable to a wide range of problematic sediments in regions outside of Antarctica with a highly detrital nature.

3.7 Conclusions

We have provided two new alternative techniques for the Ramped PyrOx ^{14}C approach which have improved our ability to date sediments with very low proportions of syndepositionally-aged material. Both techniques we have described show a large improvement in the separation of pre-aged detritus from the much smaller syndepositionally-aged fraction not only for AIO ^{14}C dating, but on conventional Ramped PyrOx analyses as well. Differences in composite and isotope dilution Ramped PyrOx ^{14}C dates may occur due to sample heterogeneity, blank contamination, and error propagation. Nevertheless, the differences between the two new techniques are small to negligible relative to the overall improvement in ages compared to AIO. Careful consideration must be taken when deciding which technique is most appropriate for a set of samples. The availability of techniques like those described herein remove limitations on geoscientists working in sediments from the Antarctic margin. Ultimately, this may allow accurate dating of sediments under ice shelves, glacial tills, or siliceous muds and oozes buried prior to the LGM. Sub-ice shelf sediments, for example, could serve as a modern analog for Cryogenian research (e.g. Hoffman et al., 2012; Vincent et al., 2000). It would also allow researchers to study ice sheet behavior not only during the deglacial period, but into the glacial period as well. Thus, by using these alternative techniques, we can not only date Antarctic marine sediments from the LGM to the present, but we can also provide chronologies beyond these horizons, where highly detrital material has precluded radiocarbon dating in the past.

CHAPTER 4:

DEGLACIAL RECORD FROM THE WESTERN ROSS SEA: ROSS ICE SHEET INSTABILITY DURING THE LGM

4.1 Note to Reader

This chapter is prepared as a manuscript for future publication.

4.2 Abstract

The Ross Embayment is among the most well-studied regions in Antarctica. Despite the relative abundance of data, the style and forcing of deglaciation of the Ross Sea sector following the Last Glacial Maximum (LGM) is challenging due to the region's considerable size, complex geometry, and difficulties in dating Antarctic glaciomarine sedimentary sequences. During the LGM, the Ross Sea basin is believed to have been covered by grounded ice that extended over most of the continental shelf. Marine sediments collected near the Drygalski Ice Tongue in the western Ross Sea reveal sequences of laminated diatomaceous muds and oozes interbedded with diamicts. This research has analyzed chronology and paleothermometry techniques designed to overcome the difficulties of analyzing sediments lacking carbonate materials and containing high proportions of relict carbon. Improved sediment chronology using Ramped PyrOx ^{14}C dating shows evidence of a dynamic ice sheet environment in the Drygalski Trough region during the Last Glacial Maximum (LGM; 20.8 to 26.6 ka BP). Relatively warm upper ocean temperatures, measured using TEX_{86} paleothermometry, likely contributed to the

instability of the ice sheet. Following this period of instability, the ice sheet re-advanced and reached its maximum extent, remaining stable until ~8.7 ka BP, when it deglaciated permanently from the region.

4.3 Introduction

During the Last Glacial Maximum (LGM; 19-26 ka BP), Antarctica's continental shelves were covered by large stable ice sheets (e.g. Anderson et al., 2002; Bentley et al., 2014; Denton and Hughes, 2002). Ice core records show millennial scale warming events through the late Holocene (EPICA Community Members, 2006), corroborated by marine and terrestrial records, including ice-rafted detritus (IRD) deposition and sea ice extent (Nielsen and Hodell, 2007), atmospheric temperature (EPICA Comminity Members, 2006) and sea surface temperatures (SSTs) in the Southern Ocean (Caniupan et al., 2011). Ice core records also show the last major deglacial transition occurred between peak LGM conditions (~21 ka BP) to mid-Holocene warmth (~9 to 5 ka BP) and constitutes a ~4 °C increase in global mean temperature) (Annan and Hargreaves, 2015), wherein atmospheric CO_2 concentrations increased ~80 ppm (from ~190 ppm to ~270 ppm) (Marcott et al., 2014; Monnin et al., 2014; Parrenin et al., 2013). During deglaciation, ice on the Antarctic margin retreated through ice streams with significant variability, and responded asynchronously to forcings including atmospheric and ocean temperatures, sea level, and retreat patterns (e.g. Bamber et al., 2007; Livingstone et al., 2012; Smith et al., 2007). A number of mechanisms have been proposed to explain variable retreat rates across different ice streams, including drainage basin size (O'Cofaigh et al., 2008), bathymetry (Schoof, 2007), and ice stream geometry (e.g. Dowdeswell et al., 2008, O'Cofaigh et al., 2008; Shipp et al., 2002).

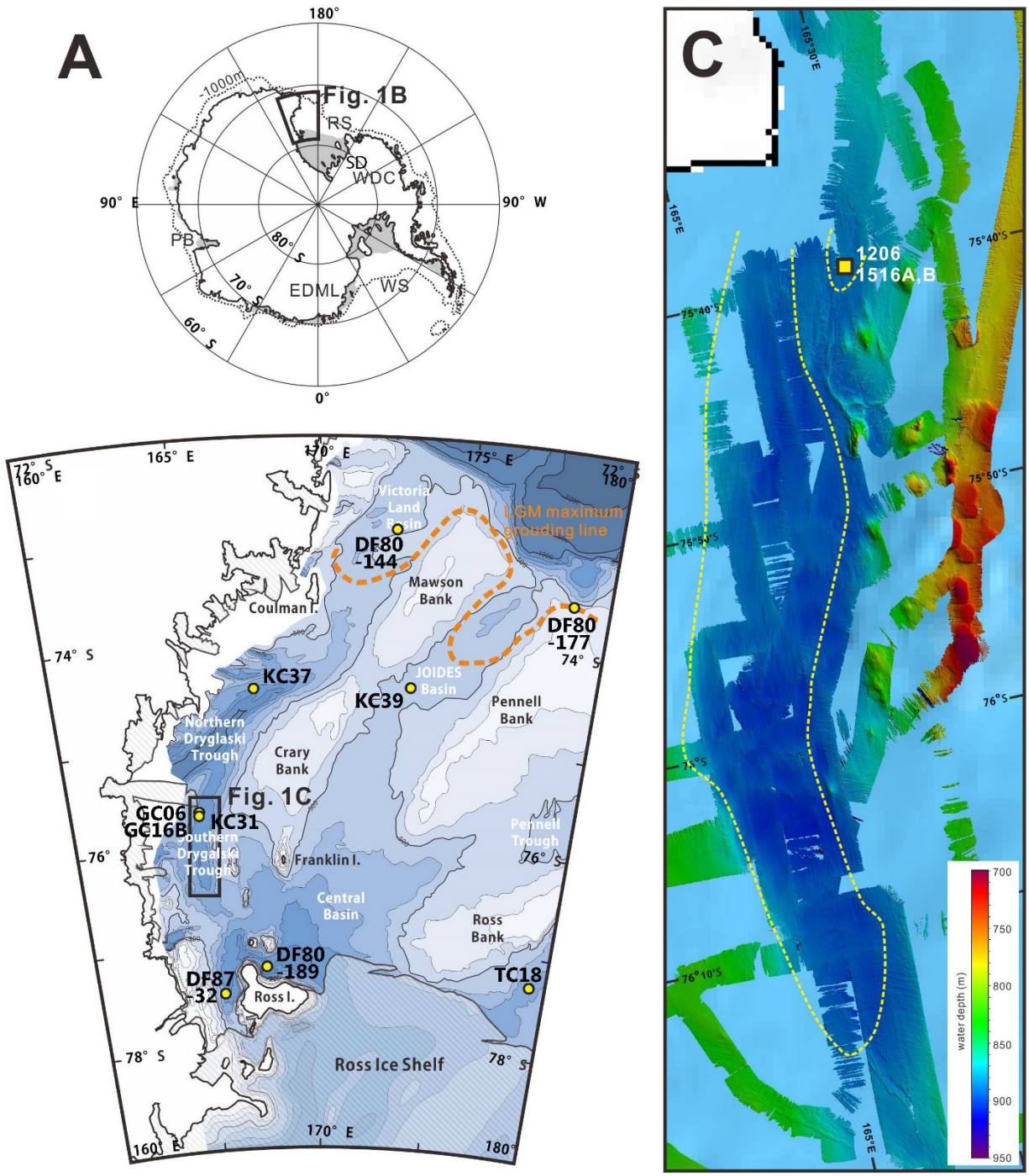

Figure 4.1. Map of study region near the Drygalski Ice Tongue (DIT). **A**. Antarctic continent. Locations of major ice cores (EDML: EPICA Dronning Maud Land, WDC: WAIS Divide, SD: Siple Dome) and drainage basins (RS: Ross Sea, WS: Weddell Sea) are shown. **B**. Western Ross ice Shelf with low resolution bathymetry and locations of other cores discussed in this study. The maximum extent of the Ross grounding line during the LGM is also shown in **B** as estimated in previous studies. **C**. Multibeam swath bathymetry of the southern Drygalski Trough with locations of cores DG12 GC06 and RS15 GC16B are shown in **C**. Yellow dashed line in **C** indicates the distribution of a seismic-transparent thin sediment layer on the seafloor composed of Holocene diatomaceous mud of detectable thickness (> 1m). The distribution of the upper mud layer is limited to water depths > 850 m, suggesting that reworking may be dominant in water depths shallower than 850 m.

The marine-based West Antarctic Ice Sheet (WAIS) has a large system of ice streams and outlet glaciers thought to be vulnerable to collapse due to the rapid removal of ice in these fast-flowing regions across an over-deepened bed (e.g. Jacobs et al., 2011; Bindschadler et al., 2003; Bougamont et al., 2003; Joughin et al., 2005; Joughin and Tulaczyk, 2002; Livingstone et al., 2012; MacAyeal, 1992; Mercer, 1978; Oppenheimer, 1998; Rignot and Jacobs, 2002; Schoof, 2007; Thomas and Bentley, 1976; Weertman, 1974). Increased water temperatures or intrusions of warm water onto an ice-covered embayment such as the Ross Sea may contribute to deglacial changes due to basal melting under an ice sheet (e.g. Joughin and Alley, 2011; MacAyeal, 1992; Pollard and DeConto, 2009; Rignot and Jacobs, 2002; Schoof, 2007). During the LGM, the Ross Sea basin was covered by grounded ice primarily fed by the WAIS, that is thought to have reached ~280,000 km^2 more than its current extent, covering the majority of the continental shelf (Figure 4.1) (Anderson et al., 2014; Anderson et al., 2002; Bentley et al., 2014; Denton and Marchant, 2000; Yokoyama et al., 2016). The presence of large, deep troughs in the Ross Sea might facilitate early initiation of deglaciation through which ice streams allowed for faster flow during the LGM, facilitating the rapid removal of ice from the continental shelf (e.g. Livingstone et al., 2012). Unlike the LGM, the modern Ross Sea is occupied by the Ross Ice Shelf (RIS), the largest ice shelf in the world (~560,000 km^2), and provides a buttress for large outlet glaciers draining the East and West Antarctic Ice Sheets (EAIS and WAIS, respectively) (e.g. Denton and Hughes, 2002; Bindshandler, 1998). Collapse of the RIS could have severe consequences for climate by disrupting Antarctic Bottom Water (AABW) production and thermohaline circulation (Clark et al., 2002; Stocker, 2003; Weaver et al., 2003), amplifying regional warming by decreasing Earth's albedo, and the eventual collapse of the WAIS (e.g. Alley and Bindschadler, 2013; McKay et al., 2008).

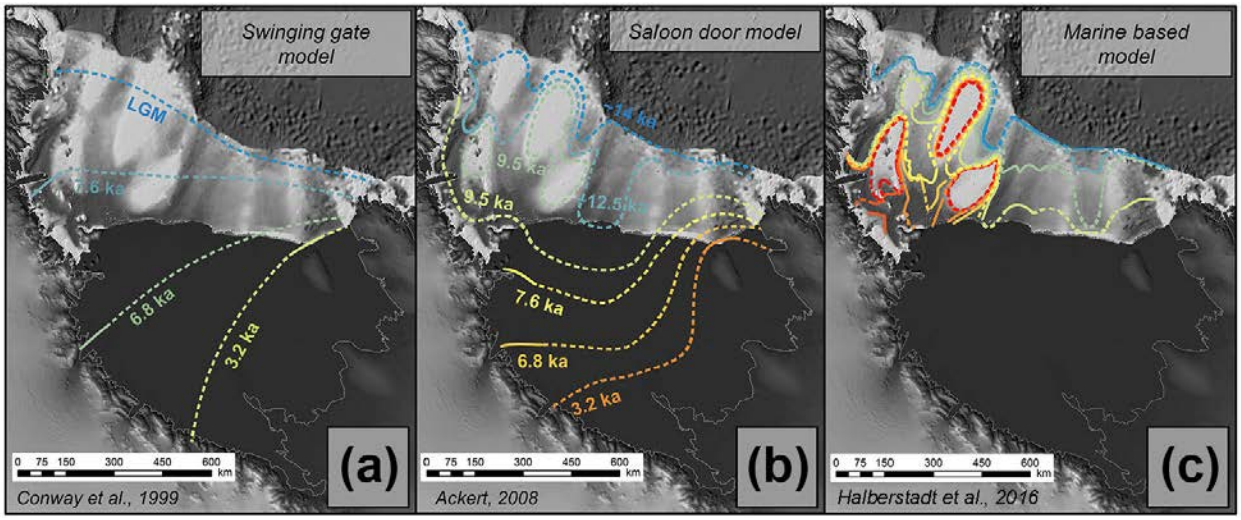

Figure 4.2. Three existing models of Ross Sea post-LGM deglaciation. (**a**) The "swinging gate model" is based on ^{14}C dates from three sites along the western Ross Sea and assumes a linear grounding line retreat that hinges just north of Roosevelt Island (Conway et al., 1999). (**b**) The "saloon-door model" includes a larger dataset that includes additional ice streams in the Ross Sea (Ackert, 2008). (**c**) The "Marine based model uses glacial morphology and compiles 20 years of multi-beam bathymetry and seismic data throughout the Ross Sea to infer complex retreat patterns with strong physiographic controls on ice-sheet drainage (Halberstadt et al., 2016). Figure modified from Halberstadt et al. (2016).

The paleodrainage of the Ross Sea basin is a crucial component to determining the mode of deglaciation during and after the LGM (Anderson et al., 1992; Greenwood et al., 2012; Halberstadt et al., 2016; Licht et al., 1999; Stuiver et al., 1981). Three main hypotheses have been used to explain the mode of Ross Sea deglaciation (Figure 4.2). The earliest hypothesis, the "swinging gate model," is so-called because it assumes a linear retreat of the grounding line hinged north of Roosevelt Island (Figure 4.2.a) (Conway et al., 1999). The "saloon-door model" incorporates a larger dataset that adds to the complexity of the deglacial reconstruction and suggests that grounding line retreat resembled two swinging doors (Figure 4.2.b) (Ackert, 2008). Most recently, Halberstadt et al. (2016) proposed the "marine-based model", which calls for complex, asynchronous retreat between troughs in the Ross Sea, with strong physiographic controls on the paleodrainage through ice streams (Figure 4.2.c). This latest glacial geomorphic reconstruction shows the best agreement with ice sheet and climate models that demonstrate significant contributions from both EAIS and WAIS to ice flow and suggest deglaciation began within Ross Sea troughs with strong bathymetric control (Golledge et al., 2014; DeConto and

Pollard, 2016; McKay et al., 2016). The marine-based model is also supported by new evidence from multibeam swath bathymetry, which suggests an early retreat of the WAIS from continental shelves and implies that coastal records account for only the final stages of glacial retreat in the Ross Sea (Lee et al., 2017a).

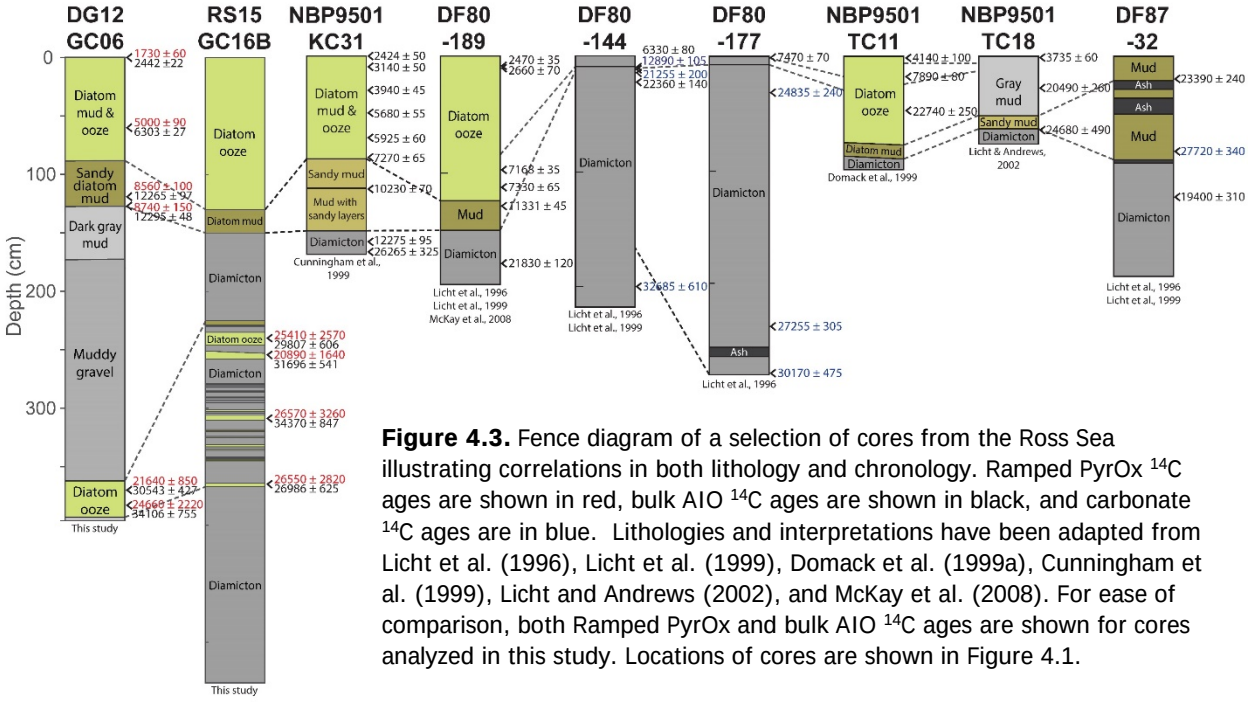

Figure 4.3. Fence diagram of a selection of cores from the Ross Sea illustrating correlations in both lithology and chronology. Ramped PyrOx ^{14}C ages are shown in red, bulk AIO ^{14}C ages are shown in black, and carbonate ^{14}C ages are in blue. Lithologies and interpretations have been adapted from Licht et al. (1996), Licht et al. (1999), Domack et al. (1999a), Cunningham et al. (1999), Licht and Andrews (2002), and McKay et al. (2008). For ease of comparison, both Ramped PyrOx and bulk AIO ^{14}C ages are shown for cores analyzed in this study. Locations of cores are shown in Figure 4.1.

Sediments in the western Ross Sea typically demonstrate a well-established retreat sequence (Figure 4.3) (Domack et al., 1999a; McKay et al., 2008). The base of this succession consists of muddy diamict interpreted as melt-out from basal debris proximal to the grounding line. Overlying this unit is a terrigenous mud interpreted as sub-ice shelf deposits. The top of this sequence consists of diatom mud and ooze indicative of open marine conditions. Variations of this sequence are indicative of a more dynamic environment, and can be found throughout the Antarctic margin (e.g. Licht et al., 1996; Licht et al., 1999; Smith et al., 2010). Cores collected within the Drygalski Trough in the western Ross Sea contain sediments that present an opportunity to examine the retreat and behavior of the WAIS through the last deglaciation. The Drygalski Trough is the westernmost trough in the Ross Sea, and contained the largest and

deepest paleo-ice stream of the Ross Sea where the EAIS and WAIS joined during the LGM; however, the respective contributions of the EAIS and WAIS in this region is still subject to debate (Anderson et al., 2014). Recent findings by Lee et al. (2017a) provide a context in which to study this depositional setting. Sediments within this region show interbedded diatom ooze and diamicton layers underlying the typical glacial to interglacial transitional facies (Lee et al., 2017b). Similar sequences have been sampled in the Prydz Channel, which drains the Lambert Glacier-Amery Ice Shelf (LG-AIS) (Domack et al., 1998; Guitard et al., 2015). These unusual lithological sequences may be indicative of multiple periods of retreat and re-advance of the Ross Ice Sheet during the last deglaciation.

This research analyzes periods of retreat and re-advance recorded in sediments from the Drygalski Trough using a compilation of dating, paleotemperature and grain size analyses to improve understanding of the timing and mechanisms forcing regional ice retreat. The timing of ice retreat remains ambiguous largely due to the many difficulties in measuring ^{14}C reliably in Antarctic sediments, with existing estimates ranging between 8.5 and 11.5 ^{14}C ka BP (e.g. Kellogg et al., 1979; Licht et al., 1999; Licht et al., 1996; McKay et al., 2016; McKay et al., 2008; Shipp et al., 1999). Ramped PyrOx ^{14}C dating targets young labile organic material contained in the sample through thermochemical separation of components (Rosenheim et al., 2008). Recent studies have shown its applicability to dating Antarctic sediments from a wide variety of settings (Rosenheim et al., 2008; Rosenheim et al., 2013b; Subt et al., 2016; Subt et al., 2017). In carbon-poor settings with low sedimentation, such as sub-ice shelf environments, advanced techniques can be applied to the Ramped PyrOx approach to more accurately date these sediments (Subt et al., 2017).

The behavior of ice sheets is inherently linked to climate and water mass conditions, though our understanding of the extent and timing of its response to environmental changes is

still limited. Ice sheet instability may have been the result of climate and water mass conditions, which are known to be an important driving mechanism for ice dynamics due to basal melting (e.g. Pritchard et al., 2012). Although ice core reconstructions have provided insight into past atmospheric temperature fluctuations, ocean temperatures proximal to Antarctica's ice sheets are largely unknown because most paleothermometers depend on the availability of biogenic carbonate. The TEX_{86} (TetraEther indeX of tetraethers consisting of 86 carbon atoms) paleothermometer is based on relative abundances of glycerol dialkyls glycerol tetraethers (GDGTs), membrane lipids from the pelagic marine archaea, Thaumarchaeota, and has shown promising results for reconstructing Antarctic-margin sea surface temperatures (SSTs) (e.g. Kim et al., 2008; Kim et al., 2010; Liu et al., 2009; Schouten et al., 2002; Shevenell et al., 2011; Tierney and Tingley, 2014; Tierney and Tingley, 2015). To determine the effects of ocean temperature on ice dynamics in the Drygalski Trough during the last glacial cycle, this we reconstruct upper ocean temperatures using TEX_{86} paleothermometry. Results provide insights into the timing of ice retreat and suggest a role for the intrusion of warm waters into the trough as a potential cause of observed glacial instability in the western Ross Sea during the LGM and deglaciation.

4.4 Methods

4.4.1 Geologic Setting

The Drygalski Trough, which is adjacent to the Drygalski Ice Tongue (DIT), in the western Ross Sea is one of seven cross-shelf glacially sculpted troughs in the Ross Sea, which formed over remnant bathymetric lows from extensional tectonics that led to the formation of the modern Ross Sea (Lawver et al., 1991), leaving a path for ice streams to flow through

preferentially (Anderson and Andrews, 1999; Cooper et al., 1991). Its maximum depth is ~1500 m within the trough near the Drygalski Ice Tongue (Brambati et al., 1997), making it the deepest trough and the site of the thickest grounded ice in the Ross Sea during the LGM (Anderson et al., 2014). During the LGM, the region was fed by merging ice streams from EAIS outlet glaciers north of Ross Island (Anderson et al., 2014; Licht et al., 1999), and the David Glacier from the WAIS. The David Glacier is one of the major outlet glaciers of the modern Ross Sea embayment (Licht et al., 1999), making it an important location for constraining ice extent and regional response to climate forcing. Previous research conducted in the western Ross Sea seeking to understand post-LGM deglaciation was hampered by the limited availability of carbonate microfossils for ^{14}C dating and regions where bulk AIO ^{14}C dates show only minimal effects (usually in the form of older ^{14}C ages than from other sources) from the incorporation of older carbon (e.g. Anderson et al., 1991; Licht et al., 1996; McKay et al., 2016).

High-resolution multibeam swath bathymetry generated during the 2015 R/V Araon expedition (Figure 4.1) shows glacially-scoured seafloor at these sites, including mega-scale glacial lineations (MSGLs) running parallel to the Drygalksi Trough (Figure 4.1.C), indicating that a large ice sheet flowed in a north-south direction, and the depth of these flow lines indicates fast ice flow in this region. Grounding zone wedges (GZWs) perpendicular to flow lines indicate past ice sheet extent. A GZW is visible just south of the study sites (Figure 4.1.C), suggesting ice was grounded proximal to the study sites. The bathymetry of this region will be more thoroughly discussed in future publications by Lee et al. (unpublished).

4.4.2 Sediment Core Descriptions

Cores DG12-BC06 and -GC06, and RS15-GC16B were collected onboard the R/V Araon during the 2012 and 2015 Korea Polar Research Institute (KOPRI) expeditions, respectively, and

subsequently stored and sampled at the KOPRI repository. Cores BC06 and GC06 (75° 39.5684' S, 165° 23.8382' E) are a box core (.34 m) and a gravity core (3.96 m), respectively, both collected at 859 m water depth. Core GC16B (75° 39.57' S, 165° 29.4282' E) is a gravity core that is 5.56 m long and was taken at 848 m water depth. The sites of GC06 and GC16B are only 272 m apart (Figure 4.1). These three cores were collected from two sites adjacent to the Drygalski Ice Tongue and display similar lithology, where samples were taken from key lithologic features of glacial retreat from each of these cores. Cores GC06 and GC16B both display interbedded diatom ooze and diamicton units.

Sediment analyses for water content, grain size, X-radiography, and magnetic susceptibility were conducted at the Korea Polar Research Institute to identify lithologic units within each core (Figure 4.3). The upper 3 cm of core BC06 consist of dark gray mud with high water content and smaller grain sizes. From 3-34 cm, a diatom mud and ooze layer shows constant high water-content, larger grain sizes and lower magnetic susceptibility. The upper 88 cm core-depth of core GC06 contains the highest water content and % TOC, smallest grain sizes, and lowest magnetic susceptibility in the core. Sediments in the underlying unit (from 88 to 127 cm core-depth) consist of sandy diatom mud and contain slightly lower water content than the overlying diatom ooze, as well as generally increasing magnetic susceptibility, increasing grain sizes, and rapidly decreasing % TOC. Underlying this layer is a dark gray mud (127 to 172 cm core-depth), which contains even lower water content than the overlying diatom mud, larger grain sizes, slightly higher magnetic susceptibility and the lowest % TOC found in this core. A muddy gravel layer (172 to 362 cm core-depth) nearly identical in water content and % TOC underlies the dark gray mud and shows decreasing grain size, and decreasing magnetic susceptibility. Due to the similarity of the dark gray mud and muddy gravel layers and the lack of visible stratigraphic difference between them (Figure 4.4.A), we identify

these two units together as diamicton, which is mostly stratified due to varying content of volcanic materials. From 362 to 393 cm core-depth in GC06, a second diatom mud and ooze unit shows relatively high water-content, small grain sizes, low magnetic susceptibility, and relatively high % TOC.

The upper 130 cm of core GC16B consists of diatom mud and ooze, and sediments from 130 to 150 cm core-depth consist of diatomaceous mud, which we assume coincide with the corresponding units in core GC06, given the proximity of the two cores, and the similarity in water content, magnetic susceptibility and % TOC trends. From 150 to 225 cm core-depth, sediments consist of a diamicton unit with low water content, %TOC values, and magnetic susceptibility. Laminated diatom mud and ooze layers containing occasional pebbles are interbedded with diamicton layers from 225 to 367 cm core-depths. The basal contact of one of these diamictons shows a thrust-like deformation consistent with a proximal grounding line or slump deposits (251-253 cm core-depth; Figure 4.4). Ramped PyrOx ^{14}C analyses of samples in this core above and below this contact were used to test if it was deposited in situ or transported. Whereas sediments deposited in chronological order are likely deposited in situ, slumps or other deformational processes would likely result in age reversals or large contamination of relict organic material.

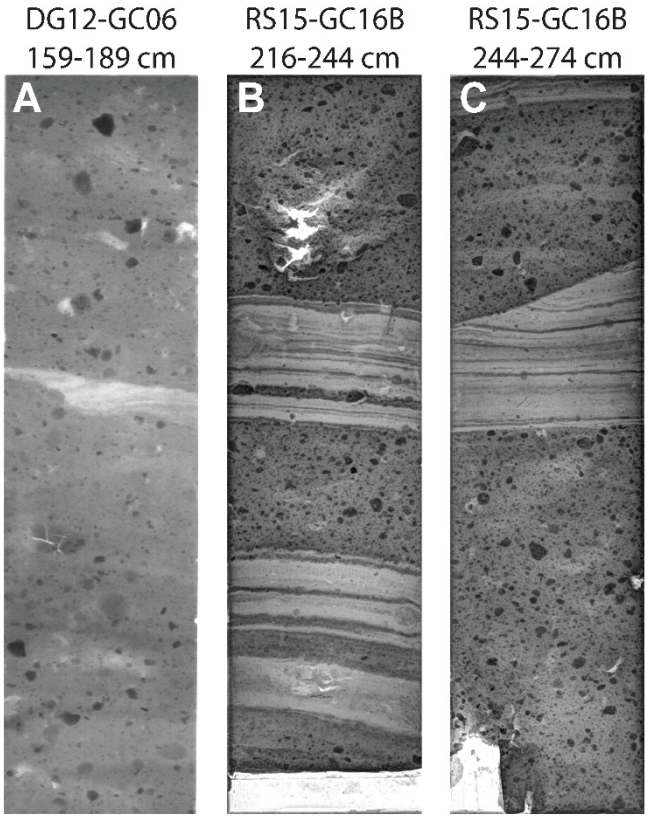

Figure 4.4. Select x-radiograph images from cores DG12-GC06 and RS15-GC16B. **A**. Transition of dark gray mud to muddy gravel in core GC06 show indistinguishable lithologies interpreted as diamict. **B** and **C**. Thrust-like deformation at basal contact diamict ~251 cm core-depth.

4.4.3 Chronology

Samples taken from each core contain insufficient carbonate microfossils for ^{14}C dating or $\delta^{18}O$ measurements. To compensate in such a situation, the bulk AIO fraction of the sample is typically used for dating instead, but this approach is not reliable for dating in highly detrital settings such as the western Ross Sea, where pre-aged organic material can bias or even overwhelm the age of sediment from transitional ice shelf and grounded glacial sediments (e.g. McKay et al., 2008). A more accurate dating tool is Ramped PyrOx ^{14}C dating, which separates organic carbon from different sources based on their thermochemical characteristics (Rosenheim et al., 2008). Preliminary AIO ^{14}C ages were analyzed by Beta Analytic Radiocarbon Dating Laboratory, and were used to determine the proportion of syndepositionally-aged carbon in the sample (f_{SA}) using equations described by Subt et al. (2017), wherein a two-endmember mixing model was used to predict the proportions of labile and relict components within each sample (Table 4.1, Appendix C1). It is typically assumed the relict component is devoid of ^{14}C, or ^{14}C-dead. Here, to ensure the highest possible accuracy in the ages was achieved, conservative estimates of the age of the labile component were based upon the lithology and character of each sample. Samples from key lithologic units were then targeted for more robust conventional Ramped PyrOx ^{14}C dating: for those samples where f_{SA} values resulted in less than 10% of the total AIO carbon, composite Ramped PyrOx ^{14}C dating was also applied to sample ultra-small splits of labile organic carbon and offset the effects of very high proportions of relict organic carbon. However, it should be noted that f_{SA} values can only be considered estimates of the proportion of the thermochemically labile component in any given sample and thus rely upon robust assumptions of the ages of labile and relict components of the sample. For cores BC06 and GC06, samples from the upper 172 cm, where lithologies ranged from diatom ooze

and sandy diatom mud to dark gray mud, the age of the labile component was assumed to be 10 ^{14}C years. This is a highly conservative estimate, even for a core-top age, due to additional effects on organic carbon from old reservoir ages in Antarctic waters, as well as potential reworking of sediment. In samples from lower diatomaceous units, the age of the labile component was assumed to be equivalent to the lowest-temperature conventional RP ^{14}C age of the nearest up-core sample (~8800 ^{14}C y). This same assumption was used for all dated samples from core GC16B, where no preliminary dating was applied. Additionally, the AIO ^{14}C age of these samples was assumed to be older than the oldest-dated sample from core GC06 (~40,000 ^{14}C years) as an additional conservative estimation for f_{SA}. The temperatures of reaction for fSA, T1, were calculated for samples analyzed using RP, and are listed in Table 4.1 (see Appendix, C2).

Table 4.1. Sample preliminary data for cores BC06, GC06 and GC16B. AIO ^{14}C ages for samples from BC06 and GC06 were measured at Beta Analytic while those from GC16B are estimations based on core GC06 and previous research.

Core	Depth (cm)	%TOC	AIO Age (^{14}C y)	±	f_{SA}	T_1 (°C)
DG12 BC06	0	1.38	3910	30	0.6154	484.3
DG12 GC06	20		5280	30	0.5189	
DG12 GC06	40		6620	30	0.4392	
DG12 GC06	60	1.09	7190	30	0.4091	425.7
DG12 GC06	80		7950	30	0.3722	
DG12 GC06	100		9640	40	0.3016	
DG12 GC06	119	0.44	14130	50	0.1724	354.4
DG12 GC06	127	0.45	12060	50	0.2231	370.2
DG12 GC06	172		30140	170	0.0437	
DG12 GC06	370	0.92	35650	280	0.0353	259.6
DG12 GC06	376		32500	220	0.0523	
DG12 GC06	383	1.08	39250	410	0.0226	242.0
RS15 GC16B	240	0.79	40000*		0.0186	248.9
RS15 GC16B	253	0.74	40000*		0.0186	246.8
RS15 GC16B	306	0.69	40000*		0.0186	239.7
RS15 GC16B	365	0.71	40000*		0.0186	240.9

* AIO ^{14}C age was not measured for these samples. Reported age is assumed based on previously-dated samples and conservative estimates.

It is important to account for the different sources of uncertainty for ^{14}C dates in this study. Blank contamination (the mixture of contaminant CO_2 in the sample during analysis) was corrected for using the equations derived by Subt et al. (2017) for both conventional and composite Ramped PyrOx analyses. The total modern carbon in one Ramped PyrOx analysis is 2.5 ± 1.4 µg. A proportion of this amount was integrated over the time required to collect each aliquot and applied to each individually. The total dead blank, which is not time-integrated, is 1.8 ± 1.5 µg and was applied whole to each aliquot (Fernandez et al., 2014). There is an inherent bias in any ^{14}C dates of sediments incorporating some amount of relict organic material due to the mixture of components from different regions and time periods. The effects of diagenesis can preferentially impact the labile organic component targeted for Ramped PyrOx ^{14}C dating. However, ^{14}C dates in this study match within error between cores, thus it is unlikely diagenesis significantly biased these data, as these effects would likely result in widely different measurements between two cores analyzed. Sediments deposited proximal to the grounding line may also incorporate higher proportions of relict organic material, thus biasing the age of the sediment. We limit the effects of this admixture by applying Ramped PyrOx to the sediments, thus providing a more effective separation of organic components in the sediments.

4.4.4 Paleotemperature Reconstruction

We have reconstructed regional paleotemperatures using TEX_{86} to investigate how ocean temperatures may have correlated with ice dynamics in the Drygalski Trough during and after the LGM. Freeze-dried samples were prepared according to methods established by Schouten et al. (2007) and Huguet et al. (2010) at the University of South Florida, wherein archaeal GDGTs were extracted through ultrasonification with dimethanol/dichloromethane

(DCM; 1:1, v/v), repeated with DCM. The extracted supernatants were dried under a stream of N_2, rinsed 3x with DCM, dried again with N_2, then refrigerated. The compounds were then filtered with a PTFE 0.4µm filter in DCM solvent before being injected into an Agilent 1200 high-performance chromatographer (HPLC) coupled to a Varian 352 Mass Spectrometer (MS), equipped with an autoinjector and ChemStation chromatography manager software. Separation of the GDGTs used to generate the TEX_{86} index was achieved on a Prevail Cyano column (2.1x150mm, 3µm), maintained at 30°C. GDGTs were eluted isocrastically with a hexane:isopropanol (99:1, v/v) mobile phase for 5 minutes, then using a linear gradient of up to 1.8% isopropanol for 45 minutes with a flow rate of 0.2 mL min^{-1}. GDGTs were detected using positive ion APCI of the eluent by single-ion mode detection (SIM) on the HPLC/MS. Peak areas from extracted ion chromatograms were manually integrated to calculate the TEX_{86} index using equation 4.1 as defined by Schouten et al. (2002):

$$TEX_{86} = \frac{[GDGT-2]+[GDGT-3]+[GDGT-5]}{[GDGT-1]+[GDGT-2]+[GDGT-3]+[GDGT-5]} \quad \text{Eq. 4.1}$$

Due to a latitudinal bias in global calibrations, regional calibrations for polar regions are often necessary (e.g. Kim et al., 2010; Pearson and Ingalls, 2013; Tierney and Tingley, 2014; Tierney and Tingley, 2015). In this study, TEX_{86} values were converted to absolute temperatures by applying a linear calibration developed by Shevenell et al. (2011), which includes Antarctic samples, produces core-top temperatures similar to the expected modern temperatures as well as a realistic range of temperatures downcore (see Appendix, C3).

The TEX_{86} paleotemperature proxy is limited by the availability of GDGTs extracted from the sample to resolve chromatographic differences that result in well-defined ratios. However, it should be noted that some degeneration may occur over time; thus, it was sometimes necessary to use very large samples from the lower diatomaceous ooze units to extract

sufficient GDGTs for accurate measurement. Error was determined using the calculated TEX_{86} index of samples extracted and run in duplicate and triplicate.

There are several different sources of uncertainty for TEX_{86} measurements. Temperature measurements from TEX_{86} paleothermometry may be biased by mixing components from different sources. A number of recent studies suggest the TEX_{86} index in the marine water column may reflect not only changes in temperature, but also other environmental factors (Elling et al., 2014; Elling et al., 2015; Hurley et al., 2016; Qin et al., 2015). Thaumarchaeota alter their cell permeability with the addition and removal of cyclopentane and cyclohexane rings (Konneke et al., 2014; Valentine, 2007) in response to environmental conditions (e.g. Elling et al., 2014; Elling et al., 2015; Hurley et al., 2016; Ingalls, 2016; Qin et al., 2015). However, these conditions are more likely to be consistent through time in a single location than over a wide variability of regions. Additionally, TEX_{86} values produce a good fit with linear global calibrations (e.g. Kim et al., 2008; Kim et al., 2010; Liu et al., 2009; Schouten et al., 2002; Shevenell et al., 2011), all of which produce the same trends, but vary in absolute values. Diagenesis can also alter TEX_{86} indices through isomerization of crenarchaeol (Shah et al., 2008), resulting in warmer temperature estimates. However, like ^{14}C dates, TEX_{86} indices match between cores within the range of uncertainty, indicating diagenetic effects are unlikely to have significantly biased data from this study.

4.5 Results

Overall, thermograph shapes used for ^{14}C chronology were consistent within lithologic units (Appendix, Figure C2, C3). For example, Samples GC06 0 and 60 cm were both sampled from the upper diatom mud and ooze layer, and display almost identical shapes. Samples GC06 119 and 127 cm were both sampled from the sandy diatom mud, and are also fairly similar in

shape, but were subject to decreasing yields with depth due to decreasing %TOC in this sedimentary unit (Appendix, Figure C2). Moreover, all samples from the lower diatom ooze units at both sites display very similar thermograph shapes with only some minor differences in the distributions of components within each sample.

Core top sediments of BC06 yielded temperatures of ~0.8 °C (~1730 ^{14}C years ago). In the upper diatom ooze unit of core GC06 (88 to 127 cm core-depth), temperatures remain relatively constant, with a generally decrease of < 0.5 ± 0.3 °C by ~5000 ^{14}C yrs BP. Temperatures then warm again by ~3.5 ± 0.6 °C through the sandy diatom mud underlying this unit by ~8000 ^{14}C yrs BP and cool by ~3.2 ± 2.0 °C ~8740 ^{14}C yrs BP. No temperatures or ages were measured within the diamicton due to very low %TOC. The lower diatom ooze unit shows a significant decrease in temperatures of ~3.0 ± 1.0 °C between ~23800 and ~21100 ^{14}C years ago. In core GC16B, TEX_{86} was not measured within the upper diatom ooze through diamict sequence as these were assumed to coincide with the upper diatom mud and ooze units of core GC06. However, TEX_{86} was measured in lower diatom ooze layers from 225 to 367 cm core-depths, and yielded temperatures ranging from ~2.3 to ~3.7 ± 0.7 °C (~20890 to ~26570 ^{14}C yrs BP), and well with values from the lower diatom ooze in core GC06.

4.6 Discussion

4.6.1 Evaluating Core Chronologies

Preliminary bulk AIO ^{14}C dating applied on 12 samples from core DG12 GC06 (Table 4.1; Appendix, Figure C4), resulted in age reversals and large biases towards older ages, implying some mixture of relict, detrital carbon. Subsequent conventional RP ^{14}C dates on 6 samples of the same core were applied to examine the original AIO chronology (Appendix, Table C3, Figure

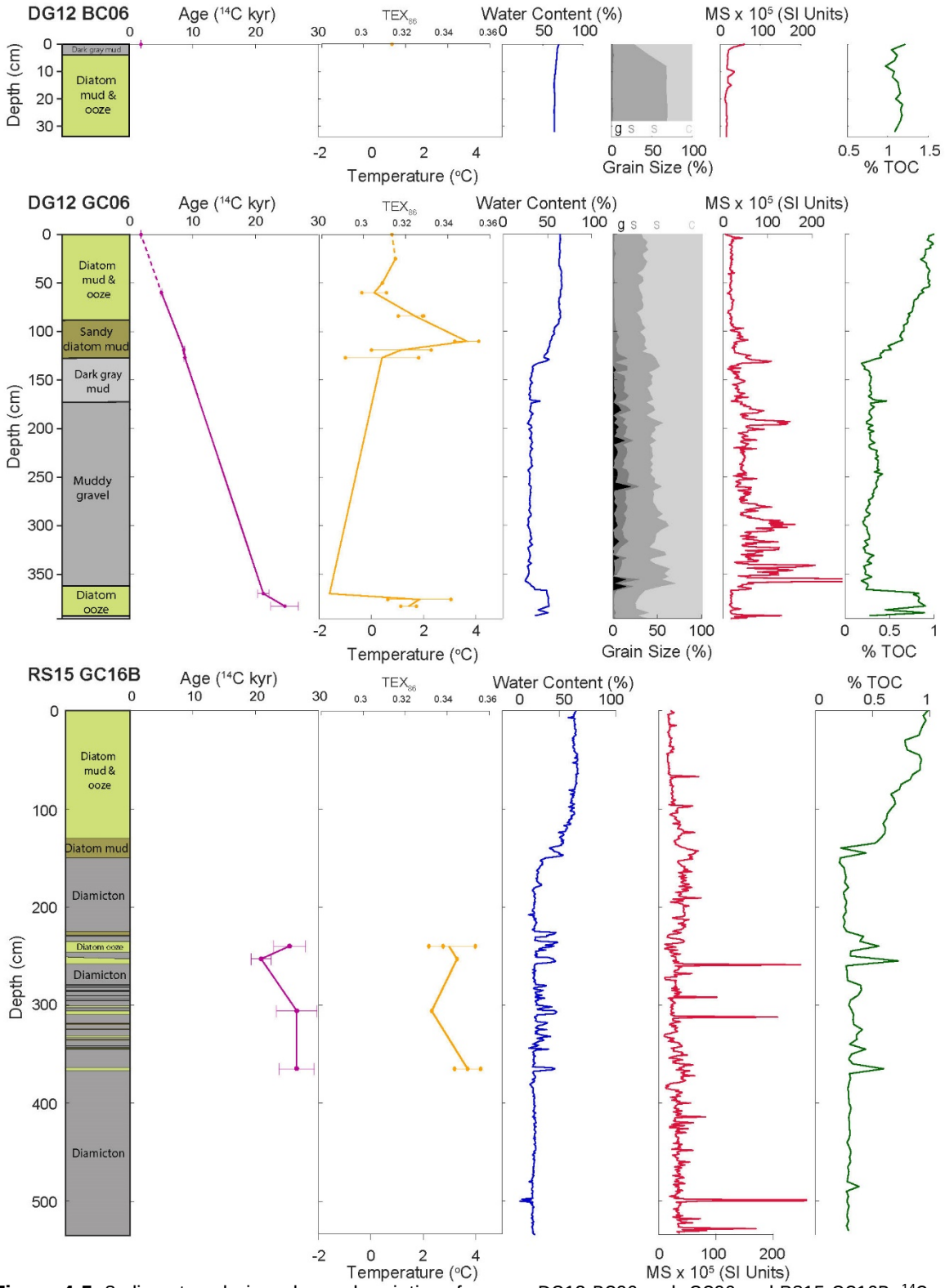

Figure 4.5. Sediment analysis and core descriptions for cores DG12-BC06 and -GC06 and RS15-GC16B. ^{14}C ages are shown as blank-corrected, uncalibrated Ramped PyrOx ages. Temperatures are shown using a linear Southern Ocean calibration (Shevenell et al., 2011). Uncertainty in temperature is based on duplicate and triplicate measurements of TEX_{86} values. Note the core-top temperature value of BC06 is shown also in GC06 for simplified comparison. Magnetic susceptibility (MS) is shown in SI units (x 10^5).

C4). In all cases, RP1 ^{14}C resulted in younger dates than in AIO ^{14}C. Conventional RP ^{14}C dates in the upper 127 cm of the core, within diatom mud and ooze layers, show multiple consecutive low-temperature splits are within error of each other- a pattern we refer to as “age plateaus.” The presence of these age-plateaus indicates there is little mixture of detrital material in the lowest-temperature aliquots and the RP1 ages are approaching the “true age” of the syndepositionally-aged material. Further down-core, these ages showed evidence of being highly detrital, as there is a large difference between the ages of the first two RP aliquots, and the calculated AIO ^{14}C ages are very old. These bottom samples were reanalyzed using composite RP ^{14}C dating (Subt et al., 2017). Conventional and composite RP ^{14}C dates are within 1 standard deviation of each other throughout core GC06, which implies that for these samples, conventional RP ^{14}C ages provide equal accuracy as composite RP. If the conventional RP1 splits were subsampled, it is likely that all splits within this interval would result in ages within error of each other. This lends confidence in the assumptions made for dating samples within these lower diatom ooze units, not only in core GC06, but also core GC16B, where no preliminary bulk AIO ^{14}C ages were available.

The existence of a deformational contact was evaluated using Ramped PyrOx ^{14}C analyses. A slight age reversal exists in the samples above and below this layer, which likely reflects a thrust-like deformation of the overlying diamicton (Figure 4.4). Such an increase in detrital material would bias the age of RP1 towards older ages, but have no effect on the remaining chronology. Indeed, the age of the uppermost sample is older than the underlying diatom ooze sediments, suggesting that sediments overlying the deformational contact were transported, either through slump deposits or proximity to the grounding line. Laminated sediments underlying this contact display ages in chronological order, and are in agreement with lower diatom ooze ages from core GC06, suggesting that sediments underlying the

deformational contact were deposited in situ. The ages of these samples may also be biased by bioturbation and/or reworking. However, the presence of well-preserved laminations within these diatom ooze and mud layers (intervals between 225 and 367 cm core-depth in core GC16B) indicates that bioturbation and reworking are not likely to have effected major changes on the sediments. The range of ages of lower diatom ooze samples in cores GC06 and GC16B are comparable, suggesting these ages are relatively accurate.

In a complex setting like the southwestern Ross Sea, where there is much evidence for the inclusion of multiple sources of organic carbon in the sediments, it is important to investigate and compare the available tools for analysis. Whereas Ramped PyrOx separates organic carbon from different sources based on their thermochemical characteristics, compound-specific ^{14}C dating exploits the heterogeneity of ^{14}C contents in sediments at the biomarker level. Both approaches have shown significant improvements on bulk AIO ^{14}C ages (Eglinton et al., 1996; Ohkouchi and Eglinton, 2006; Rosenheim et al., 2008; Subt et al., 2016; Subt et al., 2017; Wang et al., 1996). Several studies have successfully measured ^{14}C ages in the Ross Sea and show core-top ages are generally older than the ~1730 ^{14}C y core-top age of this study (Ohkouchi and Eglinton, 2006; Ohkouchi et al., 2003; Yokoyama et al., 2016). Downcore ages are more difficult to compare due to variable lithologies and accumulation rates found throughout the Ross Sea. However, the older core-top compound-specific ages suggest that the assumption that the biomarkers used for compound-specific analysis did not exist at the time that detrital material in these sediments was created is inaccurate. Analysis of specific biomarkers also requires significantly larger sample sizes (up to 350 g of dried sediment; Ohkouchi et al., 2003) than even composite Ramped PyrOx (<2 g). However, it is also important to note that the distance between sites measured with compound specific and

Ramped PyrOx approaches may influence this comparison, i.e. it is not a direct comparison given the small-scale regional differences in sedimentation patterns.

4.6.2 Constraints on the Timing and Style of Ice Retreat

Changes in temperature revealed through TEX_{86} paleothermometry reveal interesting patterns in relation the lithologic sequence of the cores in this study. This is most evident in core GC06, where TEX_{86} was measured through several lithologies (Figure 4.5; Appendix, Table C2). The past ~5.0 ^{14}C kyr have been characterized by generally slow warming upper ocean temperatures in the Ross Sea (from ~-0.1 to ~0.8°C). Apparent temperatures show relative cooling ranging from ~3.7 to ~-0.1 °C from ~8.0 to ~5.0 ka BP. These conditions were preceded by rapid warming (from ~0.4 to ~3.7°C) ~8.7 to ~8.0 ^{14}C ka BP, and cooling through the preceding ~3 ^{14}C ka BP. Although we were unable to measure temperatures from diamicton stages due to the scarcity of organic material through these time periods, temperatures are remarkably warm through lower diatom muds and oozes underlying and interlaminated with diamicton layers, which are inferred to be periods of open-water conditions ~20.8 to 26.6 ^{14}C ka BP. In the most recent deglaciation, the warmest temperatures occur prior to the deposition of diatom oozes, suggesting that warm temperatures played an important role in ice retreat.

Warm temperatures in the western Ross Sea during the LGM may be linked to CDW impinging on the continental shelf. In modern Ross Sea conditions, the strong, westward-flowing Antarctic Slope Current (ASC) is the major division between the Antarctic Surface Water (AASW) on the Ross shelf and the CDW on the lower continental slope (Smith et al., 2012). The ASC limits the transport of CDW and modified CDW (mCDW) onto the shelf (Ainley and Jacobs, 1981; Orsi and Wiederwohl, 2009; Whitworth et al., 1998). Nevertheless, heat and salt

budgets, the regional sea ice cycle, and primary productivity in the Ross Sea are all highly dependent on CDW transport to the shelf (Smith et al., 2012). Weakening ASC, caused by fluctuations in Southern Hemisphere Westerly Winds speed and position, could allow for greater on-shelf CDW transport (Dinniman et al., 2012; Dinniman et al., 2011; Spence et al., 2014).

The improved chronology in these cores illustrates more dynamic ice behavior during Holocene retreat than previously reported, supporting recent sedimentary evidence of spatial complexity (Halberstadt et al., 2016). Reconstructions of ice sheet extent have estimated post-LGM grounding line retreat through the western Ross Embayment reached the latitude of the Drygalski Ice Tongue ~12,275 uncorrected ^{14}C yr BP (9,850 cal yr BP; Anderson et al., 2014; Cunningham et al., 1999). The Drygalski Ice Tongue itself likely formed at least ~4 kyrs ago, based on ^{14}C dates of penguin guago (Baroni and Orombelli, 1994), thus this feature was not present at the time of deglaciation. The calculated and measured bulk AIO ^{14}C age of sediments in the same relative stratigraphic position in this study show a similar result (12,295 uncorrected ^{14}C yr or 9,853 cal yr BP; Table 4.1, Figure 4.5). Our RP ^{14}C chronology places the most recent retreat of the grounding line past the Drygalski Ice Tongue by ~8,740 ^{14}C yr BP (~7540 cal yr BP after applying the standard 1200 yr reservoir-age correction for this region applied to previous dates (Cunningham et al., 1999)). Although the reservoir age has likely changed over time, no ^{14}C dating technique on marine sediments can resolve potential changes in reservoir age due to the inherent bias from surrounding waters. As previous estimates of the timing of the latest grounding line retreat rely on marine bulk AIO ^{14}C dates along the western Ross Sea, which are known to be problematic (e.g. Andrews et al., 1999; Cunningham et al., 1999; Licht et al., 1999; Licht et al., 1996; McKay et al., 2008), updated Ramped PyrOc ^{14}C dates in this study produce a more accurate chronology of retreat and offer insights into the dynamic ice retreat style.

Four distinct laminated diatom ooze layers were measured in core GC16B, which were used to resolve the timing of individual retreat sequences. The bottommost two ooze units show no significant difference in ^{14}C dates, thus with the exception of the topmost diatom ooze layers, which overlies a deformational contact, ^{14}C dates of laminated diatom oozes in this core are in chronological order. The older ^{14}C age of the topmost diatom ooze layer, which also coincides with ^{14}C dates of the bottom two ooze layers is probably the result of deformation of this layer, possibly due to slumping sediments, which would likely preserve laminations, but result in an age reversal due to transport of sediment facies. There is no evidence that sediments underlying the deformation contact underwent any effects from deformation or transport, thus these sediments are interpreted to have been deposited in situ. Bulk AIO ^{14}C dates of the same sediments showed a very different chronology, with the youngest age occurring in the lowermost diatom ooze layer (Appendix, Table C3). However, advanced Ramped PyrOx ^{14}C dating was able to resolve the timing of individual retreats by removing the effects from changing proportions of relict organic material. The combined chronology and paleotemperature record can provide a great deal of information about the dynamic Ross ice sheet behavior through the LGM.

It has long been assumed that a stable ice sheet covering the Ross Embayment was at its maximum thickness and extent during the LGM (e.g. Anderson et al., 2014; Halberstadt et al., 2016; Kellogg et al., 1979; Licht et al., 1999; Licht et al., 1999; Mosola and Anderson, 2006; Shipp et al., 1999). The existence of several retreat sequences dated between 20.8 and 26.6 ka BP provides clear evidence to contradict this notion, of retreating and re-advancing ice during most of the LGM. These findings are supported by a growing body of evidence for ice sheet instability in the Ross Sea during the LGM, for which the implications have been largely ignored or misinterpreted. Licht et al., (1996; 1999) argued that ice on the middle and outer continental

shelf of the western Ross Sea was not grounded prior to and during the LGM. Tephra layers, which could only occur in open-water conditions, occur near Coulman Island. As tephra layers themselves cannot be dated, ^{14}C above and below these layers were used to determine their deposition between 22 and 26 ka BP (Figure 4.5; Licht et al., 1999). Further south, uncorrected ^{14}C dates of bulk organic material underlying diamict sediments along the Drygalski Trough coincide with calculated and measured bulk AIO ^{14}C ages of LGM retreat sequences in this study (Cunningham et al., 1999). Similarly, grounding line retreat in the middle shelf of the eastern Ross Sea sector was found to have begun ~27.5 ka BP (Bart and Cone, 2012), prior to the LGM; however, no mechanism was offered to explain this early retreat. Ages shown in Figure 4.3 show tie-points between cores in the western Ross Sea based on both isochrons and stratigraphic similarities. It is evident from the ties made between core stratigraphies (only 272 m apart) in this analysis that lithologies are not laterally continuous. This may in part be due to more dynamic Ross ice sheet responses to climate, sea level and seawater conditions than has previously been assumed for the LGM. Variations in the typical deglacial sequence may also be a sign of winnowing of

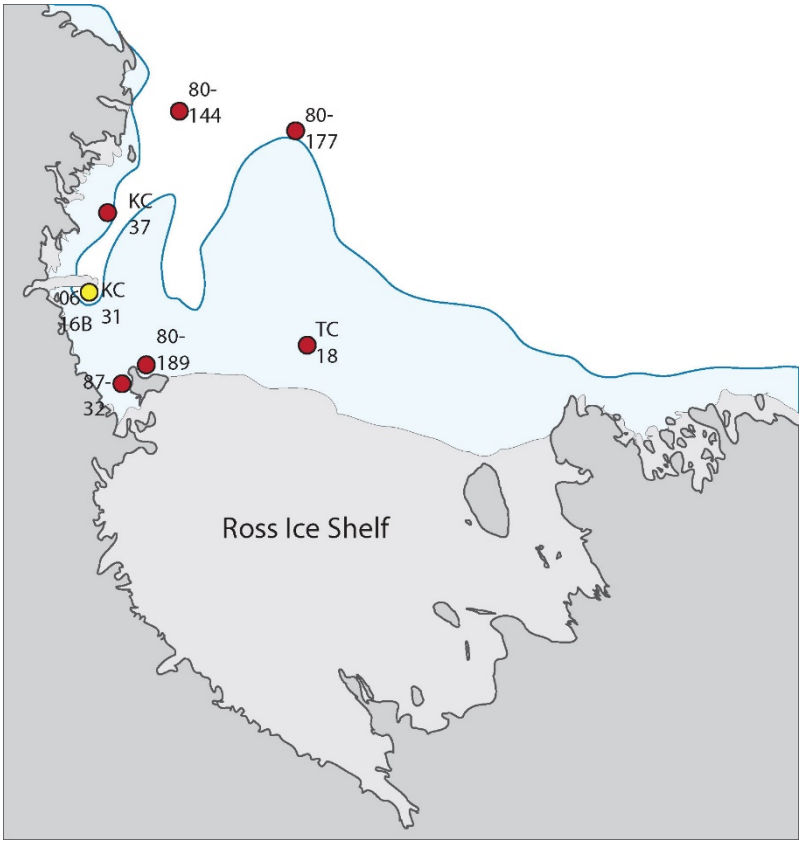

Figure 4.6. Reconstruction of grounded ice extent during the LGM. Red and yellow dots correspond with core sites discussed in Figure 4.3 and this study, respectively. Modern grounded ice extent is shown in dark gray and light gray outlines show modern ice shelf extent. Reconstructed LGM grounded ice extent is shown in blue.

older sediments by bottom currents (e.g. Licht et al., 1999; Licht, 2004; Cunningham et al., 1999).

The most likely scenario to explain the dynamic grounding line behavior in the western Ross Sea during the LGM involves a grounding line that retreated to the inner shelf along the deepest troughs prior to the LGM. Changes in water temperature and other potential forcings, such as atmospheric temperatures and CO_2 concentrations or variations in Southern Ocean circulation, caused fluctuations in the grounding line position between ~20.8 and 26.6 ka BP. Following this period of instability, the grounding line re-advanced and reached its maximum extent after ~13.8 ka BP (Licht and Andrews, 2002). An ice shelf formed after the grounding line maximum extent was attained ~8.7 ^{14}C ka BP, as evidenced by a hiatus in ^{14}C dates on the outer continental shelf (Licht et al., 1996), and sub-ice shelf sediments recovered from this region (Licht et al., 1995). Carbonate and AIO ^{14}C dates within diamicton sediments through the Drygalski and JOIDES troughs correspond to calculated bulk AIO dates in this study, and tend to occur in chronological order prior to and during the LGM (Figure 4.3) (e.g. Cunningham et al., 1999; Domack et al., 1999a; Licht et al., 1996; Licht et al., 1999; Licht and Andrews, 2002). Previous research has shown that highly detrital sediments are much more likely to produce age reversals and indistinguishably “old” dates due to changing proportions of labile and relict material in the sediments (e.g. Rosenheim et al., 2008; Rosenheim et al., 2013; Subt et al., 2016; Subt et al., 2013). Thus, the chronological ordering of these dates may also indicate sediments in the Drygalski Trough were deposited in a sub-ice shelf environment during and after the LGM. Had they been deposited in a true subglacial setting, these sediments would likely produce much older or even infinite ages due to the very high proportions of relict detrital material, which would preclude most ^{14}C dating techniques. Permanent open ocean conditions did not occur until ~8.5 ka BP (Figure 4.6).

An increase in temperature or intrusion of warm water can catalyze a sudden ice sheet collapse, even during a glacial period (e.g. Jacobs et al., 2011; Rignot and Jacobs, 2002; Schoof, 2007). Fluctuating strength and position of the Southern Hemisphere Westerly Winds could allow for warm CDW onlapping onto the continental shelf (Dinniman et al., 2012; Dinniman et al., 2011; Spence et al., 2014), which in turn likely influenced the stability of the grounding line position during the LGM. The timing of the early retreat also appears to coincide with the retreat of grounded ice from the Eastern Weddell Sea (e.g. Anderson and Andrews, 1999; Elverhoi, 1981). One or more of these events may also correspond with the Antarctic Isotope Maximum-2 (AIM2) event that has been identified through ice core CH_4 and $\delta^{18}O$ records (EPICA Community Members, 2006), which occurred between 23 and 24 ka BP and is characterized by pronounced millennial-scale variability of warming episodes prior to and during the LGM. Millennial-scale warming events have previously been observed in marine sediments through IRD deposits (Weber et al., 2014; Nielsen and Hodell, 2007) and sea ice records (Collins et al., 2012). Warmer ocean waters intruding onto the shelf in the Ross Sea may have also caused retreat of the ice stream in the the Drygalski Trough (Waddington et al., 2006),.

It is very likely that collapse occurred only regionally as a response to warm subsurface CDW intruding up-shelf through the deepest troughs of the Ross Sea, impacting an already vulnerable region of the ice sheet. However, it is still prudent to explore other potential scenarios to explain these data. One such scenario is the existence of temporary polynyas or the complete early collapse of the Ross ice sheet during the LGM. Smith et al. (2010) described similar lithologies, which were interpreted as seasonal or perennial polynyas that coincide with the LGM and Marine Isotope Stage (MIS) 2 as well as middle MIS 3. Warm upper ocean temperatures derived from this study could lead to the formation of open-ocean polynyas, which are typically formed from upwelling of warm deep water over deeper water depths might

have been possible if ice in the Drygalski Trough had no grounded ice sheet, allowing for a warm water incursion. However, the sedimentary evidence is not consistent with a polynya setting (Figure 4.5). Bathymetric data near the core sites as well as the deformational surface in the sediments both suggest these sediments were deposited proximal to the grounding line during the LGM, which would encumber the formation of multiple polynyas, as these form in regions covered by sea ice and not by ice shelves. Early collapse of the Ross ice sheet is equally unlikely, given the overwhelming evidence for grounded ice sheets through the LGM, as well as the paucity of open-water sedimentation throughout most of the Ross Sea prior to ~8ka.

The "marine-based hypothesis" for grounding line retreat in the Ross Sea provides strong evidence for asynchronous retreat between troughs (Figure 4.2), but relies mostly on existing bulk AIO ^{14}C dates to constrain the timing of the changes observed (Figure 4.3) (Halberstadt et al., 2016). This study shows evidence in support of the "marine-based" model, and applies an improved chronology and updated high-resolution multibeam bathymetry from the Drygalski Ice Tongue to show that early and rapid retreat of the grounding line occurred during the LGM (Figure 4.6). Although the maximum grounding line position in the Drygalski Trough has been well-established north of Coulman Island (Anderson et al., 2014; Halberstadt et al., 2016; Kellogg et al., 1979; Licht et al., 1999; Shipp et al., 1999), this study strongly suggests this maximum position did not occur at the LGM as has been previously assumed.

4.7 Conclusions

The improved chronology of ice behavior during and after the LGM places the most recent retreat of the grounding line in the Ross Embayment past the DIT ~8.7 ka BP, at least 1000 years earlier than previous estimates due to the separation of thermochemical components in the sediments. Prior retreats of grounded ice in the Ross Sea occurred multiple

times between 20.8 and 26.6 ka BP. Overall temperature trends suggest retreat of the grounding line was largely caused by warm ocean waters flooding the region, which may have been the result of warm CDW intrusions onto the continental shelf, facilitated by weakened Antarctic Slope Current and fluctuating strength and position of Southern Hemisphere Westerly Winds. This research challenges the assumption that ice in the Ross Sea remained grounded and stable throughout the LGM, and instead shows evidence of dynamic ice sheet responses to warmer water temperatures.

CHAPTER 5:

CONCLUSIONS

Since AIO and carbonate Antarctic sediments were first ^{14}C-dated in the George V and Adélie margin by Domack et al. (1989), it has been abundantly clear that traditional ^{14}C-dating techniques are not always accurate for Antarctic marine marginal sediments. Several inconsistencies in these first AMS ^{14}C dates illustrated the difficulties of dating Antarctic marginal marine sediments. Nevertheless, other detailed analyses of many other outlet systems along the Antarctic margins soon followed. Gordon and Harkness (1992) examined reservoir ages in Antarctic sediments and found high variability both geographically and with the type of material dated, further complicating the interpretation of ^{14}C dates in these extreme regions. Andrews et al. (1999) demonstrated additional difficulties in dating Antarctic sediments due to regional differences, changing sediment accumulation rates, and differences in the proportions of pre-aged organic C between samples. During the late 1990's and early 2000's, the first consistent AIO ^{14}C dates in the Ross Sea were measured, but required large surface age corrections (e.g. Cunningham et al., 1999; Licht et al., 1998; Licht et al., 1999; Licht et al., 1996; Shipp et al., 1999).

Despite the increasing awareness of the many problems with ^{14}C-dating of Antarctic sediments, there have also been many advances and improvements of dating approaches. This progress has allowed for the expansion of the applicability of ^{14}C dating in many regions. One example of this is the high-resolution chronology for Palmer Deep sediments achieved by combining carbonate and organic carbon ^{14}C dates that are in excellent agreement in a high-

sedimentation setting (Domack et al., 2001). Indeed, highly productive regions like the Palmer Deep pose fewer problems for dating as there is substantially less admixture of pre-aged organic material and higher accumulation rates that limit the effects of reworking. Alternative approaches to ^{14}C dating have also been employed for more problematic regions. Compound-specific ^{14}C dating of fatty acids has been applied to sediments from the Ross Sea with some success (Ohkouchi et al., 2003; Yokoyama et al., 2016), but this approach typically requires very large sample sizes that limit its application. Ramped PyrOx ^{14}C dating has significantly improved upon bulk AIO ^{14}C dating since it was first developed (Rosenheim et al., 2008). It requires substantially less sediment than CS ^{14}C dating and has produced remarkable improvement in results. These approaches have all contributed to the growing collection of information about Antarctic paleoceanography, but there is still much to be learned.

The first research project in this dissertation (Chapter 2) sought to examine the applicability of Ramped PyrOx ^{14}C dating and compare it against carbonate ^{14}C dates of similar or equal depths within the same core. The overarching hypothesis of this dissertation is that dating of Antarctic sediments can be improved using alternative techniques. The findings of this project support the hypothesis. By sampling RP1 splits at slightly lower temperatures than in previous studies, the RP ^{14}C chronology from Lapeyrère Bay is in good agreement with carbonate ^{14}C dates of equal or similar core depths. However, with the use of smaller RP1 splits, there is a higher cost in analytical uncertainty. This research also meets the main objectives of this dissertation by providing improvements on the RP ^{14}C dating technique and ameliorating the effects of pre-aged organic material in the sediments. This research also examined the application of a reservoir correction and established that when Ramped PyrOx and carbonate dates are similar, a reservoir age can be equally applied to both during the calibration. However, no ^{14}C dating technique used on marine water or sediments can remove the effects of

old reservoir ages due to the inherent bias of the ^{14}C reservoir to carbonaceous material in the ocean. Because reservoir ages through time have remained poorly constrained, reservoir corrections applied on sediments downcore, especially where changes in setting and lithology take place, should be applied cautiously. Additionally, this research showed that the common core-top age correction applied to most Antarctic ^{14}C chronologies may have insidious effects on the chronology.

The findings from the first project as well as previous Ramped PyrOx ^{14}C analyses suggested that by sampling increasingly small low-temperature splits, the resulting ^{14}C age would incorporate smaller proportions of relict organic carbon. Doing so would concentrate the labile organic component in the first split, but decreasing sample sizes would also decrease the precision due to analytical uncertainty. In the second research project of this dissertation (Chapter 3), we analyzed sediment samples from a site adjacent to the Larsen C ice shelf. These sediments were found to have been deposited in a sub-ice shelf setting, and incorporated a large proportion of relict detrital material. Based on previous Ramped PyrOx ^{14}C dating, it was intuitively inferred that the conventional Ramped PyrOx approach would not sufficiently separate the relict organic component in the sample. By analyzing the ultra-small splits required for a more accurate analysis of these samples, the analytical precision associated with such small samples would render the results to be infinite ages. For this reason, this research developed two different alternate techniques for Ramped PyrOx ^{14}C dating, which involved repeated identical analyses of the sample and/or the addition of a diluent of known age. Both alternate Ramped PyrOx ^{14}C dating techniques provide significant improvements in the accuracy of ^{14}C dates relative to other dating approaches used. Small differences between these techniques can be explained by sample heterogeneity, blank contamination, and error propagation. The findings from this project strongly support the overarching hypothesis. By

applying alternate Ramped PyrOx techniques that allow for sampling ultra-small splits of sample, we both improve the accuracy, and minimize the uncertainty. The results of this project also meet with the objectives of the dissertation through the successful development and application of alternate Ramped PyrOx techniques. In doing so, we have expanded the applicability of ^{14}C dating to new limits and provided the first sub-ice shelf sediment chronology.

Sediments in the Ross Sea and Antarctic Peninsula have been targeted for paleoceanographic studies due to their accessibility and proximity to major research stations. In this dissertation, we analyzed samples from both regions in three very different sedimentary environments. Whereas chapters 2 and 3 focused on sediments from the Antarctic Peninsula, chapter 4 focused on the Drygalski Through. Although constraints on the timing of grounding line retreat was relatively well constrained for the western Ross Sea by measuring carbonates and organic material, these estimates remained in disagreement with terrestrial estimates of ice retreat. The third and final research project of this dissertation (Chapter 4) thus focused on applying techniques developed and explored in Chapters 2 and 3 to sediments from cores taken south of the Drygalski Ice Tongue in order to address this disagreement. The lithology of these cores shows not only the most recent retreat of the grounding line, but a number of prior retreats and re-advances that indicate open-water conditions. We applied a combination of conventional and composite Ramped PyrOx ^{14}C dates to the Drygalski sediments. Our results indicated that the most recent grounding line retreat past the Drygalski Ice Tongue occurred by ~8.7 ka BP, > 2 ka earlier than past estimates had determined. The lithology of the cores analyzed in this study suggested an unstable grounding line, which retreated several times. ^{14}C dates of these sediments indicated the ice sheet instability occurred between 20.8 and 26.6 ka BP, coinciding with the LGM. When comparing conventional and composite Ramped PyrOx ^{14}C ages in two samples analyzed by both techniques, the results were nearly identical, indicating

that the application of composite Ramped PyrOx may have been over-applied. That is, fewer composites would likely have yielded the same degree of accuracy and would have been easier to analyze. The results of this study also met the objectives of this dissertation in that we expanded the application of Ramped PyrOx techniques to deeper sedimentary sequences that have often gone undated due to the high amount of relict organic material that biases the age of these sediments. To determine the possible causes of an unstable ice sheet during the LGM, we applied TEX_{86} paleothermometry, and found that warm surface waters predominated during the LGM. It is possible that an intrusion of warm CDW could have caused temporary collapses of the ice sheet in the Ross Sea, but to determine a mechanism for this intrusion, further research needs to be conducted to determine the extent of this intrusion.

The importance of sediment chronology cannot be overstated. The need for accurate dating methods in polar sediments has been one of the greatest limitations for reconstructing past events along the Antarctic margins. The research of this dissertation has demonstrating the versatility of the Ramped PyrOx ^{14}C approach for dating these sediments through the use of various new techniques. The availability of techniques like those described herein lessens the limitations on geoscientists working in sediments from the Antarctic margin. Ultimately, through innovative use of established approaches, we are now capable of accurately analyzing sediments in sub-ice shelf, subglacial and glacial settings. Besides the utility of these techniques in gaining a wider understanding of the Antarctic ice dynamics during the Late Pleistocene-Holocene glacial period, the techniques described here may prove useful for other studies as well. For example, sub-ice shelf sediments could serve as a modern analog for Cryogenian research (e.g. Hoffman et al., 2012; Vincent et al., 2000). These techniques allow researchers to study ice sheet behavior not only during the deglacial period, but into the glacial period as

well. Thus, by using these techniques, we can not only date late Quaternary Antarctic marine sediments, where highly detrital material has precluded ^{14}C dating in the past.

REFERENCES

Ackert , R., 2008. Swinging gate or Saloon doors: Do we need a new model of Ross Sea deglaciation?, Fifteenth West Antarctic Ice Sheet Meeting, Sterling, Virginia.

Adhikari, P.L., Maiti, K., Overton, E.B., Rosenheim, B.E. and Marx, B.D., 2016. Distributions and accumulation rates of polycyclic aromatic hydrocarbons in the northern Gulf of Mexico sediments. Environmental Pollution, 212: 413-423.

Ainley, D.G. and Jacobs, S.S., 1981. Sea-bird affinities for ocean and ice boundaries in the Antarctic. Deep Sea Research Part A. Oceanographic Research Papers, 28(10): 1173-1185.

Alley, R.B. and Bindschadler, R.A., 2013. The West Antarctic Ice Sheet and Sea-Level Change, The West Antarctic Ice Sheet: Behavior and Environment. American Geophysical Union, pp. 1-11.

Alonso-Sáez, L., Waller, A.S., Mende, D.R., Bakker, K., Farnelid, H., Yager, P.L., Lovejoy, C., Tremblay, J.-É., Potvin, M., Heinrich, F., Estrada, M., Riemann, L., Bork, P., Pedrós-Alió, C. and Bertilsson, S., 2012. Role for urea in nitrification by polar marine Archaea. Proceedings of the National Academy of Sciences, 109(44): 17989-17994.

Anderson, J.B. and Andrews, J.T., 1999. Radiocarbon constraints on ice sheet advance and retreat in the Weddell Sea, Antarctica. Geology, 27(2): 179-182.

Anderson, J.B., Conway, H., Bart, P.J., Witus, A.E., Greenwood, S.L., McKay, R.M., Hall, B.L., Ackert, R.P., Licht, K., Jakobsson, M. and Stone, J.O., 2014. Ross Sea paleo-ice sheet drainage and deglacial history during and since the LGM. Quaternary Science Reviews, 100: 31-54.

Anderson, J.B., Kennedy, D.S., Smith, M.J. and Domack, E.W., 1991. Sedimentary facies associated with Antarctica's floating ice masses. Geological Society of America Special Papers, 261: 1-26.

Anderson, J.B., Shipp, S.S., Bartek, L.R. and Reid, D.E., 1992. Evidence for a Grounded Ice Sheet on the Ross Sea Continental Shelf During the Late Pleistocene and Preliminary Paleodrainage Reconstruction. In: D.H. Elliot (Editor), Contributions to Antarctic Research III. American Geophysical Union, Washington, D. C., pp. 39-62.

Anderson, J.B., Shipp, S.S., Lowe, A.L., Wellner, J.S. and Mosola, A.B., 2002. The Antarctic Ice Sheet during the Last Glacial Maximum and its subsequent retreat history: a review. Quaternary Science Reviews, 21(1): 49-70.

Andrews, J.T., Domack, E.W., Cunningham, W.L., Leventer, A., Licht, K.J., Jull, A., DeMaster, D.J. and Jennings, A.E., 1999. Problems and possible solutions concerning radiocarbon dating of surface marine sediments, Ross Sea, Antarctica. Quaternary Research, 52(2): 206-216.

Ashley, G.M. and Smith, N.D., 2000. Marine sedimentation at a calving glacier margin. Geological Society of America Bulletin, 112(5): 657-667.

Baker, R.R. and Bishop, L.J., 2004. The pyrolysis of tobacco ingredients. Journal of Analytical and Applied Pyrolysis, 71(1): 223-311.

Bamber, J.L., Alley, R.B. and Joughin, I., 2007. Rapid response of modern day ice sheets to external forcing. Earth and Planetary Science Letters, 257(1): 1-13.

Barker, S., Knorr, G., Vautravers, M.J., Diz, P. and Skinner, L.C., 2010. Extreme deepening of the Atlantic overturning circulation during deglaciation. Nature Geosci, 3(8): 567-571.

Baroni, C. and Orombelli, G., 1994. Abandoned penguin rookeries as Holocene paleoclimatic indicators in Antarctica. Geology, 22(1): 23-26.

Bart, P.J. and Anderson, J.B., 2000. Relative temporal stability of the Antarctic ice sheets during the late Neogene based on the minimum frequency of outer shelf grounding events. Earth and Planetary Science Letters, 182(3-4): 259-272.

Bart, P.J. and Cone, A.N., 2012. Early stall of West Antarctic Ice Sheet advance on the eastern Ross Sea middle shelf followed by retreat at 27,500 14C yr BP. Palaeogeography, Palaeoclimatology, Palaeoecology, 335–336: 52-60.

Bentley, M.J., 1999. Volume of Antarctic Ice at the Last Glacial Maximum, and its impact on global sea level change. Quaternary Science Reviews, 18(14): 1569-1595.

Bentley, M.J., 2010. The Antarctic palaeo record and its role in improving predictions of future Antarctic Ice Sheet change. Journal of Quaternary Science, 25(1): 5-18.

Bentley, M.J., Ó Cofaigh, C., Anderson, J.B., Conway, H., Davies, B., Graham, A.G.C., Hillenbrand, C.-D., Hodgson, D.A., Jamieson, S.S.R., Larter, R.D., Mackintosh, A., Smith, J.A., Verleyen, E., Ackert, R.P., Bart, P.J., Berg, S., Brunstein, D., Canals, M., Colhoun, E.A., Crosta, X., Dickens, W.A., Domack, E., Dowdeswell, J.A., Dunbar, R., Ehrmann, W., Evans, J., Favier, V., Fink, D., Fogwill, C.J., Glasser, N.F., Gohl, K., Golledge, N.R., Goodwin, I., Gore, D.B., Greenwood, S.L., Hall, B.L., Hall, K., Hedding, D.W., Hein, A.S., Hocking, E.P., Jakobsson, M., Johnson, J.S., Jomelli, V., Jones, R.S., Klages, J.P., Kristoffersen, Y., Kuhn, G., Leventer, A., Licht, K., Lilly, K., Lindow, J., Livingstone, S.J., Massé, G., McGlone, M.S., McKay, R.M., Melles, M., Miura, H., Mulvaney, R., Nel, W., Nitsche, F.O., O'Brien, P.E., Post, A.L., Roberts, S.J., Saunders, K.M., Selkirk, P.M., Simms, A.R., Spiegel, C., Stolldorf, T.D., Sugden, D.E., van der Putten, N., van Ommen, T., Verfaillie, D., Vyverman, W., Wagner, B., White, D.A., Witus, A.E. and Zwartz, D., 2014. A community-based geological reconstruction of Antarctic Ice Sheet deglaciation since the Last Glacial Maximum. Quaternary Science Reviews, 100(0): 1-9.

Berger, W.H. and Johnson, R.F., 1978. On the thickness and the ^{14}C age of the mixed layer in deep-sea carbonates. Earth and Planetary Science Letters, 41(2): 223-227.

Berkman, P.A. and Forman, S.L., 1996. Pre-bomb radiocarbon and the reservoir correction for calcareous marine species in the Southern Ocean. Geophysical Research Letters, 23(4): 363-366.

Bianchi, T.S., Galy, V., Rosenheim, B.E., Shields, M., Cui, X. and Van Metre, P., 2015. Paleoreconstruction of organic carbon inputs to an oxbow lake in the Mississippi River watershed: Effects of dam construction and land use change on regional inputs. Geophysical Research Letters, 42(19): 7983-7991.

Bice, K.L., Birgel, D., Meyers, P.A., Dahl, K.A., Hinrichs, K.-U. and Norris, R.D., 2006. A multiple proxy and model study of Cretaceous upper ocean temperatures and atmospheric CO2 concentrations. Paleoceanography, 21(2): PA2002.

Bindschadler, R., 1998. Future of the West Antarctic Ice Sheet. Science, 282(5388): 428-429.

Bindschadler, R.A., King, M.A., Alley, R.B., Anandakrishnan, S. and Padman, L., 2003. Tidally Controlled Stick-Slip Discharge of a West Antarctic Ice. Science, 301(5636): 1087-1089.

Blunier, T., Chappellaz, J., Schwander, J., Dällenbach, A., Stauffer, B., Stocker, T., Raynaud, D., Jouzel, J., Clausen, H.B. and Hammer, C.U., 1998. Asynchrony of Antarctic and Greenland climate change during the last glacial period. Nature, 394(6695): 739-743.

Bougamont, M., Tulaczyk, S. and Joughin, I., 2003. Numerical investigations of the slow-down of Whillans Ice Stream, West Antarctica: is it shutting down like Ice Stream C? Annals of Glaciology, 37(1): 239-246.

Brachfeld, S., Domack, E., Kissel, C., Laj, C., Leventer, A., Ishman, S., Gilbert, R., Camerlenghi, A. and Eglinton, L.B., 2003. Holocene history of the Larsen-A Ice Shelf constrained by geomagnetic paleointensity dating. Geology, 31(9): 749-752.

Brambati, A., Fanzutti, G.P., Finocchiaro, F., Melis, R., Frignani, M., Ravaioli, M. and Setti, M., 1997. Paleoenvironmental Record in Core Anta91-30 (Drygalski Basin, Ross Sea, Antarctica). In: P.F. Barker and A.K. Cooper (Editors), Geology and Seismic Stratigraphy of the Antarctic Margin, 2. American Geophysical Union, Washington, D. C., pp. 137-151.

Broecker, W.S., 1963. A preliminary evaluation of uranium series inequilibrium as a tool for absolute age measurement on marine carbonates. Journal of Geophysical Research, 68(9): 2817-2834.

Burke, A. and Robinson, L.F., 2012. The Southern Ocean's Role in Carbon Exchange During the Last Deglaciation. Science, 335(6068): 557-561.

Caniupán, M., Lamy, F., Lange, C.B., Kaiser, J., Arz, H., Kilian, R., Baeza Urrea, O., Aracena, C., Hebbeln, D., Kissel, C., Laj, C., Mollenhauer, G. and Tiedemann, R., 2011. Millennial-scale sea surface temperature and Patagonian Ice Sheet changes off southernmost Chile (53°S) over the past ~60 kyr. Paleoceanography, 26(3): PA3221.

Carlson, A.E. and Clark, P.U., 2012. Ice sheet sources of sea level rise and freshwater discharge during the last deglaciation. Reviews of Geophysics, 50(4).

Carré, M., Jackson, D., Maldonado, A., Chase, B.M. and Sachs, J.P., 2016. Variability of ^{14}C reservoir age and air–sea flux of CO2 in the Peru–Chile upwelling region during the past 12,000 years. Quaternary Research, 85(1): 87-93.

Cearreta, A. and Murray, J.W., 2000. AMS ^{14}C dating of Holocene estuarine deposits: consequences of high-energy and reworked foraminifera. The Holocene, 10(1): 155-159.

Clark, P.U., Dyke, A.S., Shakun, J.D., Carlson, A.E., Clark, J., Wohlfarth, B., Mitrovica, J.X., Hostetler, S.W. and McCabe, A.M., 2009. The last glacial maximum. Science, 325(5941): 710-714.

Clark, P.U., Mitrovica, J.X., Milne, G.A. and Tamisiea, M.E., 2002. Sea-Level Fingerprinting as a Direct Test for the Source of Global Meltwater Pulse IA. Science, 295(5564): 2438-2441.

Clark, P.U. and Mix, A.C., 2002. Ice sheets and sea level of the Last Glacial Maximum. Quaternary Science Reviews, 21(1–3): 1-7.

Collins, L.G., Pike, J., Allen, C.S. and Hodgson, D.A., 2012. High-resolution reconstruction of southwest Atlantic sea-ice and its role in the carbon cycle during marine isotope stages 3 and 2. Paleoceanography, 27(3): PA3217.

Conway, H., Hall, B.L., Denton, G.H., Gades, A.M. and Waddington, E.D., 1999. Past and Future Grounding-Line Retreat of the West Antarctic Ice Sheet. Science, 286(5438): 280-283.

Cook, A., Fox, A., Vaughan, D. and Ferrigno, J., 2005. Retreating glacier fronts on the Antarctic Peninsula over the past half-century. Science, 308(5721): 541-544.

Cooper, A.K., Barrett, P.J., Hinz, K., Traube, V., Letichenkov, G. and Stagg, H.M.J., 1991. Cenozoic prograding sequences of the Antarctic continental margin: a record of glacio-eustatic and tectonic events. Marine Geology, 102(1): 175-213.

Cunningham, W.L., Leventer, A., Andrews, J.T., Jennings, A.E. and Licht, K.J., 1999. Late Pleistocene-Holocene marine conditions in the Ross Sea, Antarctica: evidence from the diatom record. The Holocene, 9(2): 129-139.

de Jong, W., Pirone, A. and Wójtowicz, M.A., 2003. Pyrolysis of Miscanthus Giganteus and wood pellets: TG-FTIR analysis and reaction kinetics. Fuel, 82(9): 1139-1147.

DeConto, R.M. and Pollard, D., 2016. Contribution of Antarctica to past and future sea-level rise. Nature, 531(7596): 591-597.

DeMaster, D.J., Ragueneau, O. and Nittrouer, C.A., 1996. Preservation efficiencies and accumulation rates for biogenic silica and organic C, N, and P in high-latitude sediments: The Ross Sea. Journal of Geophysical Research: Oceans, 101(C8): 18501-18518.

Denton, G.H. and Hughes, T.J., 2002. Reconstructing the Antarctic Ice Sheet at the Last Glacial Maximum. Quaternary Science Reviews, 21(1–3): 193-202.

Denton, G.H. and Marchant, D.R., 2000. The geologic basis for a reconstruction of a grounded ice sheet in McMurdo Sound, Antarctica, at the Last Glacial Maximum. Geografiska Annaler: Series A, Physical Geography, 82(2-3): 167-211.

Deschamps, P., Durand, N., Bard, E., Hamelin, B., Camoin, G., Thomas, A.L., Henderson, G.M., Okuno, J.i. and Yokoyama, Y., 2012. Ice-sheet collapse and sea-level rise at the Bolling warming 14,600[thinsp]years ago. Nature, 483(7391): 559-564.

Dinniman, M.S., Klinck, J.M. and Smith, W.O., 2011. A model study of Circumpolar Deep Water on the West Antarctic Peninsula and Ross Sea continental shelves. Deep Sea Research Part II: Topical Studies in Oceanography, 58(13): 1508-1523.

Dinniman, M.S., Klinck, J.M. and Hofmann, E.E., 2012. Sensitivity of Circumpolar Deep Water transport and ice shelf basal melt along the West Antarctic Peninsula to changes in the winds. Journal of Climate, 25: 4799-4816.

Domack, E.W., Amblàs, D., Gilbert, R., Brachfeld, S., Camerlenghi, A., Rebesco, M., Canals, M. and Urgeles, R., 2006. Subglacial morphology and glacial evolution of the Palmer deep outlet system, Antarctic Peninsula. Geomorphology, 75(1): 125-142.

Domack, E.W., Duran, D., Leventer, A., Ishman, S., Doane, S., McCallum, S., Amblas, D., Ring, J., Gilbert, R. and Prentice, M., 2005. Stability of the Larsen B ice shelf on the Antarctic Peninsula during the Holocene epoch. Nature, 436(7051): 681-685.

Domack, E.W. and Ishman, S., 1993. Oceanographic and physiographic controls on modern sedimentation within Antarctic fjords. Geological Society of America Bulletin, 105(9): 1175-1189.

Domack, E.W., Jacobson, E.A., Shipp, S. and Anderson, J.B., 1999a. Late Pleistocene–Holocene retreat of the West Antarctic Ice-Sheet system in the Ross Sea: Part 2—Sedimentologic and stratigraphic signature. Geological Society of America Bulletin, 111(10): 1517-1536.

Domack, E.W., Jull, A.J.T., Anderson, J.B., Linick, T.W. and Williams, C.R., 1989. Application of tandem accelerator mass-spectrometer dating to late Pleistocene-Holocene sediments of the East Antarctic continental shelf. Quaternary Research, 31(2): 277-287.

Domack, E.W., Leventer, A., Dunbar, R., Taylor, F., Brachfeld, S. and Sjunneskog, C., 2001. Chronology of the Palmer Deep site, Antarctic Peninsula: a Holocene palaeoenvironmental reference for the circum-Antarctic. The Holocene, 11(1): 1-9.

Domack, E.W., Ship, S. and Anderson, J., 1999b. Late Pleistocene–Holocene retreat of the West Antarctic Ice-Sheet system in the Ross Sea: part 1—geophysical results. Geological Society of America Bulletin, 111(10): 1486-1516.

Domack, E.W. and Williams, C.R., 1990. Fine Structure and Suspended Sediment Transport in Three Antarctic Fjords, Contributions to Antarctic Research I. Antarctic Research Series. American Geophysical Union, pp. 71-89.

Dowdeswell, J.A., Ottesen, D., Evans, J., Cofaigh, C.Ó. and Anderson, J.B., 2008. Submarine glacial landforms and rates of ice-stream collapse. Geology, 36(10): 819-822.

Eglinton, T.I., Aluwihare, L.I., Bauer, J.E., Druffel, E.R.M. and McNichol, A.P., 1996. Gas Chromatographic Isolation of Individual Compounds from Complex Matrices for Radiocarbon Dating. Analytical Chemistry, 68(5): 904-912.

Eglinton, T.I., Benitez-Nelson, B.C., Pearson, A., McNichol, A.P., Bauer, J.E. and Druffel, E.R.M., 1997. Variability in Radiocarbon Ages of Individual Organic Compounds from Marine Sediments. Science, 277(5327): 796-799.

Elderfield, H. and Ganssen, G., 2000. Past temperature and [delta]18O of surface ocean waters inferred from foraminiferal Mg/Ca ratios. Nature, 405(6785): 442-445.

Elling, F.J., Könneke, M., Lipp, J.S., Becker, K.W., Gagen, E.J. and Hinrichs, K.-U., 2014. Effects of growth phase on the membrane lipid composition of the thaumarchaeon Nitrosopumilus maritimus and their implications for archaeal lipid distributions in the marine environment. Geochimica et Cosmochimica Acta, 141(Supplement C): 579-597.

Elling, F.J., Könneke, M., Mußmann, M., Greve, A. and Hinrichs, K.-U., 2015. Influence of temperature, pH, and salinity on membrane lipid composition and TEX86 of marine planktonic thaumarchaeal isolates. Geochimica et Cosmochimica Acta, 171(Supplement C): 238-255.

Elverhoi, A., 1981. Evidence for a late Wisconsin glaciation of the Weddell Sea. Nature, 293(5834): 641-642.

EPICA Community Members, 2006. One-to-one coupling of glacial climate variability in Greenland and Antarctica. Nature, 444(7116): 195-198.

Fairbanks, R.G., 1989. A 17, 000-year glacio-eustatic sea level record: influence of glacial melting rates on the Younger Dryas event and deep-ocean circulation. Nature, 342(6250): 637-642.

Fernandez, A., Santos, G.M., Williams, E.K., Pendergraft, M.A., Vetter, L. and Rosenheim, B.E., 2014. Blank Corrections for Ramped Pyrolysis Radiocarbon Dating of Sedimentary and Soil Organic Carbon. Analytical Chemistry, 86(24): 12085-12092.

Ferrigno, J., Cook, A., Mathie, A., Williams, R., Swithinbank, C., Foley, K., Fox, A., Thomson, J. and Sievers, J., 2008. Coastal-Change and Glaciological Map of the Larsen Ice Shelf Area, Antarctica: 1940–2005. Geologic Investigations Series Map I–2600–B. Antarctica, U.S. Geological Survey, Reston, Virginia, 28 pp.

Gaglioti, B.V., Mann, D.H., Jones, B.M., Pohlman, J.W., Kunz, M.L. and Wooller, M.J., 2014. Radiocarbon age-offsets in an arctic lake reveal the long-term response of permafrost carbon to climate change. J. Geophys. Res.: Biogeosci., 119(8): 1630-1651.

Golledge, N.R., Kowalewski, D.E., Naish, T.R., Levy, R.H., Fogwill, C.J. and Gasson, E.G.W., 2015. The multi-millennial Antarctic commitment to future sea-level rise. Nature, 526(7573): 421-425.

Golledge, N.R., Menviel, L., Carter, L., Fogwill, C.J., England, M.H., Cortese, G. and Levy, R.H., 2014. Antarctic contribution to meltwater pulse 1A from reduced Southern Ocean overturning. Nature Communications, 5: 5107.

Gordon, J.E. and Harkness, D.D., 1992. Magnitude and geographic variation of the radiocarbon content in Antarctic marine life: implications for reservoir corrections in radiocarbon dating. Quaternary Science Reviews, 11(7): 697-708.

Greenwood, S.L., Gyllencreutz, R., Jakobsson, M. and Anderson, J.B., 2012. Ice-flow switching and East/West Antarctic Ice Sheet roles in glaciation of the western Ross Sea. Geological Society of America Bulletin, 124(11-12): 1736-1749.

Griffith, T.W. and Anderson, J.B., 1989. Climatic control of sedimentation in bays and fjords of the northern Antarctic Peninsula. Marine Geology, 85(2–4): 181-204.

Guitard, M., 2015. Millennial-scale variability of a major East Antarctic Outlet Glacier during the last glaciation, University of South Florida, Scholar Commons, 1 - 45 pp.

Gustavson, T.C. and Boothroyd, J.C., 1987. A depositional model for outwash, sediment sources, and hydrologic characteristics, Malaspina Glacier, Alaska: A modern analog of the southeastern margin of the Laurentide Ice Sheet. Geological Society of America Bulletin, 99(2): 187-200.

Halberstadt, A.R.W., Simkins, L.M., Greenwood, S.L. and Anderson, J.B., 2016. Past ice-sheet behaviour: retreat scenarios and changing controls in the Ross Sea, Antarctica. The Cryosphere, 10(3): 1003-1020.

Hall, B.L. and Henderson, G.M., 2001. Use of uranium-thorium dating to determine past ^{14}C reservoir effects in lakes: examples from Antarctica. Earth and Planetary Science Letters, 193(3): 565-577.

Hemingway, J.D.e.a., in prep. An inverse model for relating organic carbon thermal reactivity and isotope composition using Ramped PyrOx.

Hendy, C.H. and Hall, B.L., 2006. The radiocarbon reservoir effect in proglacial lakes: Examples from Antarctica. Earth and Planetary Science Letters, 241(3–4): 413-421.

Heroy, D.C. and Anderson, J.B., 2005. Ice-sheet extent of the Antarctic Peninsula region during the Last Glacial Maximum (LGM)—Insights from glacial geomorphology. Geological Society of America Bulletin, 117(11-12): 1497-1512.

Heroy, D.C. and Anderson, J.B., 2007. Radiocarbon constraints on Antarctic Peninsula ice sheet retreat following the Last Glacial Maximum (LGM). Quaternary Science Reviews, 26(25): 3286-3297.

Hoffman, P.F., Halverson, G.P., Domack, E.W., Maloof, A.C., Swanson-Hysell, N.L. and Cox, G.M., 2012. Cryogenian glaciations on the southern tropical paleomargin of Laurentia (NE Svalbard and East Greenland), and a primary origin for the upper Russøya (Islay) carbon isotope excursion. Precambrian Research, 206–207: 137-158.

Hughes, T., 1973. Is the West Antarctic Ice Sheet disintegrating? Journal of Geophysical Research 78, 7884–7910.

Huguet, C., Martens-Habbena, W., Urakawa, H., Stahl, D.A. and Ingalls, A.E., 2010. Comparison of extraction methods for quantitative analysis of core and intact polar glycerol dialkyl

glycerol tetraethers (GDGTs) in environmental samples. Limnology and Oceanography: Methods, 8(4): 127-145.

Hurley, S.J., Elling, F.J., Könneke, M., Buchwald, C., Wankel, S.D., Santoro, A.E., Lipp, J.S., Hinrichs, K.-U. and Pearson, A., 2016. Influence of ammonia oxidation rate on thaumarchaeal lipid composition and the TEX86 temperature proxy. Proceedings of the National Academy of Sciences, 113(28): 7762-7767.

Huybrechts, P., 2002. Sea-level changes at the LGM from ice-dynamic reconstructions of the Greenland and Antarctic ice sheets during the glacial cycles. Quaternary Science Reviews, 21(1–3): 203-231.

Ingalls, A.E., 2016. Palaeoceanography: Signal from the subsurface. Nature Geosci, 9(8): 572-573.

Ingalls, A.E., Anderson, R.F. and Pearson, A., 2004. Radiocarbon dating of diatom-bound organic compounds. Marine Chemistry, 92(1–4): 91-105.

Ingalls, A.E. and Pearson, A., 2005. Ten years of compound-specific radiocarbon analysis. Oceanography, 18(3): 18.

Issler, D.R. and Snowdon, L.R., 1990. Hydrocarbon generation kinetics and thermal modelling, Beaufort-Mackenzie Basin. Bulletin of Canadian Petroleum Geology, 38(1): 1-16.

Jacobs, S.S., Amos, A.F. and Bruchhausen, P.M., 1970. Ross sea oceanography and antarctic bottom water formation. Deep Sea Research and Oceanographic Abstracts, 17(6): 935-962.

Jacobs, S.S., Jenkins, A., Giulivi, C.F. and Dutrieux, P., 2011. Stronger ocean circulation and increased melting under Pine Island Glacier ice shelf. Nature Geoscience, 4(8): 519-523.

Joughin, I. and Alley, R.B., 2011. Stability of the West Antarctic ice sheet in a warming world. Nature Geosci, 4(8): 506-513.

Joughin, I., Bindschadler, R.A., King, M.A., Voigt, D., Alley, R.B., Anandakrishnan, S., Horgan, H., Peters, L., Winberry, P., Das, S.B. and Catania, G., 2005. Continued deceleration of Whillans Ice Stream, West Antarctica. Geophysical Research Letters, 32(22): n/a-n/a.

Joughin, I. and Tulaczyk, S., 2002. Positive Mass Balance of the Ross Ice Streams, West Antarctica. Science, 295(5554): 476-480.

Kellogg, T.B., Truesdale, R.S. and Osterman, L.E., 1979. Late Quaternary extent of the West Antarctic ice sheet: New evidence from Ross Sea cores. Geology, 7(5): 249-253.

Kim, J.-H., Schouten, S., Hopmans, E.C., Donner, B. and Sinninghe Damsté, J.S., 2008. Global sediment core-top calibration of the TEX86 paleothermometer in the ocean. Geochimica et Cosmochimica Acta, 72(4): 1154-1173.

Kim, J.-H., van der Meer, J., Schouten, S., Helmke, P., Willmott, V., Sangiorgi, F., Koç, N., Hopmans, E.C. and Damsté, J.S.S., 2010. New indices and calibrations derived from the distribution of crenarchaeal isoprenoid tetraether lipids: Implications for past sea surface temperature reconstructions. Geochimica et Cosmochimica Acta, 74(16): 4639-4654.

Kirtania, K. and Bhattacharya, S., 2012. Application of the distributed activation energy model to the kinetic study of pyrolysis of the fresh water algae Chlorococcum humicola. Bioresource Technology, 107: 476-481.

Könneke, M., Schubert, D.M., Brown, P.C., Hügler, M., Standfest, S., Schwander, T., Schada von Borzyskowski, L., Erb, T.J., Stahl, D.A. and Berg, I.A., 2014. Ammonia-oxidizing archaea use the most energy-efficient aerobic pathway for CO2 fixation. Proceedings of the National Academy of Sciences, 111(22): 8239-8244.

Lavoie, C., Domack, E.W., Pettit, E.C., Scambos, T.A., Larter, R.D., Schenke, H.W., Yoo, K.C., Gutt, J., Wellner, J., Canals, M., Anderson, J.B. and Amblas, D., 2015. Configuration of

the Northern Antarctic Peninsula Ice Sheet at LGM based on a new synthesis of seabed imagery. The Cryosphere, 9(2): 613-629.

Lawver, L., Royer, J., Sandwell, D. and Scotese, C., 1991. Evolution of the Antarctic continental margins. In: M.R.A. Thomson, J.A. Crame and J.W. Thomson (Editors), Geological evolution of Antarctica. Cambridge University Press, Cambridge, UK, pp. 533-539.

Lea, D.W., Mashiotta, T.A. and Spero, H.J., 1999. Controls on magnesium and strontium uptake in planktonic foraminifera determined by live culturing. Geochimica et Cosmochimica Acta, 63(16): 2369-2379.

Lee, J.I., McKay, R.M., Golledge, N.R., Yoon, H.I., Yoo, K.-C., Kim, H.J. and Hong, J.K., 2017a. Widespread persistence of expanded East Antarctic glaciers in the southwest Ross Sea during the last deglaciation. Geology.

Lee, J.I., Yoon, H.I., Yoo, K.C., Kim, H.J. and Hong, J.K., 2017b. Processed gridded swath bathymetry data from the Ross Sea acquired in 2013 and 2015. Marine Geoscience Data System (MGDS), Integrated Earth Data Applications (IEDA).

Leventer, A., Domack, E., Barkoukis, A., McAndrews, B. and Murray, J., 2002. Laminations from the Palmer Deep: A diatom-based interpretation. Paleoceanography, 17(3): PAL 3-1-PAL 3-15.

Leventer, A., Domack, E., Dunbar, R., Pike, J., Stickley, C., Maddison, E., Brachfeld, S., Manley, P. and McClennen, C., 2006. Marine sediment record from the East Antarctic margin reveals dynamics of ice sheet recession. GSA TODAY, 16(12): 4.

Licht, K.J. and Andrews, J.T., 2002. The ^{14}C Record of Late Pleistocene Ice Advance and Retreat in the Central Ross Sea, Antarctica. Arctic, Antarctic, and Alpine Research, 34(3): 324-333.

Licht, K.J., Cunningham, W.L., Andrews, J.T., Domack, E.W. and Jennings, A.E., 1998. Establishing chronologies from acid-insoluble organic ^{14}C dates on antarctic (Ross Sea) and arctic (North Atlantic) marine sediments. Polar Research, 17(2): 203-216.

Licht, K.J., Dunbar, N.W., Andrews, J.T. and Jennings, A.E., 1999. Distinguishing subglacial till and glacial marine diamictons in the western Ross Sea, Antarctica: Implications for a last glacial maximum grounding line. Geological Society of America Bulletin, 111(1): 91-103.

Licht, K.J., Jennings, A.E., Andrews, J.T. and Williams, K.M., 1996. Chronology of late Wisconsin ice retreat from the western Ross Sea, Antarctica. Geology, 24(3): 223-226.

Liu, Z., Pagani, M., Zinniker, D., DeConto, R., Huber, M., Brinkhuis, H., Shah, S.R., Leckie, R.M. and Pearson, A., 2009. Global Cooling During the Eocene-Oligocene Climate Transition. Science, 323(5918): 1187-1190.

Livingstone, S.J., Ó Cofaigh, C., Stokes, C.R., Hillenbrand, C.-D., Vieli, A. and Jamieson, S.S., 2012. Antarctic palaeo-ice streams. Earth-Science Reviews, 111(1): 90-128.

Lønne, I., 1995. Sedimentary facies and depositional architecture of ice-contact glaciomarine systems. Sedimentary Geology, 98(1–4): 13-43.

MacAyeal, D.R., 1992. Irregular oscillations of the West Antarctic ice sheet. Nature, 359(6390): 29-32.

Mackintosh, A., Golledge, N., Domack, E., Dunbar, R., Leventer, A., White, D., Pollard, D., DeConto, R., Fink, D. and Zwartz, D., 2011. Retreat of the East Antarctic ice sheet during the last glacial termination. Nature Geoscience, 4(3): 195-202.

Mackintosh, A.N., Verleyen, E., O'Brien, P.E., White, D.A., Jones, R.S., McKay, R., Dunbar, R., Gore, D.B., Fink, D., Post, A.L., Miura, H., Leventer, A., Goodwin, I., Hodgson, D.A., Lilly, K., Crosta, X., Golledge, N.R., Wagner, B., Berg, S., van Ommen, T., Zwartz, D.,

Roberts, S.J., Vyverman, W. and Masse, G., 2014. Retreat history of the East Antarctic Ice Sheet since the Last Glacial Maximum. Quaternary Science Reviews, 100: 10-30.

Martin, S., 2001. Polynyas. In: J.H. Steele, K.K. Turekian and S.A. Thorpe (Editors), Encyclopedia of Ocean Sciences. Academic Press, San Diego, pp. 2241-2247.

McKay, R., Golledge, N.R., Maas, S., Naish, T., Levy, R., Dunbar, G. and Kuhn, G., 2016. Antarctic marine ice-sheet retreat in the Ross Sea during the early Holocene. Geology, 44(1): 7-10.

McKay, R.M., Dunbar, G.B., Naish, T.R., Barrett, P.J., Carter, L. and Harper, M., 2008. Retreat history of the Ross Ice Sheet (Shelf) since the Last Glacial Maximum from deep-basin sediment cores around Ross Island. Palaeogeography, Palaeoclimatology, Palaeoecology, 260(1–2): 245-261.

Mead, K.A., 2012. Age estimates of holocene glacial retreat in Lapeyrere Bay, and Anvers Island Fjord, University of Houston, 90 pp.

Mercer, J.H., 1978. West Antarctic ice sheet and CO2 greenhouse effect: a threat of disaster. Nature, 271(5643): 321-325.

Michalchuk, B.R., Anderson, J.B., Wellner, J.S., Manley, P.L., Majewski, W. and Bohaty, S., 2009. Holocene climate and glacial history of the northeastern Antarctic Peninsula: the marine sedimentary record from a long SHALDRIL core. Quaternary Science Reviews, 28(27–28): 3049-3065.

Milliken, K., Anderson, J., Wellner, J., Bohaty, S. and Manley, P., 2009. High-resolution Holocene climate record from Maxwell Bay, South Shetland Islands, Antarctica. Geological Society of America Bulletin, 121(11-12): 1711-1725.

Mix, A.C., Bard, E. and Schneider, R., 2001. Environmental processes of the ice age: land, oceans, glaciers (EPILOG). Quaternary Science Reviews, 20(4): 627-657.

Mosola, A.B. and Anderson, J.B., 2006. Expansion and rapid retreat of the West Antarctic Ice Sheet in eastern Ross Sea: possible consequence of over-extended ice streams? Quaternary Science Reviews, 25(17–18): 2177-2196.

Nakada, M., Kimura, R., Okuno, J., Moriwaki, K., Miura, H. and Maemoku, H., 2000. Late Pleistocene and Holocene melting history of the Antarctic ice sheet derived from sea-level variations. Marine Geology, 167(1): 85-103.

Nielsen, S.H.H. and Hodell, D.A., 2007. Antarctic ice-rafted detritus (IRD) in the South Atlantic: Indicators of iceshelf dynamics or ocean surface conditions? 2007-1047-SRP-020, USGS, Reston, VA.

Nürnberg, D., Bijma, J. and Hemleben, C., 1996. Assessing the reliability of magnesium in foraminiferal calcite as a proxy for water mass temperatures. Geochimica et Cosmochimica Acta, 60(5): 803-814.

Ó Cofaigh, C., Davies, B.J., Livingstone, S.J., Smith, J.A., Johnson, J.S., Hocking, E.P., Hodgson, D.A., Anderson, J.B., Bentley, M.J., Canals, M., Domack, E., Dowdeswell, J.A., Evans, J., Glasser, N.F., Hillenbrand, C.-D., Larter, R.D., Roberts, S.J. and Simms, A.R., 2014. Reconstruction of ice-sheet changes in the Antarctic Peninsula since the Last Glacial Maximum. Quaternary Science Reviews, 100(0): 87-110.

Ó Cofaigh, C., Dowdeswell, J.A., Evans, J., Larter, R.D., 2008. Geological constraints on Antarctic palaeo-ice-stream retreat. Earth Surf. Process. Landforms, 33: 513–525.

Ohkouchi, N. and Eglinton, T.I., 2006. Radiocarbon constraint on relict organic carbon contributions to Ross Sea sediments. Geochemistry, Geophysics, Geosystems, 7(4): Q04012.

Ohkouchi, N. and Eglinton, T.I., 2008. Compound-specific radiocarbon dating of Ross Sea sediments: a prospect for constructing chronologies in high-latitude oceanic sediments. Quaternary Geochronology, 3(3): 235-243.

Ohkouchi, N., Eglinton, T.I. and Hayes, J.M., 2003. Radiocarbon dating of individual fatty acids as a tool for refining Antarctic margin sediment chronologies. Radiocarbon, 45(1): 17-24.

Ohkouchi, N., Eglinton, T.I., Keigwin, L.D. and Hayes, J.M., 2002. Spatial and Temporal Offsets Between Proxy Records in a Sediment Drift. Science, 298(5596): 1224-1227.

Oppenheimer, M., 1998. Global warming and the stability of the West Antarctic Ice Sheet. Nature, 393(6683): 325-332.

Orsi, A.H. and Wiederwohl, C.L., 2009. A recount of Ross Sea waters. Deep Sea Research Part II: Topical Studies in Oceanography, 56(13): 778-795.

Ottesen, D., Dowdeswell, J.A. and Rise, L., 2005. Submarine landforms and the reconstruction of fast-flowing ice streams within a large Quaternary ice sheet: The 2500-km-long Norwegian-Svalbard margin (57°–80°N). Geological Society of America Bulletin, 117(7-8): 1033-1050.

Overpeck, J.T., Otto-Bliesner, B.L., Miller, G.H., Muhs, D.R., Alley, R.B. and Kiehl, J.T., 2006. Paleoclimatic Evidence for Future Ice-Sheet Instability and Rapid Sea-Level Rise. Science, 311(5768): 1747-1750.

Pearson, A. and Ingalls, A.E., 2013. Assessing the Use of Archaeal Lipids as Marine Environmental Proxies. Annual Review of Earth and Planetary Sciences, 41(1): 359-384.

Pearson, A., McNichol, A.P., Schneider, R.J., Von Reden, K.F. and Zheng, Y., 1998. Microscale AMS ^{14}C measurement at NOSAMS. Radiocarbon, 40(1): 61-75.

Pendergraft, M.A., Dincer, Z., Sericano, J.L., Wade, T.L., Kolasinski, J. and Rosenheim, B.E., 2013. Linking ramped pyrolysis isotope data to oil content through PAH analysis. Environ. Res. Lett., 8: 044038.

Pendergraft, M.A. and Rosenheim, B.E., 2014. Varying Relative Degradation Rates of Oil in Different Forms and Environments Revealed by Ramped Pyrolysis. Environmental Science & Technology, 48(18): 10966-10974.

Please, C.P., McGuinness, M.J. and McElwain, D.L.S., 2003. Approximations to the distributed activation energy model for the pyrolysis of coal. Combustion and Flame, 133(1–2): 107-117.

Pollard, D. and DeConto, R.M., 2009. Modelling West Antarctic ice sheet growth and collapse through the past five million years. Nature, 458(7236): 329-332.

Pritchard, H.D., Ligtenberg, S.R.M., Fricker, H.A., Vaughan, D.G., van den Broeke, M.R. and Padman, L., 2012. Antarctic ice-sheet loss driven by basal melting of ice shelves. Nature, 484(7395): 502-505.

Pudsey, C., Barker, P. and Larter, R., 1994. Ice sheet retreat from the Antarctic Peninsula shelf. Continental Shelf Research, 14(15): 1647-1675.

Qin, W., Carlson, L.T., Armbrust, E.V., Devol, A.H., Moffett, J.W., Stahl, D.A. and Ingalls, A.E., 2015. Confounding effects of oxygen and temperature on the TEX86 signature of marine Thaumarchaeota. Proceedings of the National Academy of Sciences, 112(35): 10979-10984.

Rebesco, M., Domack, E., Zgur, F., Lavoie, C., Leventer, A., Brachfeld, S., Willmott, V., Halverson, G., Truffer, M., Scambos, T., Smith, J. and Pettit, E., 2014. Boundary condition of grounding lines prior to collapse, Larsen-B Ice Shelf, Antarctica. Science, 345(6202): 1354-1358.

Rignot, E. and Jacobs, S.S., 2002. Rapid Bottom Melting Widespread near Antarctic Ice Sheet Grounding Lines. Science, 296(5575): 2020-2023.

Rignot, E., Mouginot, J. and Scheuchl, B., 2011a. Ice Flow of the Antarctic Ice Sheet. Science, 333(6048): 1427-1430.

Rignot, E., Velicogna, I., van den Broeke, M.R., Monaghan, A. and Lenaerts, J.T.M., 2011b. Acceleration of the contribution of the Greenland and Antarctic ice sheets to sea level rise. Geophysical Research Letters, 38(5): n/a-n/a.

Rosenheim, B.E., Day, M.B., Domack, E., Schrum, H., Benthien, A. and Hayes, J.M., 2008. Antarctic sediment chronology by programmed-temperature pyrolysis: Methodology and data treatment. Geochemistry, Geophysics, Geosystems, 9(4): 206-216.

Rosenheim, B.E. and Galy, V., 2012. Direct measurement of riverine particulate organic carbon age structure. Geophysical Research Letters, 39(19).

Rosenheim, B.E., Roe, K.M., Roberts, B.J., Kolker, A.S., Allison, M.A. and Johannesson, K.H., 2013a. River discharge influences on particulate organic carbon age structure in the Mississippi/Atchafalaya River System. Global Biogeochemical Cycles, 27(1): 154-166.

Rosenheim, B.E., Santoro, J.A., Gunter, M. and Domack, E.W., 2013b. Improving Antarctic sediment ^{14}C dating using ramped pyrolysis: an example from the Hugo Island Trough. Radiocarbon, 55(1): 115-126.

Rosenthal, Y., Boyle, E.A. and Slowey, N., 1997. Temperature control on the incorporation of magnesium, strontium, fluorine, and cadmium into benthic foraminiferal shells from Little Bahama Bank: Prospects for thermocline paleoceanography. Geochimica et Cosmochimica Acta, 61(17): 3633-3643.

Rundle, A.S., 1973. Glaciology of the Marr Ice Piedmont, Anvers Island, Antarctica. Institute of Polar Studies Report(47).

Salonen, K., 1979. The Selection of Temperature for High Temperature Combustion of Carbon. Acta hydrochimica et hydrobiologica, 7(6): 591-597.

Santos, G.M., Southon, J.R., Drenzek, N.J., Ziolkowski, L.A., Druffel, E., Xu, X., Zhang, D., Trumbore, S., Eglinton, T.I. and Hughen, K.A., 2010. Blank assessment for ultra-small radiocarbon samples: chemical extraction and separation versus AMS. Radiocarbon, 52(2-3): 1322-1335.

Santos, G.M., Southon, J.R., Griffin, S., Beaupre, S.R. and Druffel, E.R.M., 2007. Ultra small-mass AMS ^{14}C sample preparation and analyses at KCCAMS/UCI Facility. Nucl. Instrum. Methods Phys. Res., Sect. B, 259(1): 293-302.

Sarnthein, M., Grootes, P.M., Kennett, J.P. and Nadeau, M.-J., 2013. ^{14}C reservoir ages show deglacial changes in ocean currents and carbon cycle. In: A. Schmittner, J.C.H. Chiang and S.R. Hemming (Editors), Ocean Circulation: Mechanisms and Impacts—Past and Future Changes of Meridional Overturning. American Geophysical Union, Washington, D.C., pp. 175-196.

Schoof, C., 2007. Ice sheet grounding line dynamics: Steady states, stability, and hysteresis. Journal of Geophysical Research: Earth Surface, 112(F3): F03S28.

Schoof, C., 2012. Marine ice sheet stability. Journal of Fluid Mechanics, 698: 62-72.

Schouten, S., Hopmans, E.C., Schefuß, E. and Sinninghe Damsté, J.S., 2002. Distributional variations in marine crenarchaeotal membrane lipids: a new tool for reconstructing ancient sea water temperatures? Earth and Planetary Science Letters, 204(1–2): 265-274.

Schouten, S., Huguet, C., Hopmans, E.C., Kienhuis, M.V.M. and Sinninghe Damsté, J.S., 2007. Analytical Methodology for TEX86 Paleothermometry by High-Performance Liquid

Chromatography/Atmospheric Pressure Chemical Ionization-Mass Spectrometry. Analytical Chemistry, 79(7): 2940-2944.

Schreiner, K.M., Bianchi, T.S. and Rosenheim, B.E., 2014. Evidence for permafrost thaw and transport from an Alaskan North Slope watershed. Geophysical Research Letters, 41(9): 3117-3126.

Shah, S.R., Mollenhauer, G., Ohkouchi, N., Eglinton, T.I. and Pearson, A., 2008. Origins of archaeal tetraether lipids in sediments: Insights from radiocarbon analysis. Geochimica et Cosmochimica Acta, 72(18): 4577-4594.

Shevenell, A., Ingalls, A., Domack, E. and Kelly, C., 2011. Holocene Southern Ocean surface temperature variability west of the Antarctic Peninsula. Nature, 470(7333): 250-254.

Shipp, S., Anderson, J. and Domack, E., 1999. Late Pleistocene–Holocene retreat of the West Antarctic Ice-Sheet system in the Ross Sea: Part 1—Geophysical results. Geological Society of America Bulletin, 111(10): 1486-1516.

Shipp, S.S., Wellner, J.S. and Anderson, J.B., 2002. Retreat signature of a polar ice stream: sub-glacial geomorphic features and sediments from the Ross Sea, Antarctica. Geological Society, London, Special Publications, 203(1): 277-304.

Smith, J.A., Bentley, M.J., Hodgson, D.A., Roberts, S.J., Leng, M.J., Lloyd, J.M., Barrett, M.S., Bryant, C. and Sugden, D.E., 2007. Oceanic and atmospheric forcing of early Holocene ice shelf retreat, George VI Ice Shelf, Antarctica Peninsula. Quaternary Science Reviews, 26(3): 500-516.

Smith, J.A., Hillenbrand, C.-D., Kuhn, G., Klages, J.P., Graham, A.G.C., Larter, R.D., Ehrmann, W., Moreton, S.G., Wiers, S. and Frederichs, T., 2014. New constraints on the timing of West Antarctic Ice Sheet retreat in the eastern Amundsen Sea since the Last Glacial Maximum. Global and Planetary Change, 122: 224-237.

Smith, J.A., Hillenbrand, C.-D., Pudsey, C.J., Allen, C.S. and Graham, A.G., 2010. The presence of polynyas in the Weddell Sea during the Last Glacial Period with implications for the reconstruction of sea-ice limits and ice sheet history. Earth and Planetary Science Letters, 296(3): 287-298.

Smith, W.O., Sedwick, P.N., Arrigo, K.R., Ainley, D.G. and Orsi, A.H., 2012. The Ross Sea in a Sea of Change. Oceanography, 25(3): 90-103.

Spence, P., Griffies, S.M., England, M.H., Hogg, A.M., Saenko, O.A. and Jourdain, N.C., 2014. Rapid subsurface warming and circulation changes of Antarctic coastal waters by poleward shifting winds. Geophysical Research Letters, 41(13): 4601-4610.

Stammerjohn, S.E., Martinson, D.G., Smith, R.C. and Iannuzzi, R.A., 2008. Sea ice in the western Antarctic Peninsula region: Spatio-temporal variability from ecological and climate change perspectives. Deep Sea Research Part II: Topical Studies in Oceanography, 55(18): 2041-2058.

Stocker, T.F., 2003. Global change: South dials north. Nature, 424(6948): 496-499.

Stoner, J.S., Channell, J.E.T., Hillaire-Marcel, C. and Mareschal, J.-C., 1994. High-resolution rock magnetic study of a Late Pleistocene core from the Labrador Sea. Canadian Journal of Earth Sciences, 31(1): 104-114.

Stuiver, M., Denton, G.H., Hughes, T.J. and Fastook, J.L., 1981. History of the marine ice sheet in West Antarctica during the last glaciation: a working hypothesis. The last great ice sheets: 319-436.

Stuiver, M., Pearson, G.W. and Braziunas, T.F., 1986b. Radiocarbon age calibration of marine samples back to 9000 cal yr BP. Radiocarbon, 28(2B): 980-1021.

Stuiver, M. and Polach, H.A., 1977. Discussion; reporting of C-14 data. Radiocarbon, 19(3): 355-363.

Subt, C., Fangman, K.A., Wellner, J.S. and Rosenheim, B.E., 2016. Sediment chronology in Antarctic deglacial sediments: Reconciling organic carbon ^{14}C ages to carbonate ^{14}C ages using Ramped PyrOx. The Holocene, 26(2): 265-273.

Subt, C., Yoon, H.I., Yoo, K.C., Lee, J.I., Leventer, A., Domack, E.W. and Rosenheim, B.E., 2017. Sub-ice shelf sediment geochronology utilizing novel radiocarbon methodology for highly detrital sediments. Geochemistry, Geophysics, Geosystems, 18(4): 1404-1418.

Sugden, D.E., Marchant, D.R., Denton, G.H., 1993. The case for a stable east Antarctic Ice Sheet: the background. Geografiska Annaler Series A, Physical Geography, 75(4): 151-154.

Swart, P.K., 2015. The geochemistry of carbonate diagenesis: The past, present and future. Sedimentology, 62(5): 1233-1304.

Thomas, R.H. and Bentley, C.R., 1978. A model for Holocene retreat of the West Antarctic Ice Sheet. Quaternary Research, 10(2): 150-170.

Tierney, J.E. and Tingley, M.P., 2014. A Bayesian, spatially-varying calibration model for the TEX86 proxy. Geochimica et Cosmochimica Acta, 127: 83-106.

Tierney, J.E. and Tingley, M.P., 2015. A TEX(86) surface sediment database and extended Bayesian calibration. Scientific Data, 2: 150029.

Uchida, M., Shibata, Y., Ohkushi, K.i., Yoneda, M., Kawamura, K. and Morita, M., 2005. Age discrepancy between molecular biomarkers and calcareous foraminifera isolated from the same horizons of Northwest Pacific sediments. Chemical Geology, 218(1–2): 73-89.

Valentine, D.L., 2007. Adaptations to energy stress dictate the ecology and evolution of the Archaea. Nat Rev Micro, 5(4): 316-323.

Van Geel, B. and Mook, W.G., 1989. High-Resolution ^{14}C Dating of Organic Deposits Using Natural Atmospheric ^{14}C Variations. Radiocarbon, 31(2): 151-155.

Vaughan, D. and Doake, C., 1996. Recent atmospheric warming and retreat of ice shelves on the Antarctic Peninsula. Nature, 379(6563): 328-331.

Vaughan, D.G., Marshall, G.J., Connolley, W.M., King, J.C. and Mulvaney, R., 2001. Devil in the Detail. Science, 293(5536): 1777-1779.

Vincent, F.W., Gibson, E.J.A., Pienitz, R., Villeneuve, V., Broady, A.P., Hamilton, B.P. and Howard-Williams, C., 2000. Ice Shelf Microbial Ecosystems in the High Arctic and Implications for Life on Snowball Earth. Naturwissenschaften, 87(3): 137-141.

Waddington, E.D., Conway, H., Steig, E.J., Alley, R.B., Brook, E.J., Taylor, K.C. and White, J.W.C., 2005. Decoding the dipstick: Thickness of Siple Dome, West Antarctica, at the Last Glacial Maximum. Geology, 33(4): 281-284.

Wang, Y., Amundson, R. and Trumbore, S., 1996. Radiocarbon Dating of Soil Organic Matter. Quaternary Research, 45(3): 282-288.

Weaver, A.J., Saenko, O.A., Clark, P.U. and Mitrovica, J.X., 2003. Meltwater Pulse 1A from Antarctica as a Trigger of the Bølling-Allerød Warm Interval. Science, 299(5613): 1709-1713.

Weber, M.E., Clark, P.U., Kuhn, G., Timmermann, A., Sprenk, D., Gladstone, R., Zhang, X., Lohmann, G., Menviel, L., Chikamoto, M.O., Friedrich, T. and Ohlwein, C., 2014. Millennial-scale variability in Antarctic ice-sheet discharge during the last deglaciation. Nature, 510: 134.

Weertman, J., 1974. Stability of the Junction of an Ice Sheet and an Ice Shelf. Journal of Glaciology, 13(67): 3-11.

Wellner, J.S., Lowe, A.L., Shipp, S.S. and Anderson, J.B., 2001. Distribution of glacial geomorphic features on the Antarctic continental shelf and correlation with substrate: implications for ice behavior. Journal of Glaciology, 47(158): 397-411.

Whitworth, T., Orsi, A.H., Kim, S.J., Nowlin, W.D. and Locarnini, R.A., 2013. Water Masses and Mixing Near the Antarctic Slope Front, Ocean, Ice, and Atmosphere: Interactions at the Antarctic Continental Margin. American Geophysical Union, pp. 1-27.

Wigley, T.M.L., Kelly, P.M., Eddy, J.A., Berger, A. and Renfrew, A.C., 1990. Holocene Climatic Change, ^{14}C Wiggles and Variations in Solar Irradiance [and Discussion]. Philosophical Transactions of the Royal Society of London. Series A, Mathematical and Physical Sciences, 330(1615): 547-560.

Williams, E.K., Rosenheim, B.E., Allison, M., McNichol, A.P. and Xu, L., 2015. Quantification of refractory organic material in Amazon mudbanks of the French Guiana Coast. Marine Geology, 363: 93-101.

Williams, E.K., Rosenheim, B.E., McNichol, A.P. and Masiello, C.A., 2014. Charring and non-additive chemical reactions during ramped pyrolysis: Applications to the characterization of sedimentary and soil organic material. Organic Geochemistry, 77(0): 106-114.

Wright, A.P., Siegert, M.J., Le Brocq, A.M. and Gore, D.B., 2008. High sensitivity of subglacial hydrological pathways in Antarctica to small ice-sheet changes. Geophysical Research Letters, 35(17): L17054.

Wycech, J., Kelly, D.C. and Marcott, S., 2016. Effects of seafloor diagenesis on planktic foraminiferal radiocarbon ages. Geology, 44(7): 551-554.

Xiao, W., Frederichs, T., Gersonde, R., Kuhn, G., Esper, O. and Zhang, X., 2016. Constraining the dating of late Quaternary marine sediment records from the Scotia Sea (Southern Ocean). Quaternary Geochronology, 31: 97-118.

Yamane, M., Yokoyama, Y., Miyairi, Y., Suga, H., Matsuzaki, H., Dunbar, R.B. and Ohkouchi, N., 2014. Compound-specific ^{14}C dating of IODP Expedition 318 Core U1357A obtained off the Wilkes Land Coast, Antarctica. Radiocarbon, 56(3): 1009-1017.

Yokoyama, Y., Anderson, J.B., Yamane, M., Simkins, L.M., Miyairi, Y., Yamazaki, T., Koizumi, M., Suga, H., Kusahara, K., Prothro, L., Hasumi, H., Southon, J.R. and Ohkouchi, N., 2016. Widespread collapse of the Ross Ice Shelf during the late Holocene. Proceedings of the National Academy of Sciences, 113(9): 2354-2359.

Yokoyama, Y., Lambeck, K., De Deckker, P., Johnston, P. and Fifield, L.K., 2000. Timing of the Last Glacial Maximum from observed sea-level minima. Nature, 406(6797): 713-716.

APPENDIX A:
PERMISSION TO REPRODUCE PUBLISHED WORKS

The following is taken directly from the SAGE Publishing webpage detailing permissions for the author of:

Subt, C., K.A. Fangman, J.S. Wellner, and B.E. Rosenheim (2016), Sediment chronology in Antarctic deglacial sediments: Reconciling organic carbon ^{14}C ages to carbonate ^{14}C ages using Ramped PyrOx, *The Holocene*, *26*(2), 265-273.

"If you are a SAGE journal author requesting permission to reuse material from your journal article, please note you may be able to reuse your content without requiring permission from SAGE. Please review SAGE's author re-use and archiving policies at https://us.sagepub.com/en-us/nam/journal-author-archiving-policies-and-re-use for more information."

The following is taken directly from the Geochemistry, Geophysics, Geosystems webpage detailing permissions for the author of:

Subt, C., H.I. Yoon, K.C. Yoo, J.I. Lee, A. Leventer, E. Domack, and B. Rosenheim (2017), Sub-ice shelf sediment geochronology utilizing novel radiocarbon methodology for highly detrital sediments, *Geochemistry, Geophysics, Geosystems*, 18(4), 1404-1418.

"AUTHORS - If you wish to reuse your own article (or an amended version of it) in a new publication of which you are the author, editor or co-editor, prior permission is not required (with the usual acknowledgements). However, a formal grant of license can be downloaded free of charge from RightsLink if required."

APPENDIX B:

SUPPLEMENTAL INFORMATION FOR CHAPTER 3

B1. ^{14}C Blank Corrections based on 3-component mixing model of modern blank, dead blank, and sample material

RP analysis is a versatile approach that can be used for any organic material. Thus, the characterization of blank contaminants must be applicable for general use. Our approach for blank correction follows the methods of Santos et al. (2007) and Fernandez et al. (2014). The measured fraction modern (subscript M) can be written as a mixture of three components, the unknown sample material (subscript U), the "^{14}C-dead" blank (subscript dead), and the "^{14}C-modern" blank (subscript mod):

$$\delta_M = f_{dead}\delta_{dead} + f_{mod}\delta_{mod} + f_U\delta_U \quad \text{Eq. B1.1}$$

Where δ is the fraction modern (Fm) value, as described by Stuiver and Polach [1977], f is the fraction or proportion, and:

$$\sum_{i=1}^{n} f_i = 1 \quad \text{Eq. B1.2}$$

Fm values above are written as deltas to convey the similarities of a multi-component isotopic mixing model. If we know the mass (m) of the sample and the masses of the two blank contamination components, the f's can be written as follows:

$$f_{dead} = \frac{m_{dead}}{m_{dead} + m_{mod} + m_U} \quad \text{Eq. B1.3}$$

$$f_{mod} = \frac{m_{mod}}{m_{dead} + m_{mod} + m_U} \quad \text{Eq. B1.4}$$

$$f_U = \frac{m_U}{m_{dead} + m_{mod} + m_U} \quad \text{Eq. B1.5}$$

Where:

$$\sum_{i=1}^{n} f_i = f_{dead} + f_{mod} + f_U = \frac{m_{dead}+m_{mod}+m_U}{m_{dead}+m_{mod}+m_U} = 1 \qquad \text{Eq. B1.6}$$

To solve for the unknown, we rearrange equation B1.1 as follows:

$$\delta_U = \frac{(\delta_M - f_{dead}\delta_{dead} - f_{mod}\delta_{mod})}{f_U} \qquad \text{Eq. B1.7}$$

We can then simplify equation B1.7 by writing all fraction terms as masses (substituting equations B1.3 to B1.5 in for their respective *f* variables in equation B1.7), and cancelling terms that are multiplied by the fraction modern of the dead blank ($\delta_d = 0$):

$$\delta_U = \delta_M + \delta_M \left[\frac{m_{dead}}{m_U}\right] + \delta_M \left[\frac{m_{mod}}{m_U}\right] - \delta_{mod} \left[\frac{m_{mod}}{m_U}\right] \qquad \text{Eq. B1.8}$$

From equation B1.8, we can derive an expression for the propagated analytical uncertainty as well as the uncertainties of the masses of blank contamination from:

$$\sigma_y^2 = \sum_{i=1}^{n} \sigma_{x_i}^2 \left(\frac{\partial y}{\partial x_i}\right)^2 \qquad \text{Eq. B1.9}$$

Where y=f(x_1, x_2,…,x_i).

Substituting equation B1.8 into equation B1.9, we have:

$$\sigma_{\delta_U}^2 = \sigma_{\delta_M}^2 \left[1 + \frac{m_{dead}+m_{mod}}{m_U}\right]^2 + \sigma_{m_d}^2 \left[\frac{\delta_M}{m_U}\right]^2 + \sigma_{m_{mod}}^2 \left[\frac{\delta_M - \delta_{mod}}{m_U}\right]^2 +$$

$$\sigma_{m_U}^2 \left[\frac{(\delta_{mod} m_{mod} - \delta_M m_{dead} - \delta_M m_{mod})}{m_U^2}\right]^2 \qquad \text{Eq. B1.10}$$

B2. Estimation of the fraction of syndepositionally-aged material and its temperature of combustion

We conducted a binary mixing model in which we assumed the sample consisted of two endmembers: a ^{14}C-live endmember (f_{live}) and a ^{14}C-dead endmember (f_{dead}). Thus:

$$f_{live} + f_{dead} = 1 \quad \text{Eq. B2.1}$$

We can calculate the fraction modern (Fm) values of the combined endmembers (δ_C) utilizing the weighted averaged Fm values of the ^{14}C-live material (δ_{live}) and ^{14}C-dead material (δ_{dead}):

$$\delta_c = f_{live}(\delta_{live}) + f_{dead}(\delta_{dead}) \quad \text{Eq. B2.2}$$

Here we assume that all ^{14}C-live material belongs to the fraction of syndepositionally-aged material, the ^{14}C-dead material was detrital, and the combined endmembers were equivalent to the measured bulk AIO ^{14}C age, where:

$$f_{live} = f_{SA} \quad \text{Eq. B2.3}$$

$$f_{dead} = f_{detrital} \quad \text{Eq. B2.4}$$

$$\delta_c = \delta_M \quad \text{Eq. B2.5}$$

By substituting equations B2.3 to B2.5 into equation B2.2 and assuming $\delta_{detrital}$=0, this equation can be simplified to:

$$\delta_M = f_{SA}(\delta_{SA}) \quad \text{Eq. B2.6}$$

To calculate f_{SA} for each sample, we used a conservative estimation of δ_{SA} based on the additional assumptions of a linear accumulation rate, a reservoir age of 1600 years and an uncorrected age of 13,000 years at 192 cm – a reasonable estimate for the deglaciation of the northern Antarctic Peninsula.

To calculate the temperature of combustion of the estimated amount of syndepositionally-aged material (T_1), we utilized initial sample RP analyses normalized for the number of points to

determine the CO_2 evolution of each sample. In every RP analysis, the CO_2 evolution recorded the time, temperature and pCO_2 collected at any given time.

For each sample, individual pCO_2 values were summed to determine the area under the curve (A):

$$A = \sum_{i=1}^{n} pCO_{2_i} \quad \text{Eq. B2.7}$$

Where A = f(T). The value of f_{SA} calculated for the sample using equation B2.6 was then multiplied by the total area under the curve to determine the area associated with f_{SA}.

$$A_{SA} = f_{SA}(A) \quad \text{Eq. B2.8}$$

T_1 is the temperature at which A_{SA} has been collected.

B3. Isotope dilution correction

All calculations for ^{14}C measurements are made using fraction modern (Fm) values, as described by Stuiver and Polach (1977). Isotope dilution is essentially the mixture of two components (unknown and surrogate), thus the measured Fm value (δ) can be expressed by the following equation:

$$\delta_M = f\delta_U + (1-f)\delta_S \qquad \text{Eq. B3.1}$$

where f is the fraction of the unknown relative to the total mass (unknown + surrogate), and subscripts M, U and S are the measured, unknown and surrogate (diluent), respectively.

To correct for the addition of a surrogate, equation B3.1 can be rearranged to solve for the Fm of the unknown (δ_U) as follows:

$$\boldsymbol{\delta_U = \frac{\delta_S - \delta_M - f\delta_s}{-f}} \qquad \text{Eq. B3.2}$$

To account for the associated uncertainty, the equation for propagation of error can be utilized to derive the uncertainty of δ_U:

$$\sigma_y^2 = \sum_{i=1}^{n} \sigma_{x_i}^2 \left[\frac{\partial y}{\partial x_i}\right]^2 \qquad \text{Eq. B3.3}$$

This equation can be expanded using the three variables of equation B3.2 into:

$$\sigma_{\delta_U}^2 = \sigma_f^2 \left[\frac{\partial}{\partial f}\right]^2 + \sigma_{\delta_S}^2 \left[\frac{\partial}{\partial \delta_S}\right]^2 + \sigma_{\delta_M}^2 \left[\frac{\partial}{\partial \delta_M}\right]^2 \qquad \text{Eq. B3.4}$$

The complete derived equation is thus:

$$\boldsymbol{\sigma_{\delta_U}^2 = \sigma_f^2 \left[\frac{\delta_S - \delta_M}{f^2}\right]^2 + \sigma_{\delta_S}^2 \left[1 - \frac{1}{f}\right]^2 + \sigma_{\delta_M}^2 \left[\frac{1}{f}\right]^2} \qquad \text{Eq. B3.5}$$

B4. A comparison of the propagation of uncertainty for Composite and Isotope Dilution techniques

The associated uncertainties of the composite and isotope dilution approaches are the result of the corrections that need to be applied to each. In the case of the composite approach, the blank correction is applicable, but in the case of isotope dilution, both the blank correction, and the correction for the addition of a surrogate are applicable. Thus, changes in variables incorporated into the blank correction affect both techniques. Contrarily, changes in variables incorporated into the isotope dilution correction affect only the isotope dilution techniques.

Please note that the uncertainty associated with the composite approach when only one run has been completed is the propagated error for a sample analyzed with the traditional approach.

The uncertainty associated with the composite technique was calculated by applying a blank correction to the measured Fm values of each sample. Because this technique incorporates the measured ages with the modern and dead blank contamination associated with the Ramped PyrOx (RP) approach, the Fm value can be corrected using equation B1.8, and the associated uncertainty can be propagated for the blank correction using equation B1.10.

Because certain amounts of modern and dead blank contamination are incorporated into each aliquot, it is important to account for the additional blank from the combination of multiple aliquots of the same sample involved in the composite technique. The modern blank is time-dependent (Fernandez et al., 2014), so the fraction of the collection time for individual aliquots relative to the total time it takes for a run to complete must be added for all combined aliquots and multiplied by the mass of the modern blank used in equation B1.10.

The uncertainty associated with the isotope dilution technique also involves the application of a blank-correction, which is applied first in the same way as described above for the composite

technique. The blank-corrected age is then corrected for the addition of a surrogate using equation B3.3. The associated uncertainty can then be calculated using equation B3.5.

Below are several examples of how the uncertainty of a sample is impacted using both the composite and the isotope dilution techniques when different important variables are changed.

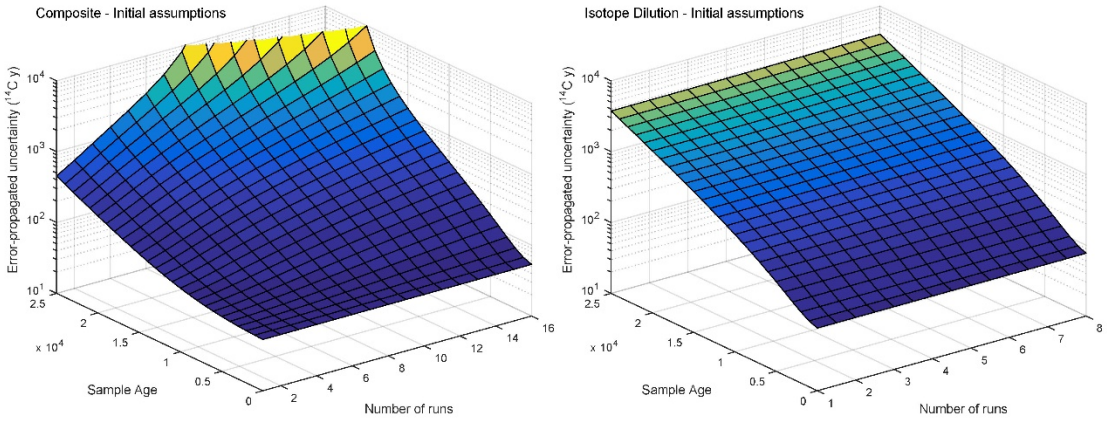

Figure B1. Initial assumptions made for Figure 3.8. f=0.7, δ_S=1.039 (Ox-I), m_U=120 mg C, mod blank values consistent with reported values in the text. It is also assumed here that the 'Sample Age' refers to the "actual age" of the sample, which is assumed to be equal to the age of the sample after it has been blank-corrected, and if applicable, isotope dilution-corrected.

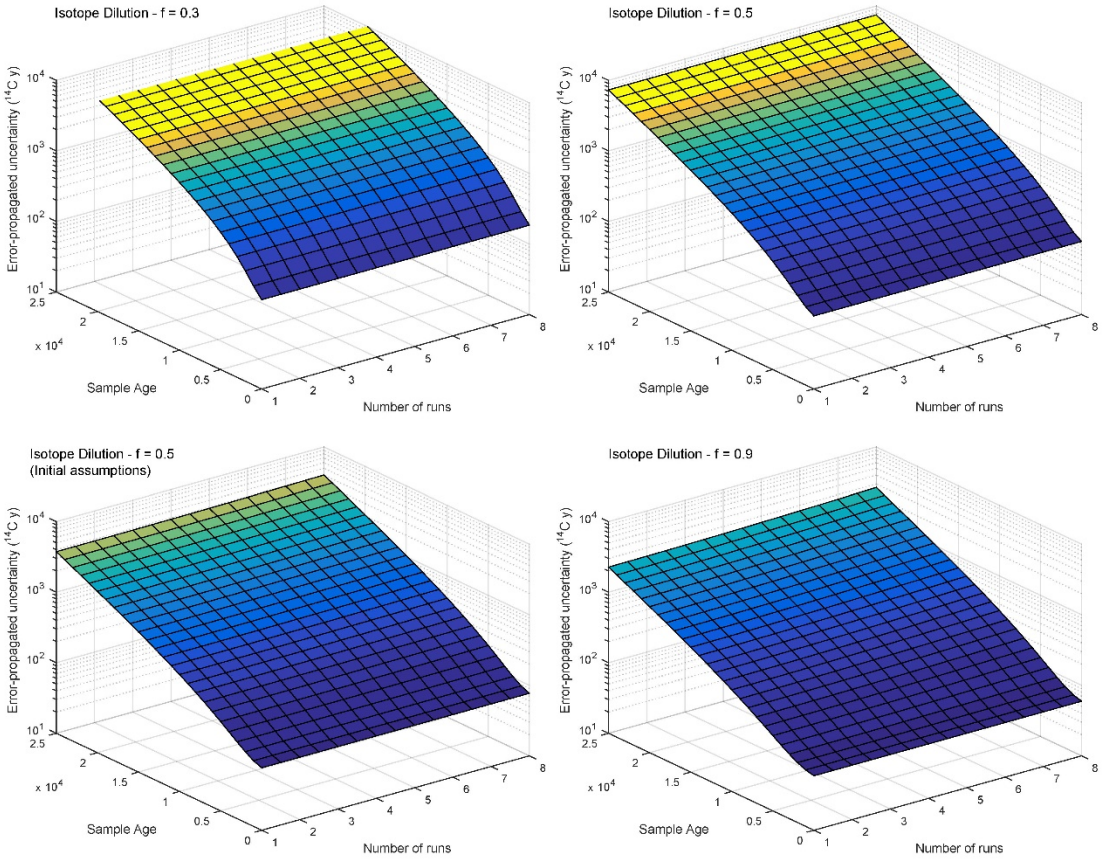

Figure B2. Effects of changes in *f* on uncertainty. Changes in *f* (fraction of sample relative to the surrogate) only affect corrections for isotope dilution.

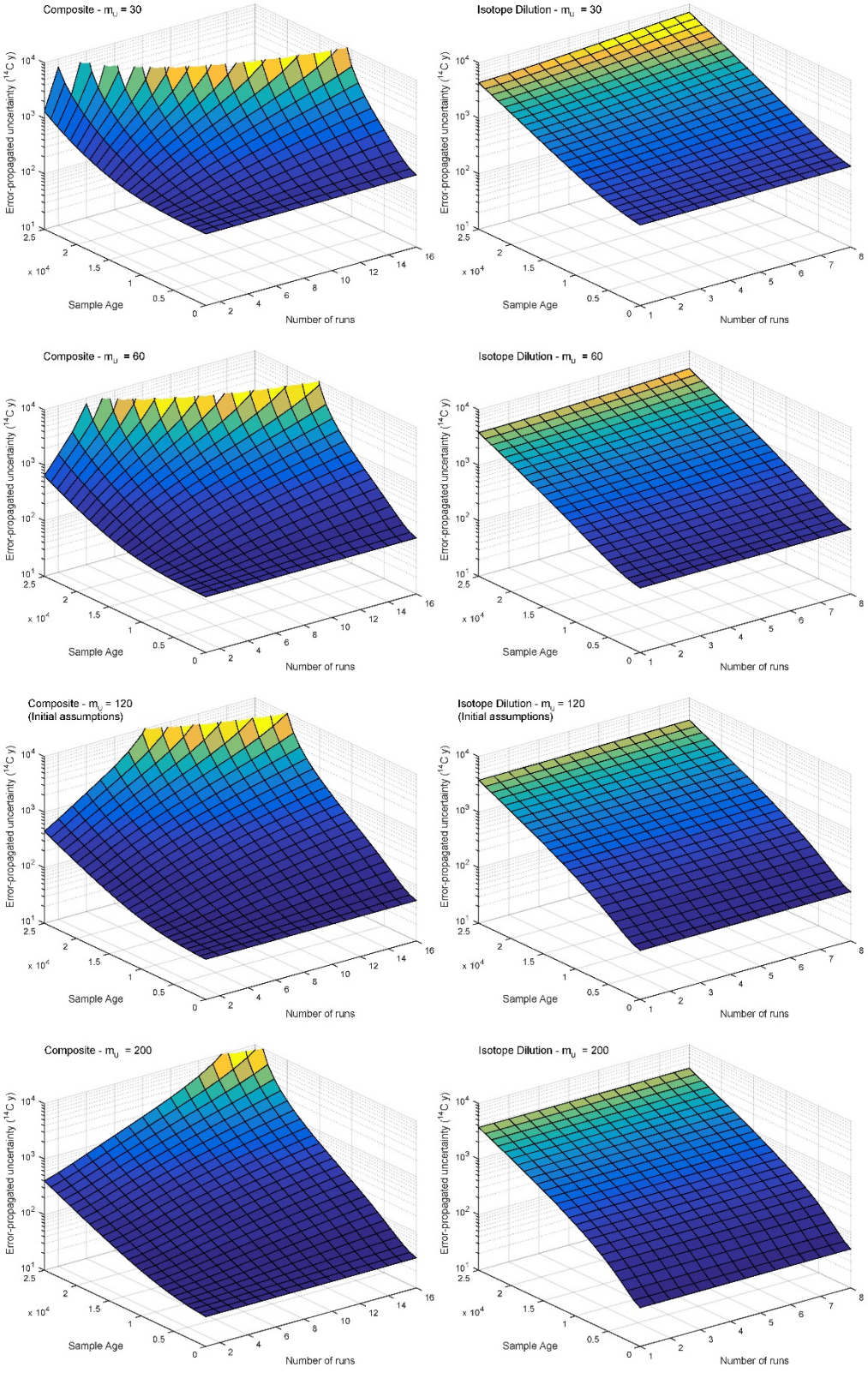

Figure B3. Effects of changes in mass (m_U) on uncertainty. Changes in mass (m_U) affects both composite and isotope dilution (because it is incorporated into the blank correction.

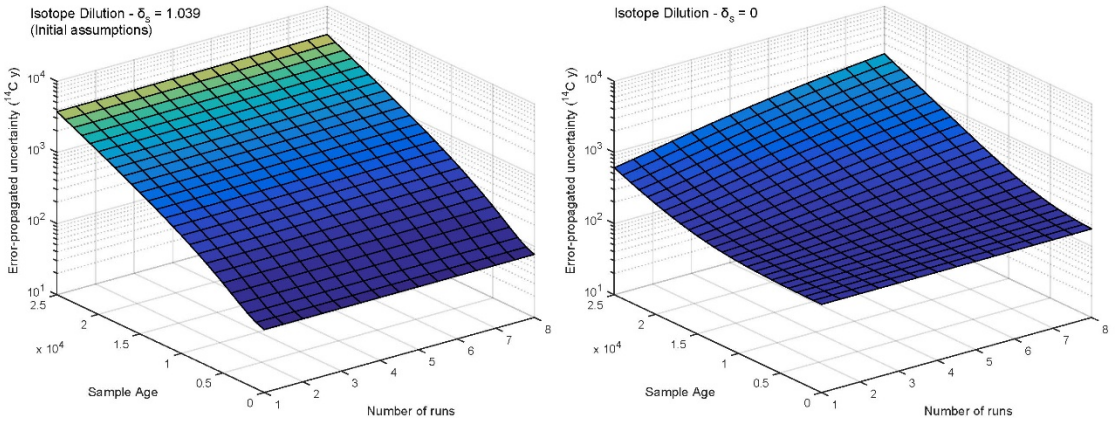

Figure B4. Effects of changes in δ_U on uncertainty. Changes in δ_U (the Fm value of the surrogate) only affects isotope dilution.

B5. Extended figures and tables

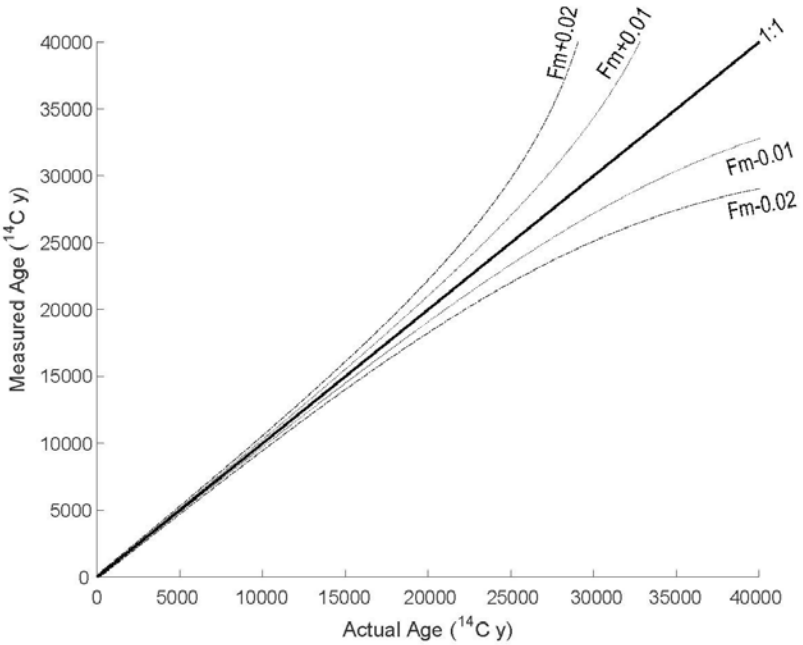

Figure B5. ^{14}C age offsets resulting from slight inaccuracies in the measured Fm value. Relatively small inaccuracies in the measured Fm value (±0.01 or ±0.02) can result in large discrepancies with the actual value when converted to ^{14}C years, especially for older samples.

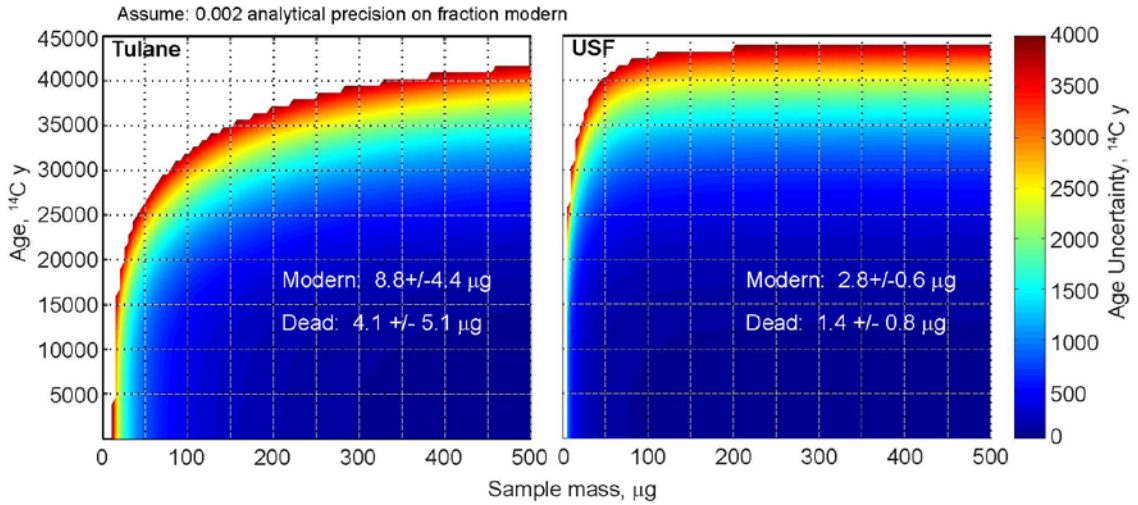

Figure B6. Recent changes in the propagated uncertainty resulting from improvements in blank contamination. The blank correction of the Ramped PyrOx system has recently been reduced from originally published Tulane values (Fernandez et al., 2014) by replacing Teflon tubing with steel.

Table B1. Information on all RP analyses and individual aliquots collected for each technique in this study. Bulk AIO analyses were used as preliminary shape runs, but were not analyzed for ^{14}C. Organic carbon recovered from each analysis is reported as %OC. Times of collection for lowest-temperature aliquots are reported as they are required for accurate blank contamination correction.

Depth (cm)	Type	Lab number	Date	Mass (mg)	T_1 (ºC)	Time RP1 (min)	%OC in RP1	m_U RP1 (µmol C)	m_U RP2 (µmol C)	m_U RP3 (µmol C)	m_U RP4 (µmol C)	m_U RP5 (µmol C)
0	Bulk	DB995	2014-10-19	60.55	800	155		15.88				
	Conventional	DB1002	2014-11-06	380.78	288	52	0.191	15.155	13.575	46.858		
		DB1079	2014-12-13	380.92	319	64	0.155	12.316	12.917	17.418	33.348	6.682
85	Bulk	DB994	2014-10-19	60.52	774	146		34.027				
	Conventional	DB1220	2015-06-15	179.34	400	82	0.148	11.982	18.318	22.06	32.79	18.524
	Composite	DB1003	2014-11-07	177.86	217	39	0.029	2.36	16.897	63.33		
		DB1004	2014-11-12	177.92	219	37	0.030	2.431	18.73	58.637		
		DB1005	2014-11-12	177.77	222	40	0.033	2.69	19.391	57.935		
		DB1006	2014-11-13	177.85	215	38	0.031	2.473	18.433	61.753		
		DB1007	2014-11-13	177.8	217	36	0.032	2.58	19.311	59.73		
		DB1009	2014-11-17	177.83	219	48	0.022	1.766	23.418	55.848		
		DB1013	2014-11-21	177.82	215	49	0.021	1.675	12.254	61.367		
		DB1018	2014-11-21	177.82	270	57	0.032	2.578				
		DB1021	2014-11-21	177.78	269	52	0.027	2.166				
		DB1035	2014-11-28	177.75	272	60	0.031	2.495				
	Isotope Dilution	DB1017	2014-11-21	177.76	274	58	0.032	2.603				
		DB1022	2014-11-21	177.75	270	55	0.028	2.223				
		DB1025	2014-11-23	177.71	270	55	0.024	1.89				
		DB1027	2014-11-24	177.77	271	65	0.027	2.194				
		DB1029	2014-11-25	177.78	270	71	0.027	2.196				
		DB1032	2014-11-27	177.75	272	60	0.028	2.228				
		DB1033	2014-11-27	177.82	270	60	0.027	2.203				
		DB1034	2014-11-28	177.76	270	61	0.028	2.246				
	Ox-I	DB1091	2014-12-15	0.212	196	38		4.18				
95	Bulk	DB993	2014-10-18	59.74	751	145		20.9				
	Composite	DB1049	2014-12-04	285.74	274	62	0.024	2.29	15.42	79.345		
		DB1050	2014-12-05	285.68	287	67	0.027	2.623	16.254	78.831		
		DB1051	2014-12-05	285.73	305	72	0.032	3.03				
		DB1058	2014-12-08	285.85	290	62	0.027	2.637				
		DB1059	2014-12-08	285.76	286	61	0.026	2.466				
		DB1071	2014-12-12	285.69	287	63	0.026	2.525				
		DB1072	2014-12-12	285.64	289	63	0.026	2.459				
		DB1073	2014-12-12	285.7	287	62	0.026	2.495				
		DB1074	2014-12-12	285.68	287	64	0.027	2.559				
	Isotope Dilution	DB1080	2014-12-13	285.71	288	58	0.028	2.681				
		DB1081	2014-12-13	285.74	288	61	0.031	2.98				
		DB1088	2014-12-14	285.7	288	62	0.033	3.156				
		DB1089	2014-12-15	285.73	288	60	0.031	2.98	11.632	88.905		
	Ox-I	DB1092	2014-12-15	0.213	171	35		4.08				
192	Bulk	DB989	2014-10-11	120.79	768	149		80				
	Conventional	DB1221	2015-06-16	146.51	397	83	0.155	13.011	18.238	25.67	13.404	11.99
	Composite	DB1037	2014-11-30	150.97	340	78	0.050	4.274	15.626	59.645		
		DB1038	2014-12-01	150.93	345	72	0.051	4.424				
		DB1039	2014-12-02	150.99	346	75	0.050	4.304				
	Isotope Dilution	DB1036	2014-11-30	150.91	339	77	0.046	3.961	13.595	62.909		
		DB1043	2014-12-02	150.92	339	73	0.049	4.242				
	Ox-I	DB1090	2014-12-15	0.441	201	39		6.9095				

Table B2. Fm values are reported in raw format, blank-corrected (BC) and isotope dilution-corrected (ID) where applicable.

Depth (cm)	Type	Fm raw	± (1σ)	Fm BC	± (1σ)	Fm ID	± (1σ)
0	Conventional RP1	0.6288	0.002	0.6320	0.0035		
0	Conventional RP1	0.6518	0.0023	0.6558	0.0043		
0	Conventional RP5	0.0238	0.0026	0.0173	0.0048		
85	Conventional RP1	0.1339	0.0008	0.1316	0.0023		
85	Conventional RP5	0.0086	0.0005	0.0060	0.0016		
192	Conventional RP1	0.1171	0.0009	0.1148	0.0022		
192	Conventional RP5	0.0152	0.0007	0.0114	0.0024		
85	Composite RP1	0.3559	0.0013	0.3295	0.0177		
95	Composite RP1	0.3013	0.0014	0.2747	0.0171		
192	Composite RP1	0.1720	0.0011	0.1540	0.0118		
85	Isotope Dilution RP1	0.5721	0.0016	0.5565	0.0132	0.3546	0.0187
95	Isotope Dilution RP1	0.5189	0.0014	0.5121	0.0082	0.2849	0.0118
192	Isotope Dilution RP1	0.6239	0.0019	0.6240	0.0051	0.2017	0.0105

APPENDIX C:

SUPPLEMENTAL INFORMATION FOR CHAPTER 4

C1. Matlab ® code for the calculation of f_{SA} as defined by Subt et al. (2017).

```
function [ fSA, runs ] = altRP1( Meas14C, Mod14C, TOC)
%AltRP: This function serves to provide an estimation of the
%proportion of syndepositionally-aged carbon (carbon that was modern
%at the time of deposition). We use a binary mixing model with two
%endmembers- one modern and one dead as in the methods outlined by
%Subt et al (2017). From this, we also calculate the number of runs
%required to accumulate this proportion from this sample if each run
%uses 400 mg of sample (the maximum mass allowed for the dirt burner).
%We account for %TOC and fSA to estimate the mass that should be
%targeted for Ramped PyrOx analyses. Depending on the nature of the
%sample, this function may also provide recommendations on the best
%course of action to take to ensure the best results.
%Inputs:
%Meas14C: is the bulk AIO 14C age of the sample. This age can be
%either measured directly for sample where fSA is needed, or it can be
%assumed based on best-guess or nearest-age approximations. Care
%should be taken with assumed ages, as the proportions of relict and
%young carbon have been shown to change drastically downcore in some
%cases. If the closest age approximation is from a different
%lithological unit, then it is more likely that the results from fSA
%will be inaccurate.
%Mod14C: is a best-guess estimate of the age of the sample in
%question. Although probably not 100 accurate, this age should be
%based on the most robust assumptions available and knowledge of the
%sampling region, lithologic unit, sedimentation rates, etc.
%TOC: Is the total organic carbon of the sample in units of per cent.
%Cristina Subt, University of South Florida, July, 2017
FmDead = 0;
%convert inputs to Fm
FmLive = exp(Mod14C/-8033);
%create vectors
flive = 0.00001:0.00001:1;
fdead = 1-flive;
CombinedFm = zeros(1,10000);
CombinedAge = zeros(1,10000);
```

```
AgeDiff = zeros(1,10000);
%Calculate fSA
for i = 1:length(flive)
    CombinedFm(i) = flive(i)*FmLive+fdead(i)*FmDead;
    CombinedAge(i) = -8033*log(CombinedFm(i));
    AgeDiff(i) = Meas14C-CombinedAge(i);
    idx = find(AgeDiff <= 0,1,'last');
    fSA = flive(1,idx);
end
fprintf('fSA = %i\n', fSA)
%Calculate amount of modern carbon
modC = ((fSA*1.2)/12)*1000;
%Start with some basic values
runs = 1;
targetmass = 120/TOC; %this is the target mass for 100 umol C
totsamp = targetmass*runs;
%Calculate the number of runs and target mass for the sample
if modC/10 >= 1
    if TOC >= 0.3
        disp(['This sample contains enough for ' num2str(modC/10) '
umol C in the first split of a 100 umol run and does not require
multiple analyses'])
        disp(['runs = ' num2str(runs)]);
        disp(['Target Mass = ' num2str(targetmass)]);
    else
        while targetmass > mass
            runs = runs+1;
            targetmass = totsamp/runs;
        end
        disp(['This sample contains enough for ' num2str(modC/10) '
umol C in the first split of a 100 umol run but requires multiple
analyses to account for very low %TOC']);
        disp(['runs = ' num2str(runs)]);
        disp(['Target Mass = ' num2str(targetmass)]);
    end
else
    if TOC >= 0.3
        runs = ceil(10/modC);
        disp('This sample requires multiple analyses because the
required proportion of carbon from the sample is very small');
        disp(['runs = ' num2str(runs)]);
        disp(['Target Mass = ' num2str(targetmass)]);
    else
        runs = ceil(10/modC);
        totsamp = targetmass*runs;
        while targetmass > mass
            runs = runs+1;
            targetmass = totsamp/runs;
        end
        disp('This sample requires multiple analyses because the
required proportion of carbon from the sample is very small.
Additional runs will also be required to account for very low %TOC');
```

```
        disp(['runs = ' num2str(runs)]);
        disp(['Target Mass = ' num2str(targetmass)]);
    end
end
```

C2. Matlab ® code for the calculation of T_1 as defined by Subt et al. (2017).

```
function [ T1 ] = T1( DBrun, p )
%This function takes a normal dirt burner run file and calculates the
%temperature at which the first split should be taken to sample the
%proportion given in the input (fSA).

%Inputs:
%datafile:  Standard Dirtburner .txt data file containing the
following
%(unlabeled) columns:
%Temperature | Date | Time | pCO2
%fSA: This is a proportion of the pCO2 that you wish to sample from
%the given run.

%Load Data and Results files
Data=load(DBrun);
T=Data(:,3);
CO2=Data(:,2);

%Calculate T1
C = cumsum(CO2);
Amt = p*max(C);
idx = find(C <= Amt,1,'last');
T1 = T(idx,1);
fprintf('T1 is %i.\n',T1)
```

C3. Regional TEX_{86} calibration study

Due to latitudinal bias, global calibrations do not often produce accurate results (e.g. Kim et al., 2010; Pearson and Ingalls, 2013; Tierney and Tingley, 2014; Tierney and Tingley, 2015). Instead, regional calibrations for polar regions may be necessary. To convert resulting TEX_{86} values to absolute temperatures, we applied several calibration routines and examined their differences. Table C1 lists the calibrations used in this study, which include several linear temperature calibrations (Kim et al., 2008; Liu et al., 2009; Schouten et al., 2002), the low-temperature calibration of Kim et al. (2010), a Southern Ocean calibration (Shevenell et al., 2011), and the BAYSPAR calibration routine which utilizes a Bayesian regression approach that varies the calibration as a function of geographical location (Tierney and Tingley, 2014; Tierney and Tingley, 2015). Table C1 also shows the equations used for each, and henceforth, we refer to specific calibrations by the calibration numbers listed in this table. In the case of calibration 4, the TEX_{86} index is calculated differently for low- and high-temperature regions, thus different calibration equations are used in each case (only the low-temperature calibration is shown in Table 4.2 as it is directly relevant to this study). TEX_{86}^{L} is calculated as follows:

$$TEX_{86}^{L} = \log_{10}\left(\frac{[GDGT-2]}{[GDGT-1]+[GDGT-2]+[GDGT-3]}\right) \qquad \text{Eq. C3.1}$$

Table C1. Sediment core-top TEX_{86} calibrations applied in this study. Calibrations are referenced in text by calibration number, relative to their chronological order. Table modified from Tierney and Tingley (2014).

Number	Range (°C)	Equation	n	r^2	Inputs	SST data	Reference
1	0 - 30	$TEX_{86} = 0.015T + 0.28$	40	0.92	15 locations (all data)	WOA98	Schouten et al., 2002
2	5 - 30	$T = -10.78 + 56.2TEX_{86}$	223	0.94	No Red Sea, SSTs < 5°C, residuals > 1σ	WOD	Kim et al., 2008
3	-3 - 30	$T = 50.475 - 16.332(^{1}/_{TEX_{86}})$	287	0.82	All data	WOA94	Liu et al., 2009
4	-3 - 30	$T = 38.6 + 68.4TEX_{86}^{L}$	396	0.86	No Red Sea	Satellite	Kim et al., 2010
5	-2 - 30	$TEX_{86} = 0.0125T + 0.3038$	230	0.82	Kim et al., 2008 data & 7 sites in Antarctic Peninsula	Satellite	Shevenell et al., 2011
SST-6 subT-7	-2 - 30	BAYSPAR (online)	1095	N/A	All data	WOA09	Tierney & Tingley, 2015

Temperature reconstructions were compared using seven different TEX_{86}-temperature calibrations (Appendix, Figure C1, Table C2). All calibrations show the same general trends, but have significant differences in absolute temperatures. For example, with the exception of calibration 4, which utilizes a different TEX_{86} index (TEX_{86}^{L}), all calibrations show that the coldest temperatures occurred ~21,000^{14}C yrs ago (DG12 GC06 370 cm).

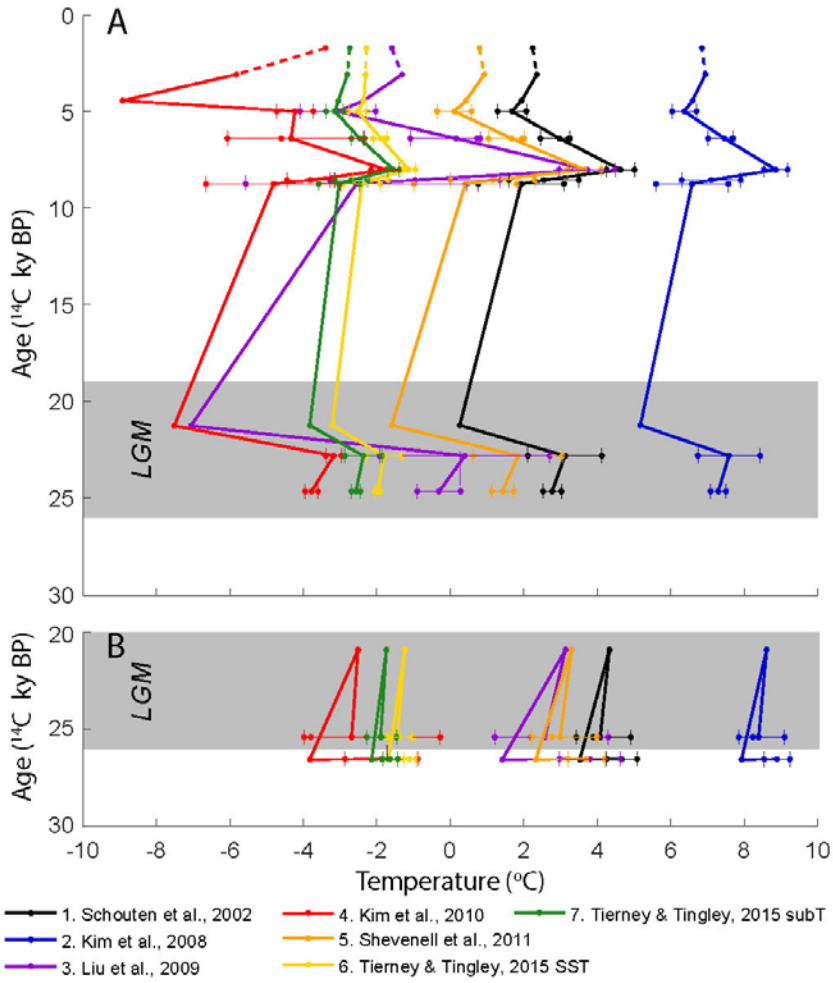

Figure C1. Temperature reconstructions for cores DG12-BC06 and -GC06 (A) and RS15-GC16B (B) according to multiple calibration routines. Temperature is plotted against blank-corrected, uncalibrated, low-temperature Ramped PyrOx ^{14}C dates. Note that core-top values from BC06 are shown with GC06.

Calibrations 3 and 4 show the largest deviations from the overall trend, though this is caused by different reasons. In the case of calibration 3, the overall trends remain the same as in other calibrations, but the positive and negative changes are greatly exaggerated, as it is a nonlinear calibration that uses inverse TEX_{86} values. Calibration 4 uses TEX_{86}^{L}, which does not include the crearchaeol regiosomer (GDGT-5) in its calculation (see equation 4.2). Despite its high concentrations, Kim et al. (2005) found that GDGT-5 may not play an important role in the temperature adaptation of archaea in subpolar regions. However, observations by Shah et al.

(2008) suggest the opposite, that GDGT-5 is important for SST prediction. Moreover, the original TEX_{86} equation is a more well-established and statistically robust expression of GDGT cyclization (e.g. Schouten et al., 2002; Tierney and Tingley, 2014). Overall, calibrations 3 and 4 show the lowest resulting temperatures, and calibration 2 results in the highest overall temperatures.

The regional applicability of these TEX_{86} calibration routines was examined for the southwestern Ross Sea. The archaeal distribution in the Ross Sea indicates living archaea are most abundant at depths > 250 m water depth (e.g. Alonso-Saenz et al., 2012). Modern mean annual water temperatures vary with depth, ranging from ~0.25 °C near the surface to ~-2 °C at depth (Jacobs et al., 1970). Based on this range of values, calibrations 1, 2 and 4 all produce calibrated temperatures too high or too low to be considered accurate (Figure 4.5). Calibration 3 shows a core-top temperature nearer to modern mean SSTs, but produced an unrealistically wide range of temperatures for this time period. Although calibration 4 is recommended by its authors for low-temperature regions, most calibrated temperatures are below freezing point (-1.8 °C) that would impede long-term open-water conditions and are inconsistent with modern and estimated LGM conditions. Calibrations 6 and 7 produce more realistic temperatures, however core-top temperatures show >2°C difference from expected modern temperatures. Calibration 5, which is a linear calibration that includes Antarctic samples, produces the core-top temperature nearest to the expected modern temperatures as well as a realistic range of temperatures and is therefore the most appropriate existing calibration for this set of samples, and we use values yielded from this calibration in the text of this chapter to refer to temperature. Although choosing an appropriate calibration is important for determining absolute temperatures, general trends between most calibrations remain the same (with the

exception of TEX_{86}^{L}), thus the use of changes in trends can be a useful tool for making observations of changing water temperatures through time.

C4. Extended figures and tables

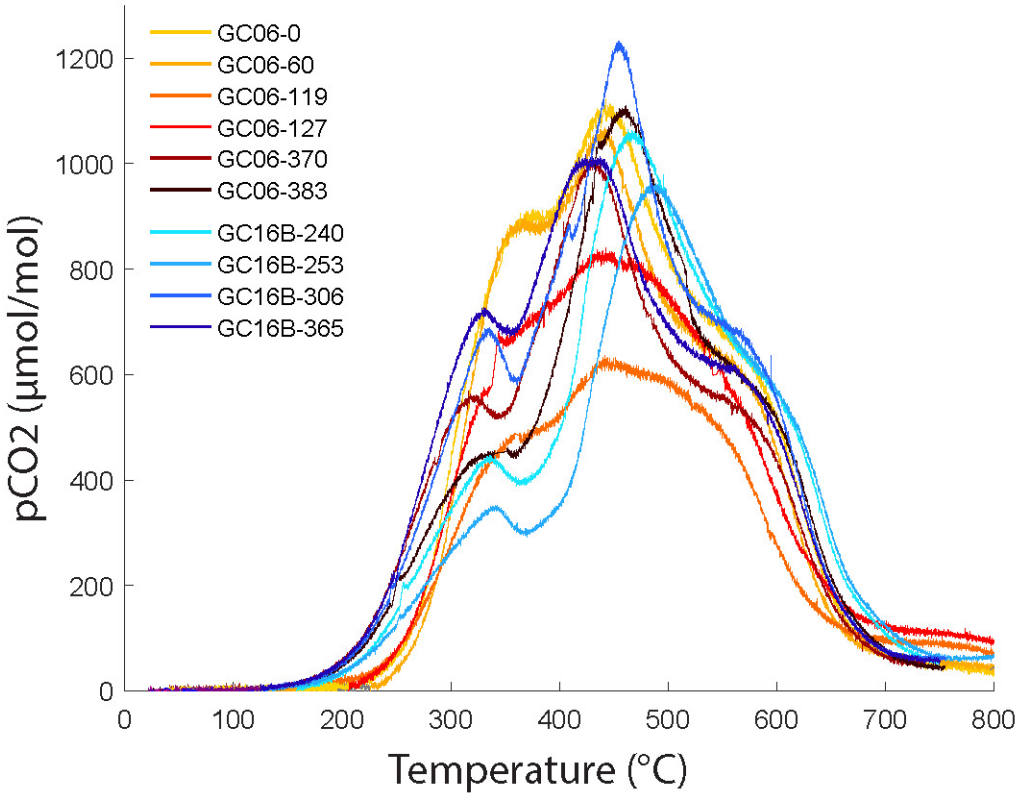

Figure C2. Thermographs of all samples analyzed for Ramped PyrOx ^{14}C in Chapter 4.

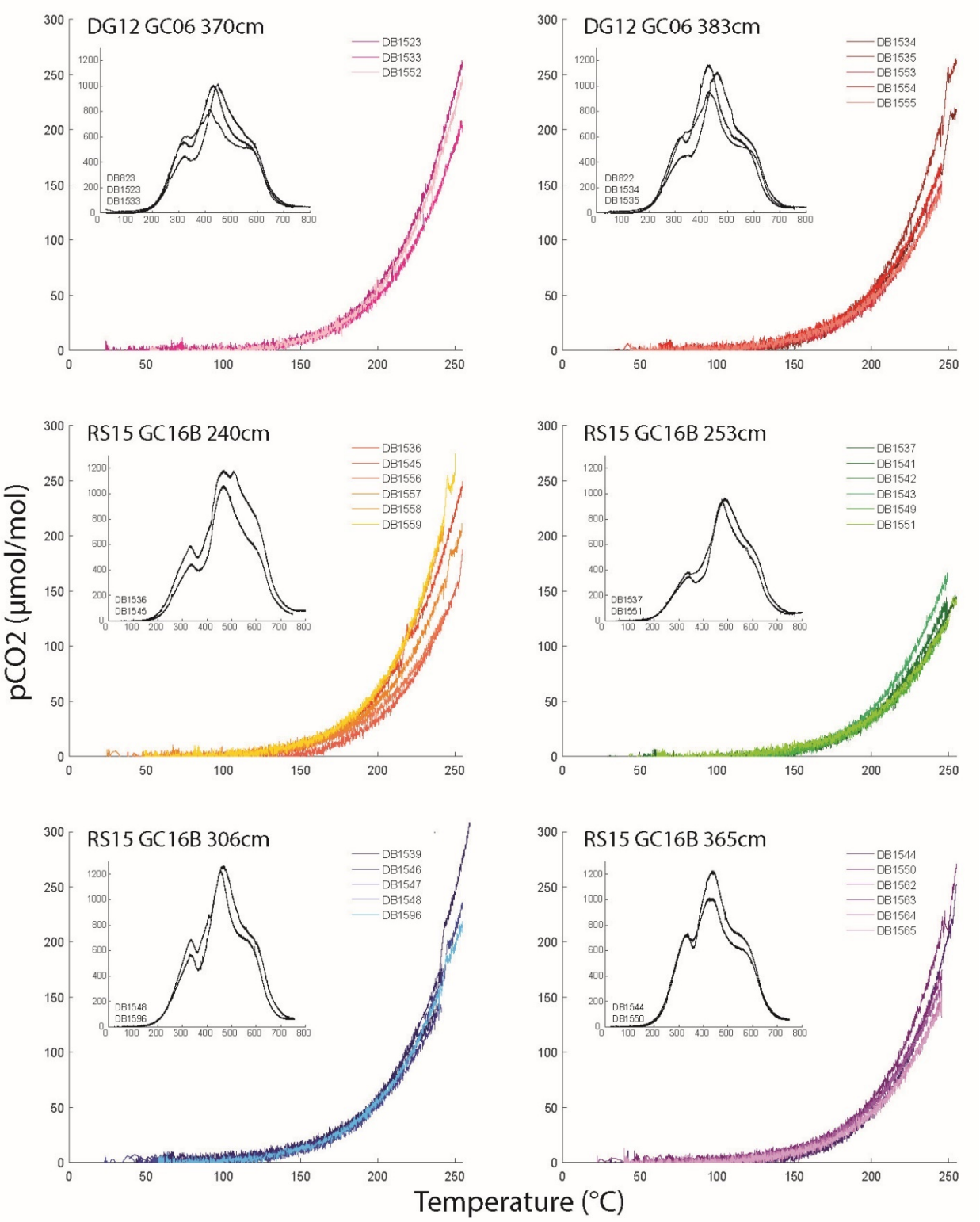

Figure C3. pCO_2 evolution along the temperature ramp for all composite RP sample analyses. Full RP analyses were carried out to evaluate the overall replicability of analyses, and are depicted in insets for each sample.

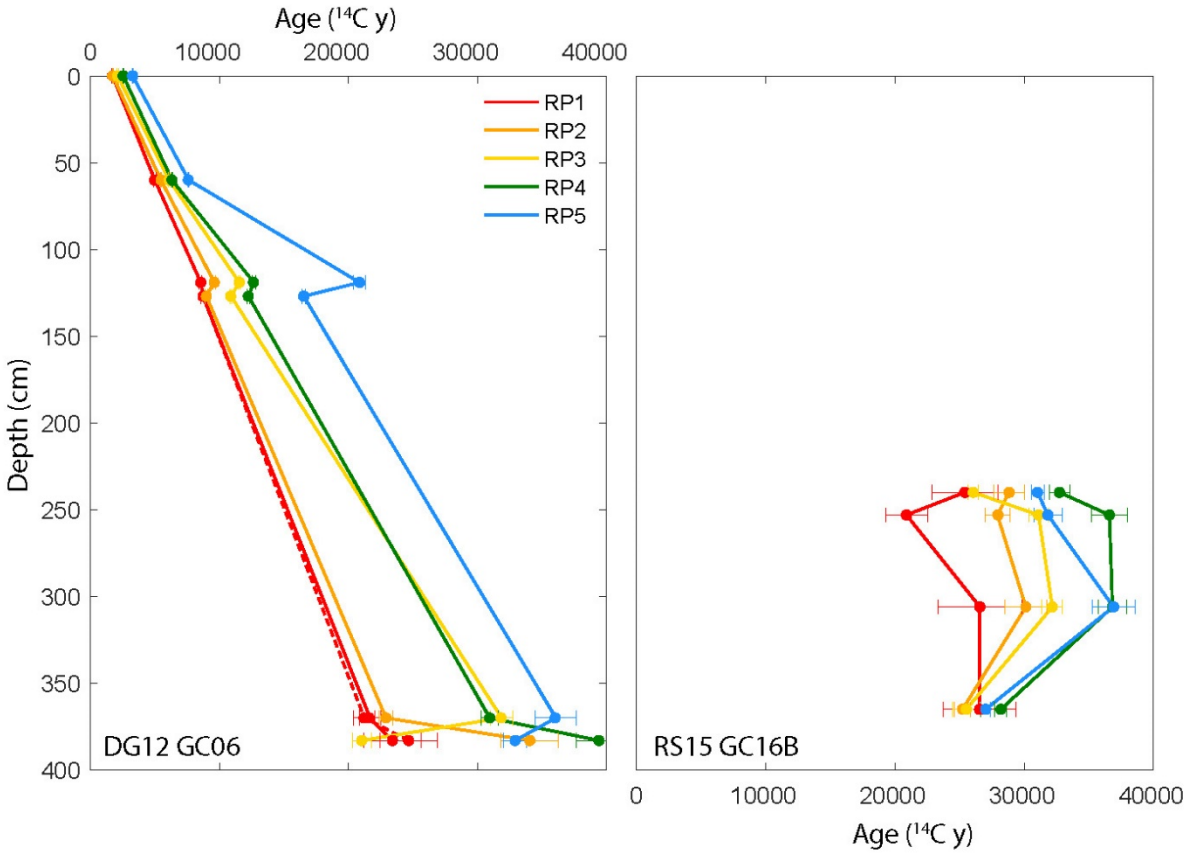

Figure C4. RP ^{14}C ages of cores DG12-BC06 and -GC06, and RS15-GC16B. Conventional RP1 ages are denoted by the dashed line alongside associated composite RP ages for the bottom two samples of core GC06. Ages are shown in blank-corrected ^{14}C years BP, and are reported in Appendix Table C2.

Table C2. TEX_{86} and BIT values for cores BC06, GC06 and GC16B. Temperatures reported were calculated using the linear calibration of Shevenell et al. (2011). Alternate calibrations were also applied and shown in Figure 4.2. Ages reported represent the lowest-temperature splits of Ramped PyrOx ^{14}C dating.

Core	Depth (cm)	Date of analysis	TEX_{86}	BIT	Temperature (°C)	Age (^{14}C y BP)	±
DG12 BC06	0	2017-05-04	0.3137	0.0934	0.7920	1730	60
DG12 GC06	25	2017-03-25	0.3154	0.3644	0.9254		
DG12 GC06	50	2017-03-05	0.3091	0.3522	0.4243		
DG12 GC06	60	2017-05-05	0.3111	0.2146	0.5821	5000	90
DG12 GC06	60	2017-06-20	0.2993	0.2201	-0.3601		
DG12 GC06	84	2017-05-04	0.3289	0.2375	2.0075		
DG12 GC06	84	2017-05-08	0.3283	0.1708	1.9613		
DG12 GC06	84	2017-06-12	0.3167	0.2921	1.0358		
DG12 GC06	110	2017-05-05	0.3438	0.3052	3.1966		
DG12 GC06	110	2017-06-20	0.3552	0.3201	4.1134		
DG12 GC06	119	2017-05-05	0.3039	0.2120	0.0077	8560	100
DG12 GC06	119	2017-06-12	0.3325	0.2931	2.2938		
DG12 GC06	127	2017-05-05	0.2914	0.2150	-0.9900	8740	150
DG12 GC06	127	2017-06-12	0.3265	0.3614	1.8127		
DG12 GC06	370	2017-03-25	0.2839	0.1457	-1.5935	21240	850
DG12 GC06	376	2017-05-04	0.3117	0.1373	0.6331		
DG12 GC06	376	2017-06-12	0.3419	0.3195	3.0482		
DG12 GC06	383	2017-05-04	0.3179	0.2042	1.1282	24660	2220
DG12 GC06	383	2017-05-08	0.3254	0.2353	1.7255		
RS15 GC16B	240	2017-05-05	0.3537	0.2501	3.9937	25410	2570
RS15 GC16B	240	2017-05-08	0.3315	0.2180	2.2181		
RS15 GC16B	240	2017-06-12	0.3384	0.2789	2.7643		
RS15 GC16B	253	2017-03-05	0.3450	0.3565	3.2972	20890	1640
RS15 GC16B	306	2017-03-05	0.3329	0.3656	2.3283	26570	3260
RS15 GC16B	365	2017-05-05	0.3438	0.2448	3.2035	26550	2820
RS15 GC16B	365	2017-06-20	0.3563	0.2708	4.1996		

Table C3. Radiocarbon ages from multiple dating techniques for Drygalski samples. Ages are reported in blank-corrected ^{14}C years BP and were measured using Ramped PyrOx ^{14}C dating. Bulk AIO ^{14}C ages were calculated using the weighted mean of all Ramped PyrOx ^{14}C ages of each sample. Table 4.1 shows preliminary bulk AIO ^{14}C ages.

Core	Depth (cm)	split	$\delta^{13}C$	µmol CO_2	Composite runs	Fm	±	Age (^{14}C y BP)	±	Bulk AIO Age (^{14}C y)	±
DG12 BC06	0	1	-25.05	19.955	1	0.8064	0.0054	1730	60	2442	22
DG12 BC06	0	2	-22.74	18.789	1	0.8039	0.0056	1750	60		
DG12 BC06	0	3	-23.64	24.756	1	0.7667	0.0045	2130	50		
DG12 BC06	0	4	-23.84	39.927	1	0.7282	0.0027	2550	30		
DG12 BC06	0	5	-24.21	36.571	1	0.6651	0.0027	3280	35		
DG12 GC06	60	1	-25.32	12.459	1	0.5369	0.0059	5000	90	6303	27
DG12 GC06	60	2	-25.07	28.941	1	0.5059	0.0027	5470	45		
DG12 GC06	60	3	-24.81	22.769	1	0.4676	0.0031	6110	60		
DG12 GC06	60	4	-25.43	25.921	1	0.4547	0.0028	6330	50		
DG12 GC06	60	5	-24.4	33.419	1	0.3874	0.0021	7620	45		
DG12 GC06	119	1	-27.04	14.067	1	0.3444	0.0042	8560	100	12265	97
DG12 GC06	119	2	-26.39	16.289	1	0.3023	0.0034	9610	100		
DG12 GC06	119	3	-25.45	25.757	1	0.2375	0.0023	11550	80		
DG12 GC06	119	4	-25.49	16.81	1	0.2065	0.0030	12670	120		
DG12 GC06	119	5	-21.17	12.448	1	0.0745	0.0041	20860	440		
DG12 GC06	127	1	-27.69	9.552	1	0.3371	0.0060	8740	150	12295	48
DG12 GC06	127	2	-26.67	16.789	1	0.3263	0.0034	9000	90		
DG12 GC06	127	3		23.983	1	0.2572	0.0024	10910	80		
DG12 GC06	127	4		29.327	1	0.2174	0.0021	12260	80		
DG12 GC06	127	5		29.092	1	0.1276	0.0018	16540	120		
DG12 GC06	370	1	-29.01	14.903	1	0.0673	0.0034	21680	410	30856	478
DG12 GC06	370	2	-28.5	22.826	1	0.0196	0.0024	31610	980		
DG12 GC06	370	3	-27.11	22.67	1	0.0134	0.0024	34650	1450		
DG12 GC06	370	4	-28.82	28.477	1	0.0150	0.0019	33710	1040		
DG12 GC06	370	5	-23.87	8.788	1	0.0423	0.0062	25420	1180		
DG12 GC06	370	1	-27.45	10.021	3	0.0711	0.0075	21240	850	30543	427
DG12 GC06	370	2	-27.67	14.305	1	0.0577	0.0036	22920	510		
DG12 GC06	370	3	-28.1	29.374	1	0.0189	0.0020	31870	860		
DG12 GC06	370	4	-27.93	38.084	1	0.0212	0.0017	30950	640		
DG12 GC06	370	5	-28	26.787	1	0.0112	0.0022	36060	1560		
DG12 GC06	383	1	-29.32	16.064	1	0.0542	0.0032	23420	480	31749	498
DG12 GC06	383	2	-29	25.025	1	0.0203	0.0022	31300	870		
DG12 GC06	383	3	-28.09	26.625	1	0.0110	0.0021	36210	1510		
DG12 GC06	383	4	-28.23	24.545	1	0.0149	0.0022	33770	1210		
DG12 GC06	383	5	-27.37	15.15	1	0.0233	0.0035	30210	1210		
DG12 GC06	383	1		9.789	5	0.0464	0.0128	24660	2220	34106	755
DG12 GC06	383	2	-29.05	13.361	1	0.0144	0.0040	34050	2230		
DG12 GC06	383	3	-28.18	30.986	1	0.0210	0.0019	31040	740		
DG12 GC06	383	4	-28.19	42.472	1	0.0074	0.0016	39460	1730		
DG12 GC06	383	5	-28.59	32.792	1	0.0166	0.0019	32910	900		
RS15 GC16B	240	1	-28.42	11.032	6	0.0423	0.0135	25410	2570	29807	606
RS15 GC16B	240	2	-28.69	12.488	1	0.0276	0.0042	28830	1220		
RS15 GC16B	240	3	-27.72	32.409	1	0.0390	0.0019	26070	390		
RS15 GC16B	240	4	-27.75	36.74	1	0.0170	0.0017	32750	820		
RS15 GC16B	240	5	-27.91	59.313	1	0.0210	0.0013	31050	510		
RS15 GC16B	253	1	-27.89	9.616	6	0.0742	0.0151	20890	1640	31696	541
RS15 GC16B	253	2	-28.76	14.417	1	0.0309	0.0037	27940	960		
RS15 GC16B	253	3	-28.01	29.304	1	0.0208	0.0020	31100	780		
RS15 GC16B	253	4	-28.23	35.114	1	0.0105	0.0018	36620	1370		
RS15 GC16B	253	5	-28.47	21.305	1	0.0190	0.0026	31820	1100		
RS15 GC16B	306	1	-28.62	10.164	6	0.0366	0.0148	26570	3260	34370	847
RS15 GC16B	306	2	-28.76	11.172	1	0.0235	0.0047	30120	1600		
RS15 GC16B	306	3	-28.33	34.966	1	0.0182	0.0018	32180	790		
RS15 GC16B	306	4	-28.38	54.582	1	0.0102	0.0014	36850	1090		
RS15 GC16B	306	5	-27.8	27.177	1	0.0101	0.0021	36870	1710		
RS15 GC16B	365	1	-28.66	11.665	6	0.0367	0.0129	26550	2820	26986	625
RS15 GC16B	365	2	-28.99	15.583	1	0.0432	0.0034	25240	640		
RS15 GC16B	365	3	-27.95	9.531	1	0.0417	0.0054	25520	1040		
RS15 GC16B	365	4	-27.7	37.253	1	0.0299	0.0017	28180	460		
RS15 GC16B	365	5	-28.46	51.197	1	0.0346	0.0015	27020	350		